Slow and Steady: 4-Phenylthiobutanoic Acid Inhibits Histone Deacetylase 8 to Enhance Post-Acute Kidney Injury Repair

by

Hwa In Han

B.S., College of William & Mary, 2014

Submitted to the Graduate Faculty of the

School of Medicine in partial fulfillment

of the requirements for the degree of

Doctor of Philosophy

University of Pittsburgh

2020

UNIVERSITY OF PITTSBURGH

SCHOOL OF MEDICINE

This dissertation was presented

by

Hwa In Han

It was defended on

May 29, 2020

and approved by

Jacqueline Ho, M.D., Department of Pediatric Nephrology

Penelope Morel, M.D., Department of Immunology

Kyle Orwig, Ph.D., Department of Obstetrics, Gynecology & Reproductive Services

Michael Tsang, Ph.D., Department of Developmental Biology

Dissertation Director: Neil Hukriede, Ph.D., Department of Developmental Biology

Slow and Steady: 4-Phenylthiobutanoic Acid Inhibits Histone Deacetylase 8 to Enhance Post-Acute Kidney Injury Repair

Hwa In Han, PhD

University of Pittsburgh, 2020

Acute kidney injury (AKI) is a rapid decline in kidney function that is associated with high mortality and morbidity rates, affecting 1 in 5 adults worldwide [1]. While damaged renal tubular epithelial cells (RTECs) undergo reparative process to proliferate and replace the damaged epithelium, it is not a robust mechanism. The initial damage is followed by a cross-talk of innate immune system and RTECs resulting in exacerbation of inflammation, fibrosis, and sometimes irreversible damage. Despite the prevalence and severity of AKI, no FDA approved therapeutics exist to replace damaged or lost RTECS. Therefore, it is imperative to screen, identify, and understand mechanisms with which candidate therapeutics can enhance repair. Our group identified 4-phenylthiobutanoic acid (PTBA) and developed analogs to enhance renal repair when treated post-AKI. However, the protein target(s) as well as the mechanisms responsible for enhanced recovery are not completely understood. Here, we used a zebrafish larvae AKI model to visualize RTEC cellular response during PTBA treatment. We also characterized the zebrafish immune response during AKI and the effect of PTBA on modulating the innate immune cell response. Lastly, we used *in vivo* and *in vitro* methods to identify the target of PTBA, Histone deacetylase 8 (HDAC8). Using knockout *hdac8* (*hdac8*$^{-/-}$) zebrafish, we showed a similarly enhanced recovery of *hdac8*$^{-/-}$ as we saw in animals treated with PTBA. We further demonstrated the *hdac8*$^{-/-}$ show changes cell cycle dynamics and epithelial to mesenchymal transition. Taken together, our work provides another step forward in pro-regenerative compound development.

Table of Contents

List of Tables

List of Figures

Preface

γH2ax: Phosphorylated H2A histone family member X; biomarker for DNA double-strand breaks

3G8: Unknown antigen on zebrafish proximal tubule cells

a6F: Na+K+ ATPase alpha-1 subunit monoclonal antibody

AA-AKI: Aristolochic acid-AKI

AKI: Acute kidney injury

Cdh17: Cadherin17; pronephros epithelial marker

Chk1: Checkpoint kinase 1

DAPI: 4’,6-diamidino-2-phenylindole

DMSO: Dimethyl sulfoxide

E-cad: E-cadherin; cadherin1

EdU: 5-ethynyl-2'-deoxyuridine; nucleoside analog of thymidine

EMT: Epithelial to mesenchymal transition

Gent-AKI: Gentamicin-induced AKI

GFP: Green fluorescent protein

gtshβ: Grouper thyroid stimulating hormone beta

HDAC: Histone deacetylase

HDI: Histone deacetylase inhibitor

HS: Heat shock

Hsp70: 70 kilodalton heat shock protein

IF: Immunofluorescence

IRI-AKI: Ischemia-reperfusion injury-AKI

ISH: *in situ* hybridization

Kim-1/ Havcr1: Kidney injury molecule-1/ Hepatitis A virus cellular receptor 1

Lyz: Lysozyme

mCh: mCherry

Mpeg1: Macrophage expressed gene 1

p21: Cyclin-dependent kinase inhibitor 1

Pax2a: Paired box gene 2

PCNA: Proliferating cell nuclear antigen

pH3: Phospho-Histone3; marker of G2/M

PT: Proximal tubule

PTBA: Phenylthiobutanoic acid

UPHD25/ M4PTB: Analog of PTBA; methyl-4-(phenylthiol)butanoate

UUO-AKI: Unilateral ureteric obstruction- AKI

RA: Retinoic acid

Ro41-5253: Potent selective retinoic acid receptor-α antagonist

RTEC: Renal tubular epithelial cells

SMC3: Structural maintenance of chromosomes 3

TUNEL: Terminal deoxynucleotidyl transferase dUTP nick end labeling; assay for apoptosis

PCI-34051: Selective HDAC8 inhibitor

Vim: Vimentin

Acknowledgements

"It is the long history of humankind (and animal kind, too) that those who learned to collaborate and improvise most effectively have prevailed."

-Charles Darwin

Neil, for all your mentorship, infectious excitement and dedication to science,

My thesis committee members, Jackie, Penny, Kyle, and Michael, for all your insightful feedback and academic support,

The zebrafish community for all your invaluable feedback, reagents, and techniques,

DLAR for your dedication to animal health,

Dr. Paul Heideman, my undergraduate mentor, for his dedication to teaching,

Everyone in the Hukriede Lab, particularly:

Michael M. for your excellence in microinjections and sharing all the laughs, the space heater, and snacks with me,

Amanda C. for your excellent expertise in proteomics and your contribution to this work,

Aneta P. for your encouragement and expertise in the field of AKI and bread-making,

Christine C. for encouraging my career development and your contribution to this work,

Eugenel E. for your expertise in molecular biology, your contribution to this work, and being an amazing partner and my best friend,

My family and friends, particularly my sister, Ji, Mom, Dad, and the Pittsburgh climbing community, for their constant and never-ending support and inspiration in life…I am humbled and

grateful to have grown whilst working with all of the amazing, hardworking people mentioned above. ***Thank you.***

1.0 Background

1.1 Kidney development, structure, and function

1.1.1 Mammalian kidney development

During development, the vertebrate kidney transitions through the three distinct kidney structures that are marked by increasing numbers and organization of nephrons. They are termed pronephros, mesonephros, and metanephros, in the order of the least number of nephrons to the greatest number of nephrons. In the mammalian, avian, and reptilian kidney, the pronephros and mesonephros arise during the embryonic development then become vestigial structures [2]. Further along in embryonic development, the metanephric kidney is formed, becoming the final kidney structure used throughout the life of the animal [2,3]. In the teleost and amphibian kidney, the pronephros serves as a functional embryonic kidney until a second wave of nephrogenesis occurs to form the mesonephros, the final kidney structure used by the adult animal [4].

The mammalian kidney arises from the intermediate mesoderm (IM) during development, specializing into different cell types via spatially and temporally regulated molecular signals [3,5]. The renal progenitor cells (RPC) that co-express LIM homeobox1 (Lhx1)/ Paired box gene 2 (Pax2)/ Paired box gene 8 (Pax8) are first observed in a set of bilateral epithelial tubes called the Wolffian duct [6] (Figure 1A). The rostral ducts function as the pronephric tubule but disintegrates overtime [2]. The elongated, caudal duct give rise to branching nephrons and serves as the mesonephros [2] (Figure 1B). The metanephric kidney forms at the caudal end of the Wolffian duct [6] (Figure 1B). The Wolffian duct is juxtaposed to metanephric mesenchyme (MM) and the two

tissues exchange various signals to initiate metanephros formation. RET tyrosine kinase (Ret) and Glial cell line-derived neurotrophic factor (GDNF) signaling is required for the Wolffian duct to invade the MM then branch, determining the final number of nephrons in the metanephric kidney [7] [8] [9](Figure 1B,C). Subpopulations of cells in the cap mesenchyme (CM) express various multipotent progenitor markers that differentiate into different kidney cell types (Figure 1D). Subpopulation of Forkhead transcription factor D $(Foxd)^{+}$ cells differentiate to interstitial cells and Fetal liver kinase-1 $(Flk1)^{+}$ cells contribute to the renal vasculature [10] [11]. Cells co-expressing SIX Homeobox 2 (Six2) and CREB-binding protein/p300-interacting transactivator with ED-rich tail 2 (Cited2) undergo mesenchymal to epithelial transition (MET) to become renal vesicles [12] [13] (Figure 1D). The renal vesicles continue to specify, receiving complex signaling cascade to initiate segmentation specification (Figure 1D). For example, the glomerulus is specified by Wilm's tumor1 (Wt1) and the proximal segment is specified by Pax2 [4] (Figure 1). During specification, the renal vesicle undergoes structural changes into a comma-shaped body, a s-shaped body, then ultimately to a fully differentiated and segmented nephron (Figure 1D). Each fully differentiated nephron is composed of segments expressing various transporters to reuptake solutes and water to reabsorb essential molecules and maintain osmotic balance.

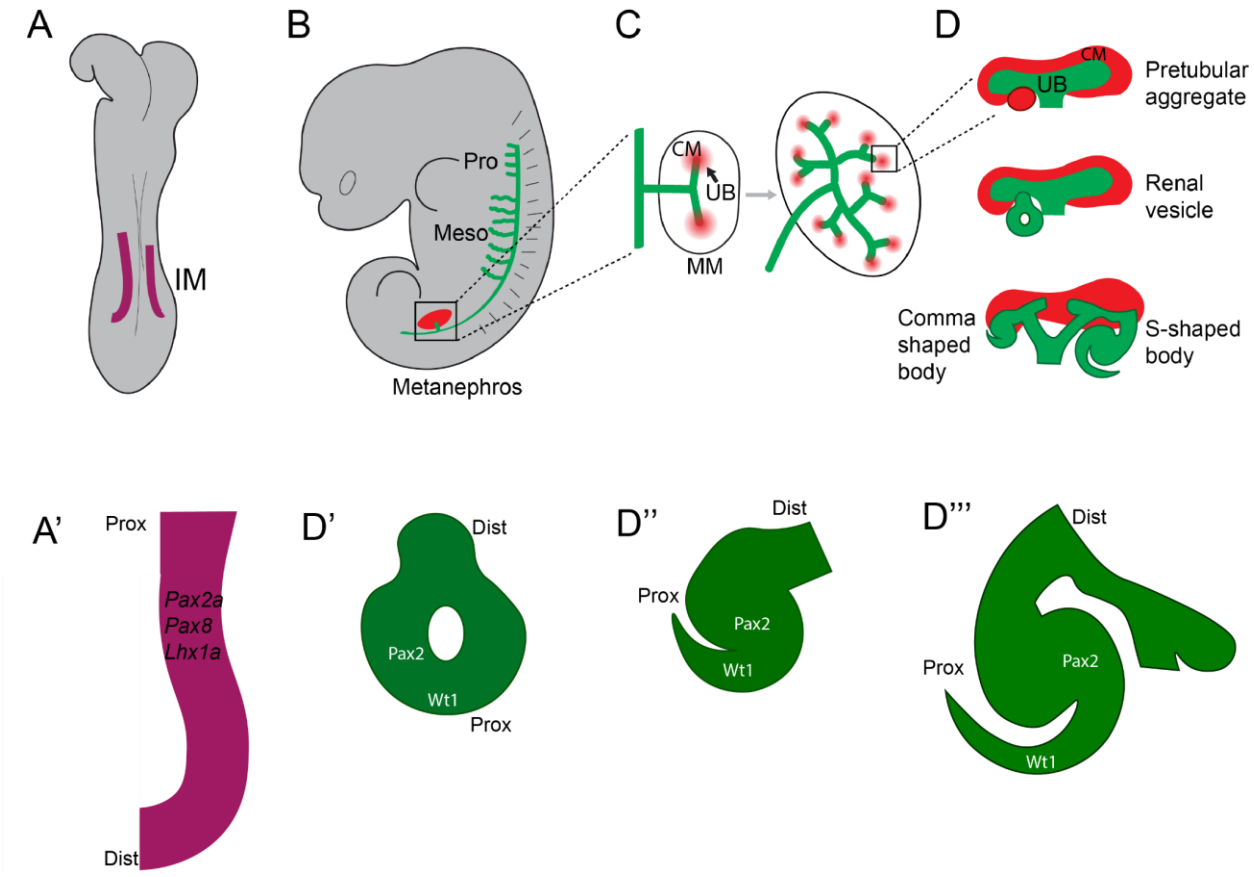

Figure 1 Mammalian kidney development

Stages of mouse kidney development. (A) Intermediate Mesoderm (IM, purple) specification at E8 (A') The renal progenitor cells within IM (purple) express Pax2a, Pax8, and Lhx1a (B) Pro-, meso-, metanephros formation. Wolffian duct (Green) is the original epithelial tube that becomes elongated from rostral to caudal. (C) Menatenprhos organogenesis at E11-E13.5. Ureteric bud branches Cap mesenchyme (CM), ureteric bud (UB), metanephric mesenchyme (MM). (D) Nephrogenesis. Pretubular aggregate continue to specify to renal vesicle (D'), comma shaped body (D''), and s-shaped body (D'').

1.1.2 Zebrafish kidney development

The zebrafish kidney undergoes similar developmental signaling pathways as the mammalian kidney. The RPCs co-express *lhx1a/pax2a/pax8* within the IM in the tailbud stage [14] [15] (Figure 2A). Like the mammalian system, the RPCs undergo MET transition to form two

bilateral tubules that eventually form the two pronephric kidneys. Within the IM the RPC field responds to a retinoic acid (RA) gradient secreted from the outer paraxial mesoderm (Figure 2B), with the high caudal RA specifying the glomerular and proximal segments [16] [3]. Like the mammalian glomerulus, the zebrafish glomerulus requires *wt1* expression while *pax2a* and *pax8* are required for proximal tubule segmentation (Figure 2B). By 24 hours post fertilization (hpf), the segmentations become distinct and the pronephros becomes functional at 72-96hpf [17] (Figure 2). At 10dpf, zebrafish undergo postembryonic metamorphosis from larva to juvenile [18]. Concurrently, the second wave of nephrogenesis occurs, resulting in the mesonephros comprised of hundreds of nephrons [18]. The mesonephric anlagen form on top of and then fuse with the pronephric tubules, with increased expression of RPC which epithelialize into renal vesicle-like bodies to elongate into nascent nephrons and fuse with the pronephric tubule [18]. The mesonephros serves as the terminal functioning kidney for adult zebrafish.

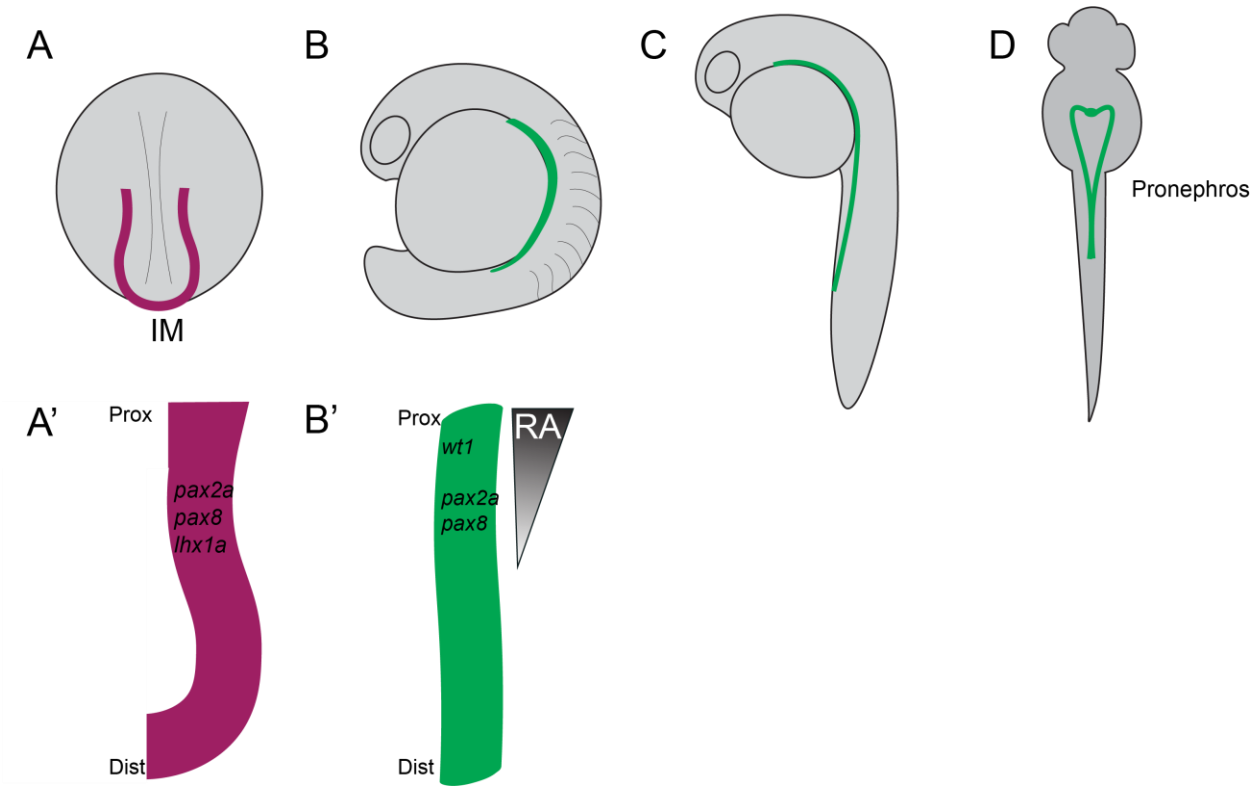

Figure 2 Zebrafish kidney development

Stages of zebrafish kidney development. (A) Intermediate Mesoderm (IM, purple) specification at 12hpf (A') The renal progenitor cells within IM (purple) express *pax2a*, *pax8*, and *lhx1a.* (B) Pronephros epithelialization 16-24hpf. (B') Proximal versus distal segmentation is determined by (among other factors) RA gradient and *wt1a*, *pax2a*, and *pax8* expression. (C) Differentiation of pronephric tubule and glomerulus 30-40hpf (D) Top view of zebrafish pronephros. They are composed of two bilateral nephrons with one fused glomerus.

1.1.3 Nephron segmentation

In the human metanephric kidney, the branching process results in a complex kidney approximately 200,000 to 2 million nephrons, each nephron serving as a working unit of filtration [19] (Figure 3A). In comparison, the zebrafish kidney pronephric kidney is simpler, resulting in two nephrons (Figure 3B). However, the function of the metanephric and pronephric nephrons both function to filter blood, excrete metabolites, uptake essential nutrients, and produce urine as its

final product [20]. The mammalian nephron is comprised of single sheet of renal tubular epithelial cells (RTECs) and is segmented into the glomerulus, proximal tubule (PT), Loop of Henle, distal tubule (DT), and collecting duct (CD) (Figure 3A,C). Main segments the zebrafish are comprised of a glomerulus, PT, DT, and cloaca (Figure 3B,D). While the mammalian and zebrafish have differing numbers of nephrons, each nephron's segmentation is well conserved (Figure 3A,B). For example, both the mammalian and zebrafish glomerulus express *Nephrin*, *Podocin*, and *Mafb* and are composed of podocytes with fenestrated barriers and capillaries to receive and filter blood into the nephron [4]. Both the mammalian and zebrafish PT express variants of Na^+K^+ATPase to absorb the majority of the solutes and water prior to passing the filtrate through the rest of the nephron [4].

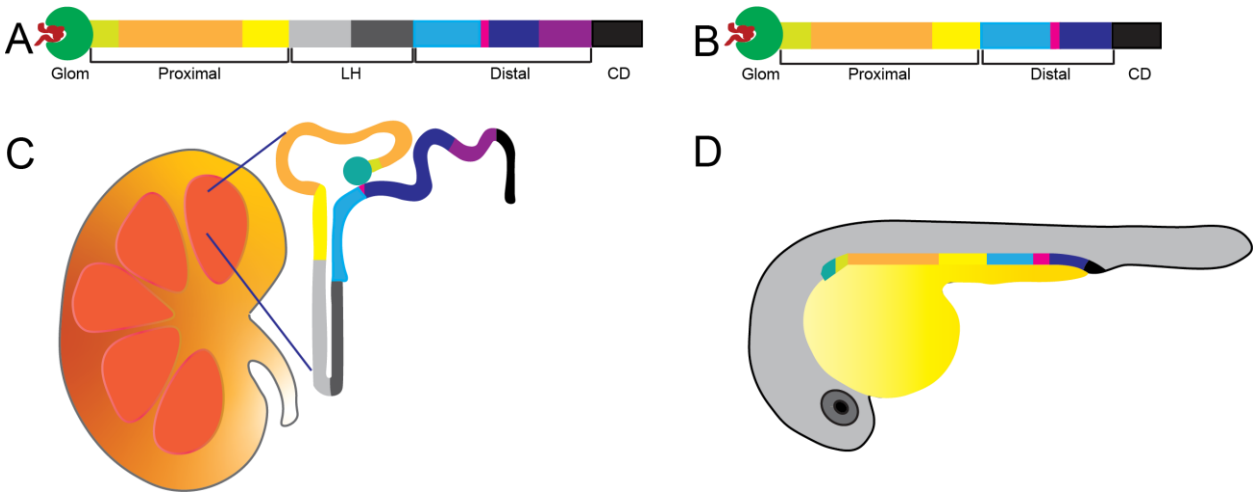

Figure 3 Mammalian metanephric kidney and larval zebrafish pronephric kidney

(A-B) Schematic segmentation sepecification of the nephron in mammals aunnd zebrafish. The blood is supplied by the tuft of capilarries (red) which is then filtered through the glomerulus (Glom, green). The resulting filtrate moves through the entire nephron from left to right: proximal tubule further segmented into the neck (light green), proximal convoluted tubule (orange), and proximal straight tubule (orange); Loop of Henle (greys, only in mammals); distal tubule further segmented into tall ascending limb (blue), macula densa (magenta, mammals) or corpuscle of Stannius (magenta, zebrafish), distal convoluted tubule (dark purple), and connecting tubule (light purple, only in mammals); and collecting duct or cloaca (CD, black). (A) mammalian nephron. (B). zebrafish nephron. (C) Schematic diagram of the mammalian metanephric kidney and the orientation of the nephron within the kidney. (D) Schematic diagram of the zebrafish pronephric kidney.

1.2 Acute kidney injury

1.2.1 Definition, epidemiology, and classification

Acute kidney injury (AKI) represents a disease spectrum with numerous contributing causes [21]. It is defined as an abrupt decline in kidney function measured by change in serum creatinine level greater than or equal to 1.5 times baseline within 7 days [22]. In the US alone, 577

experience AKI for every 100,000 persons and the incidence is higher in the hospital setting [1]. In a hospital episode of care, 21.6% adults and 33.7% children experience AKI worldwide [23]. Due to its prevalence, AKI presents very a heavy burden on the American health care system, costs ranging from $5.45 billion to $24.0 billion dollars in associated medical costs per year [24].

Due to a wide range of causes, AKI is categorized via their anatomical references to the kidney: pre-renal, intrinsic, and post- renal. Pre-renal causes are processes in which the underlying kidney function is normal but the blood flow to the kidney is reduced [1]. Intrinsic causes are processes in which there is a direct pathological issue to four major components of the kidney [1]. The major components under duress include glomerular, interstitial, tubular, and vascular. One main example of intrinsic AKI is nephrotoxic agents, such as an aminoglycoside antibiotic gentamicin, which is actively transported into the renal tubular cells and disrupts phospholipids, releases ROS, and activates intrinsic apoptosis pathways [25] [26]. Post-renal causes comprise of those that result in blockage of urinary flow such as kidney stones or blood clots in the urinary tract [1].

1.2.2 Risks and treatment

Despite the research effort, AKI continues to be a problematic and concerning disease due to its increasing rate, rising from 600,000 cases in 2001 to 3.1 million in 2011, with an average mortality rate of 23.9% [27] [28]. Risk factors include the aging population, increasing cases of cardiovascular diseases, diabetes mellitus, pre-existing proteinuria, sepsis, and exposure to commonly prescribed medications during hospital stay such as NSAIDs and aminoglycoside drugs [28]. The above mentioned diseases, along with others such as shock, acute decompensated heart failure, pre-eclampsia, cardiac surgery, and cancer are contributing comorbidities that often put already hospitalized patients at a higher risk of developing AKI [28] [27].

Current established methods of care remain supportive. Few examples presented are: discontinuation of nephrotoxic agents and diuretics, radiocontrast procedures, and close management of patient volume status and perfusion pressure [29] [30]. The ultimate goal of these measures is to maintain hemodynamic stability and to avoid worsening of the damage that can potentially lead to irreversible loss of kidney function brought on by chronic kidney disease (CKD) or end stage renal disease (ESRD). Successful recovery from an episode of AKI is not always guaranteed [31] [32]. Upon irreversible injury, patients are moved from preventative measures to renal replacement therapy (RRT). Even with RRT, patients who undergo AKI suffer from a significantly higher short term and long term mortality and morbidity rates [27,33]. Taken together, AKI is a prevalent condition that takes a heavy toll on millions of patients a year on a global level. Unfortunately, the lack of therapeutics to directly resolve the damage contributes to worsening of quality of life as well as a heavy toll on healthcare resources.

1.2.3 Cellular pathophysiology

AKI is a complicated condition due to various etiologies that lead to dysfunction of the kidney. The human kidney harbors at least 43 different cell types, each playing a critical role for homeostasis of the body [34]. Therefore, it is not only important to understand the roles they play during homeostasis but also how they contribute to pathophysiology of AKI. The major cell types of interest that play an active role in the progression of AKI are: epithelial, vascular, interstitial, and immune components [20]. Of those components, the next sections will focus on epithelial and immune components, the two major components affected in our model of AKI.

1.2.3.1 Epithelial component

During an episode of AKI, the initial cellular injury observed in the kidney is the PT [20]. The PT is particularly vulnerable to injury due to its critical and heavy role in reuptake of the majority of the filtered molecules, like glucose, amino acids, salt, water, as well as nephrotoxins [35]. The current knowledge in injury and repair mechanisms have been established using the mammalian models of AKI [20] [36](Figure 4). Injury results in rapid loss of cytoskeletal integrity and cell polarity [37]. These include loss and mislocalization of membrane proteins, transporters, cell adhesion molecules, such as Na^+K^+ATPase, tight junction, and adherens junction, respectively [20] [38] (Figure 4B). RTEC death and loss of adhesion weakens the barrier between the nephron and the interstitium of the kidney, resulting in permeability and backflow of the filtrate without proper and specific reabsorption, further creating systemic osmoregulatory problems [20] (Figure 4C).

Multiple genes and proteins are differentially regulated in the injured kidney in humans and experimental models of AKI. In the injured PT, highly upregulated genes are: *Kidney injury molecule-1* (*Kim-1*), *Neutrophil gelatinase-associated lipocalin (Ngal*), *Tissue inhibitor of metalloproteinases 2* (*Timp-2*), and *Insulin like growth factor binding protein* (*Igfbp-7*) [38] [39] [40] [41] [42]. KIM-1 is a phosphatidyl serine receptor and is reported to participate in autophagy of injured RTECs as well as aid in leukocyte recruitment [43] [44] [39] [45]. NGAL, an iron-transporter, is another biomarker upregulated in the injury setting. It is known to form complexes with other iron-binding proteins, reduce superoxide formation and thereby subsequent cellular injury [46]. More recently identified markers of injury are TIMP-2 and IGFBP7 [47] [41] [42]. They are proposed to induce cell cycle arrest and may serve as an earlier injury signal during an episode of AKI before the condition becomes irreversible [41].

1.2.3.2 Adaptive Repair

Since renal biopsies are not often performed in AKI patients, the underlying repair physiology and histopathology have been largely defined using rodent models [48] [49] . These studies have identified key cellular players during AKI events, including roles for the RTECs and the immune system. In steady state, the RTECs have approximately 1% baseline proliferation [50] [51]. At the onset of injury, however, the rate of cell cycle increases dramatically to replace the large number of lost cells due to necrosis and apoptosis [38] [52]. The enhanced population of RTECs are derived from surviving RTEC population that dedifferentiate, migrate along the basement membrane, proliferate and re-differentiate [53] [54] [52](Figure 4E,F). The differentiation process involves re-expression of mesenchymal genes normally expressed during development but silenced in developed kidneys, such as *Neural cell adhesion molecule* (*Ncam*) and *Vimentin* (*Vim*) [55] [56] [57] [58] [59] [60] [61]. RTECs also express *Sox9* and *Pax2*, which are developmentally critical genes for embryonic PT differentiation. During divisions, RTECs that co-expressed Kim-1, Vimentin, Sox9, Ki67 expand clonally, suggesting that a population of injured, dedifferentiating cells enter cell cycle and expand to repopulate the epithelium [62] [52]. The question still remains whether a select subpopulation of regenerative cells exists or all RTECs have the ability to stochastically initiate the repair [63] [55].

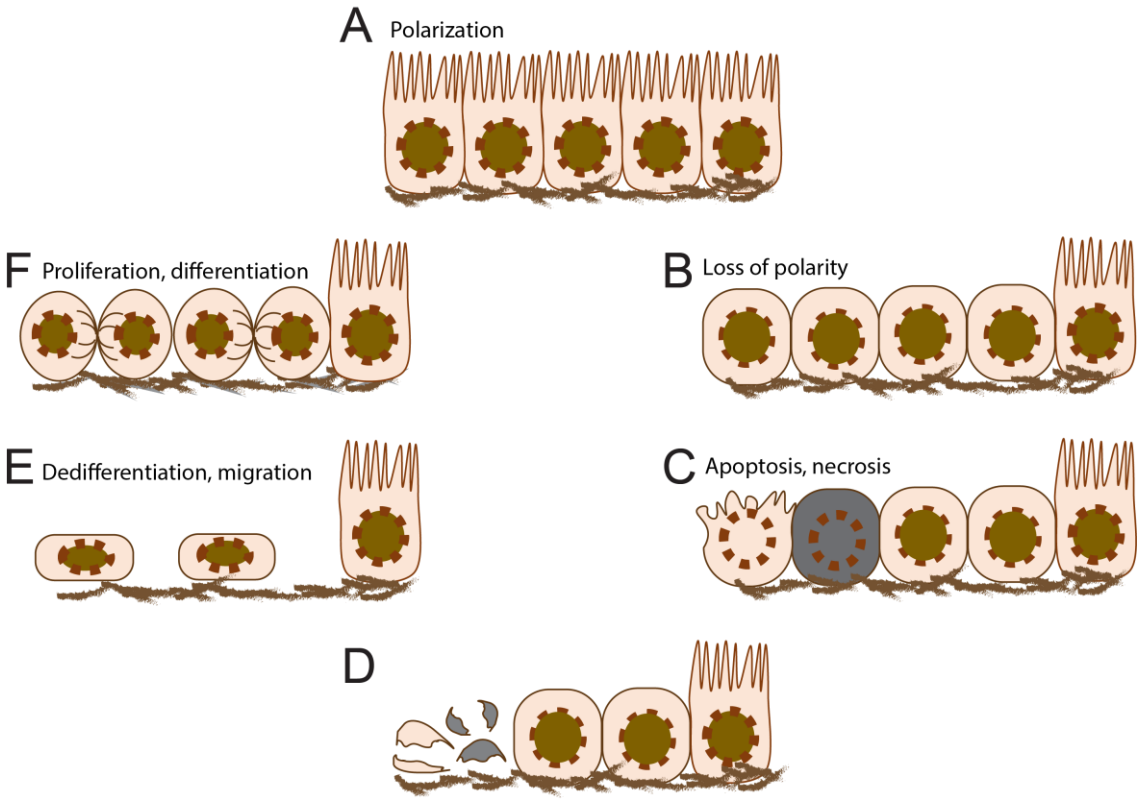

Figure 4. RTEC cellular pathophysiology during AKI

(A) Healthy, polarized proximal tubule RTECs express polarity-specifc proteins, such as basolateral Na^+K^+ATPase, adheren junction, and tight junction. (B) Upon injury to the PT, the cells initially lose epithelilal polarity, resulting in mispolarization of proteins mentioned above. (C) Cells undergo apoptosis (beige cell) necrosis (grey cell), expression of injury and inflammatory molecules such as Kim-1. (D) Cells delaminate off of the basement membrane (brown streaks) (E) Remaining cells undergo epithelial-mesenchymal-transition and reactivate developmental genes (flattened cells) such as Pax2, Sox9. (F) The reactivated cells proliferate and repopulate the damaged epithelium, expressing Ki67 or PCNA and redifferentiate into polarized epithelium

1.2.3.3 Maladaptive repair

It has been reported that only 26.6% of patients with an incidence of AKI will have sustained recovery [32]. On the other hand, a large percentage of patients with AKI progress to a worsened, irreversible condition such as CKD or ERSD [32]. This epidemiological study suggests that success of kidney repair is variable. The maladaptive repair is the result of a severe injury that

presents with marked inflammation and fibrosis [64] [65]. As such, there needs to be a deeper understanding of the molecular mechanisms that contribute to maladaptive repair. There are two cell types that undergo great transcriptional changes during AKI that contribute to the irreversible damage: the innate immune system and RTECs [66] [67] [36] [20]. The proceeding sections will expand further on RTECs and the innate immune system in the kidney and its roles in AKI and repair.

RTECs play a heavy role in maladaptive repair by enhancing their pro-fibrotic factor expression, prolonged mesenchymal state, and prolonged interactions with the immune system. Injured cells express and secrete cytokines that will alert and recruit the innate immune system, such as monocyte chemotactic protein (Mcp-1), Tumor Necrosis Factor α (Tnfα), Tissue Growth Factor-β-1 (Tgfβ-1) [67] [68]. This innate injury response is further exacerbated by cell cycle arrest. It has been shown RTECs that are arrested at G2/M phases of the cell cycle increase expression of profibrotic factors, Tgfβ-1, Connective tissue growth factor (Ctgf), and Platelet-derived growth factor b (Pdgf-b) [68]. These factors enhance innate immune system activity and induce autocrine and paracrine effects on nearby RTECs. Tgfβ-1 drives epithelial to mesenchymal transition (EMT), a process that allows a polarized RTEC interacting with basement membrane in steady state, to undergo a transcriptional change to a mesenchymal phenotype [69]. The mesenchymal cells gain heightened migratory capacity, invasiveness, and production of ECM components [69]. The mesenchymal cells, as they sustain their profibrotic response, fail to differentiate and contribute to tubular atrophy [70] [71]. Studies have shown sufficiency and requirement of RTEC-specific Snai1 and Twist, two mesenchymal transcription factors, to worsen interstitial fibrosis and inhibit normal polarity and repair of the epithelium in mouse ischemia- reperfusion injury AKI (IRI-AKI) [72,73]. EMT is also associated with RTEC cell cycle arrest. With Snai1 and Twist expression, the cells were more likely to undergo G2/M arrest [72] [73]. Conditional deletion of the two transcription factors

resulted in less cellular arrest in the mouse kidney and cell culture system [72] [73]. Another model has shown that Snai1 modulates various cyclins and checkpoint proteins to induce cellular arrest [74].

1.3 Cell cycle behavior during AKI

1.3.1 Cell cycle components

RTEC cell cycle has gained interest as an early detectable biomarker of injury over markers that manifest after injury has gone too far [41] [47]. However, cell cycle dynamics and their effect on repair mechanisms in RTECs is not yet been completely understood. In eukaryotic cells, cell cycle is categorized into four phases, G1, S, G2, and M. Each phase is distinguished by specific molecular markers, cyclins, cyclin-dependent kinases (CDKs), and cyclin-dependent kinase inhibitors (CKIs) that regulate progression through the four phases [75] (Figure 5). G1 starts with cellular growth, mRNA synthesis, and protein translation that is important for future cellular duplication [75]. S is marked by DNA replication, in which cells become increase their DNA from 2n to 4n, wherein *n* depicts the haploid DNA content of the genome [75]. G2 is the second growth phase, marked with heavy protein synthesis for the cell to undergo division or M, mitosis [75]. In M, the cell divides into two daughter cells. This phase is further subdivided into prophase, metaphase, anaphase, telophase, and cytokinesis.

There are three major proteins that regulate entry into the cell cycle. Phase-specific cyclins (A, B, D, E) are upregulated in expression during their corresponding phase [75] (Figure 5). Cyclin-dependent kinase (CDK) expression is less variable during phases, but their activity is dependent on interactions with phase-specific cyclins [75] (Figure 5). Phase-specific coupling of cyclins and

CDKs then activates downstream transcription of cell cycle related genes through a cascade of phosphorylation events of downstream target factors. In order to avoid errors in DNA replication or resolve DNA damage, cells utilize a braking mechanism to repair prior to division. This negative inhibition of cell cycling is controlled by the third type of modulator, phase specific CDK inhibitors (CKI). The CKIs are classified into two separate groups based on their targets: Inhibitors of CDK4 (INK4) and CDK interacting protein/Kinase inhibitory protein (CIP/KIPs) [75] (Figure 5). INK4 proteins inhibit CDK4 and thus inhibit the CDK4/6/cyclin D complex. CIP/KIPs exhibit a wider activity against other cyclins/CDKs [75] (Figure 5).

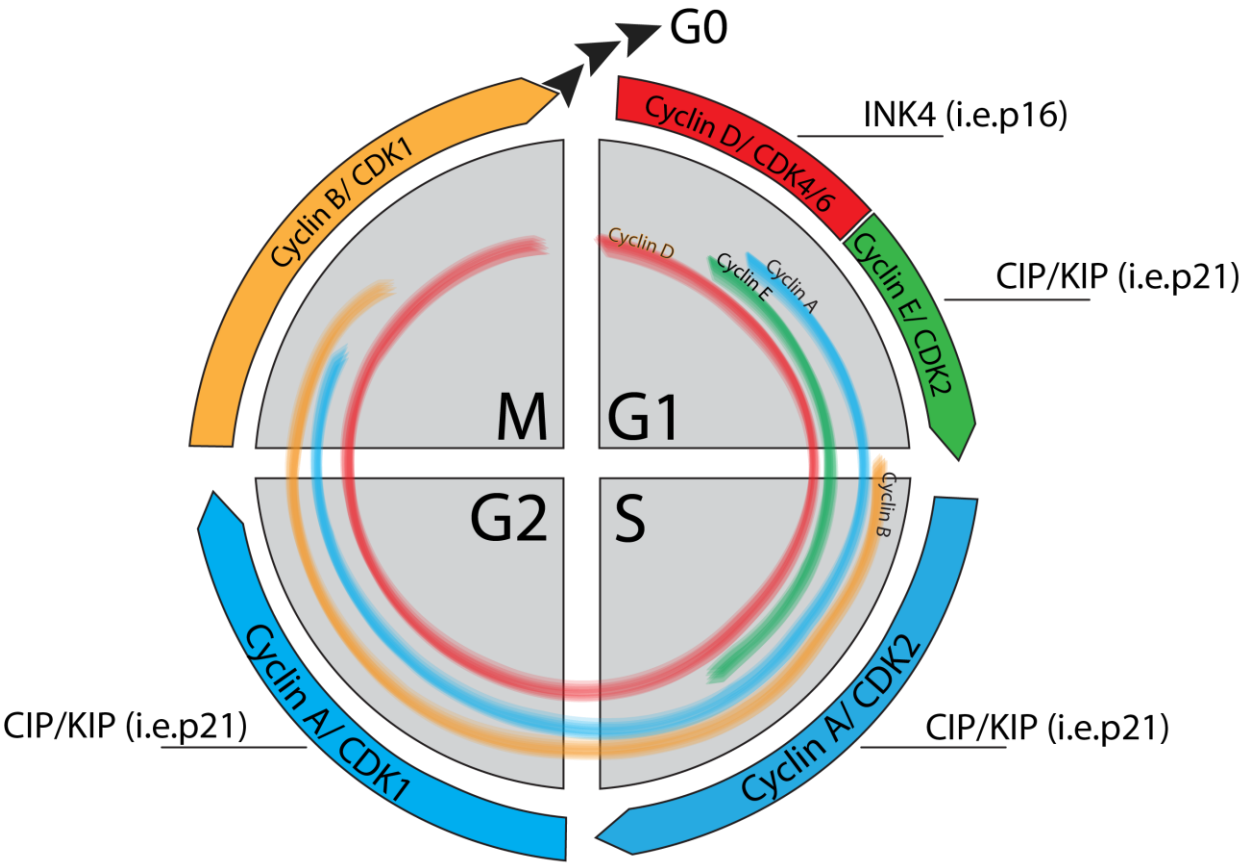

Figure 5 Cell cycle and associated cyclins, CDKs, and CKIs

The schematic of 4 cell cycle phases, G1, S, G2, M (grey). Each phase is regulated by cycle specific activation of Cyclin/CDK complexes (red, green, blue, orange arrows), which then have downstream phosphorylation and transcription cascades required to transition to the next phase. Cyclin expression is relatively unchanging (red, green, blue, orange lines) but the presence of CDKs are cell cycle specific. Upon damage, they are inhibited by CKIs (black text). G1 transition requires coupling and activation of CyclinD/ CDK4/6 (red) and subsequent Cyclin E/ CDK2 (green). This checkpoint can be inhibited by CKIs INK4 and CIP/KIP family proteins. S transition requires coupling and activation of CyclinA/ CDK2 (blue). This checkpoint is inhibited by CKIs, CIP/KIP. G2 transition requires coupling and activation of Cyclin A/CDK1 (blue). This checkpoint is inhibited by CKIs, CIP/KIP. M phase is regulated by Cyclin B/ CDK1 (orange) and are inhibited by CIP/KIP.

1.3.2 RTEC cell cycle under injury

RTECs undergo a tightly regulated cell cycling mechanism. During steady state of a mature kidney, most cells rest at G_0 and about 1% of the cell population will actively enter cell cycle to replace cells undergoing apoptosis or delamination via filtrate movement [76] [50] [75]. In the setting of injury however, cells undergo active cycling and some become arrested by CKIs until repair occurs [75]. In experimental models of AKI, including ischemia reperfusion injury (IRI-AKI), aristolochic acid (AA-AKI) and gentamicin (gent-AKI), RTECs undergo DNA damage [67]. DNA damage response (DDR) complexes are initial complexes that recognize DNA breaks and activate a downstream phosphorylation and transcriptional cascade to repair DNA. The two main DDR proteins are Ataxia telangiectasia mutated (ATM) and/or Ataxia telangiectasia and Rad3-related protein (ATR). They trigger downstream phosphorylation and transcription cascades that ultimately result in either apoptosis, necrosis, G2/M, or G1/S arrest.

In DNA damage response, DDR factors activate CKI and induce arrest. Depending on the phase of arrest, G1, S, or G2, DDR factors interact with different cell cycle-specific factors and result in different gene profiles and variable recovery outcomes (Figure 6). Specifically, in G1, ATM recognizes the DNA break and phosphorylates the adjacent histone variant H2AX (γH2AX or p-H2A.X), which then recruits other repair factors to the DNA break [77]. At the lesion, ATM and Checkpoint kinase 2 (Chk2) are turned on to stabilize p53, which then induces transcriptional activation of a CKI, *p21* [78] (Figure 6). DNA damage induces p21 expression and it serves as the main brake from transitioning from G1 to S [79]. During G1/S transition, cells express a series of Cyclin/ CDK coupling checkpoints, initiated by Cyclin D/ CDK4/6, then Cyclin E/ CDK2 [79] (Figure 6). These Cyclin/CDK complexes bind to p21 during injury, thereby halting the progression from G1 to S [79].

In G1, the cell cycle recovery, or release from G1 to S, is reversible [78]. In G1 arrested cells, p21 imposes a cell cycle arrest by simply preventing the accumulation of Cyclin E/Cdk2 [78] (Figure 6). This step can be reversed by a phosphatase that deactivates cell cycle inhibitor components, which then allows re-accumulation of Cyclin E/ Cdk2 and a reversible transition to S-phase [78] (Figure 5). This may be a reason why G1 arrest in the kidney has a positive effect during injury. In the kidney, halting G1 progression to S in the injury setting appears to result in a positive repair response. G1/S arrested RTECs expressed higher p21, followed by enhanced RTEC proliferation and AKI recovery [67] [47]. Other means of G1 arrest such as pharmacological inhibition of CDK2 resulted in less severe nephrotoxicity [80]. Pharmacological inhibition of CDK4/6, another checkpoint protein for G1/S transition, also resulted in enhanced repair [81] [82] [83]. Conversely, *p21*-deficient mice show more cells entering cell cycle due to unregulated checkpoints but ultimately result in more damage after injury due to unregulated cell division cell death [84] [85]. Together, these results suggest that G1 induced arrest and increase in p21 activity enhance recovery by preventing propagation of genetic defects and preserving bio-energetically insufficient resources during duress of an injury [47].

During the G2 arrest, the checkpoint is regulated by Cyclin A/CDK1 and Cyclin B/CDK1 to assess whether the DNA replication and damage is resolved prior to cellular division [75] (Figure 5, Figure 6). In G2, damage is recognized by ATM, Chk2, ATR, and Chk1 and these factors stabilize p53 and activate p21. This DDR cascade results in inhibition of CDK1/Cyclin B [78] (Figure 6). Additional mechanisms of G2/M inhibition are p38 and TGF-β, which also induce p21 activation [86] (Figure 6).

Cell cycle recovery from G2 to M is less likely. Compared to G1 arrest, p53 and p21 have additional functions in G2 arrest. In G2 arrest, p53 and p21 also drive transcriptional repression

and degradation of pro-mitotic genes and proteins, such as *Cyclin A*, *Cyclin B1*, and Plk1[78]. Lacking such pro-mitotic transcripts and proteins prevents cell cycle recovery, or resumption of the normal cell cycle [87] [88] [89] [90]. Cells that retain G2 DNA profile but lack G2/M protein due to premature degradation are then committed to irrecoverable arrest and cellular senescence, secreting inflammatory cytokines, such as IL-1α, IL-1β, IL-6, IL-8, MCP-1, CCN2, and TGF-β1 [91] [92] [93] [88] [94] [90]. G2/M arrest is associated with poor prognosis of AKI, suggesting the negative role it plays in maladaptive repair, potentially due to irrecoverable cell cycle arrest [71] [67] [95]. RTECs arrested at G2/M have shown a significant increase in the production (?) pro-fibrotic growth factors, such as TGF-β, Collagen 1, and CTGF [67] [96] [97] [98]. As discussed above, p21 protects RTECs from AKI in less severe models of AKI [99] [100] [85]. However, as shown by the G2/M irrecoverable arrest, p21 serves a dual purpose in RTECs [95]. In a more severe injury model of AKI to CKD, p21 expression is detrimental as *p21*-loss of function mice showed enhanced renal repair [84]. Overall, the G1 and G2 phase arrests are functionally distinct and have different implications for cell cycle recovery and survival following the induction of arrest.

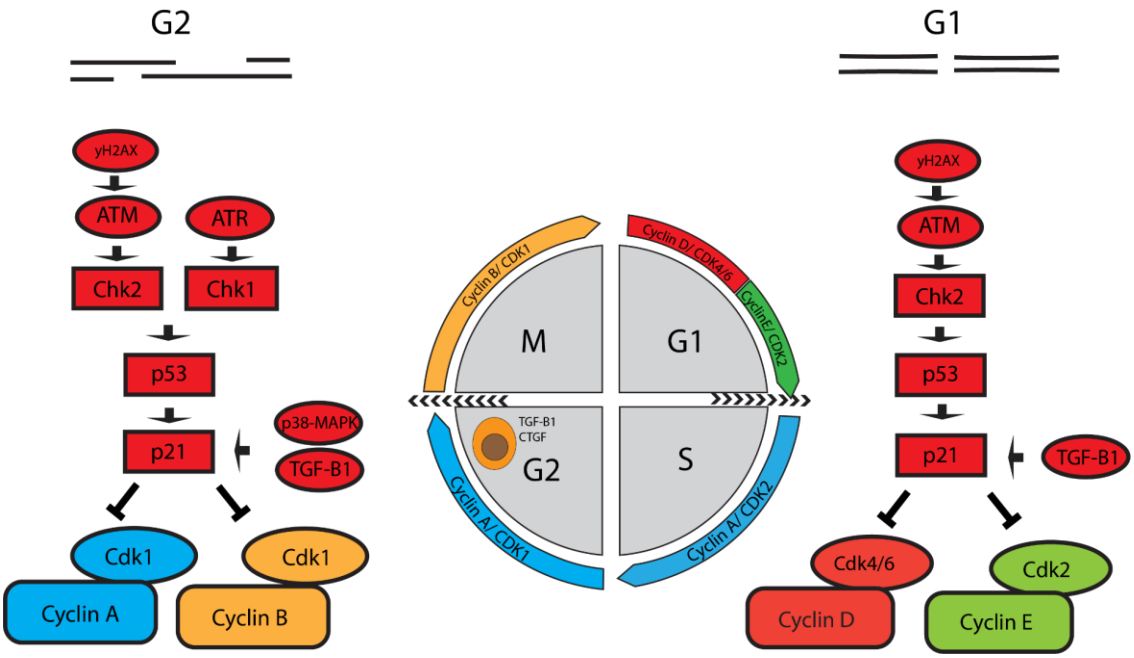

Figure 6 DNA damage signaling in G1 and G2 arrest

DNA damage response pathway varies between cell cycle due to presence of cell cycle machinery available during each checkpoint. In G1, ATM and yH2AX are activated. This allows further cascade of, Chk2, p53, and p21 activation that ultimately inhibits Cyclin D/ CDK4/6 and Cyclin E/ CDK2. In RTECs, non-DNA damage stressor can also induce arrest, such as TGF-β, which also enhacnes transcription of p21 via unknown mechanisms. In G2, ATM and its downstream cascade is also active. Additional DDR in G2 is ATR, which activates Chk1, p53, p21. In RTECs, non-DNA damage stressors induce arrest, such as p38-MAPK and TGF-β. They both enhance transcription of p21.

1.4 Innate immune system activation in AKI

1.4.1 Macrophages

1.4.1.1 Origin and function

After the initial insult to kidney tubules, both the damaged tubular cells and recruited immune cells release inflammatory factors. This initial damage response is critical for regenerative

capacity of the kidney, as well as other organs. Various models of AKI (i.e. sepsis, ischemia, nephrotoxins) all converge at a similar inflammatory response: increased expression of Damage-Associated Molecular Pattern (DAMPs), Toll-like Receptors (TLRs) from damaged tubular cells. This response acts as a signal to recruit leukocytes, macrophages and neutrophils serving as the first line of defense. Macrophages were once viewed as a single population of phagocytic cells derived from one lineage from the bone marrow [101]. However, later studies delineated two distinct lineages from which macrophages originate: embryonic and bone marrow-derived macrophages [102]. These two populations have varying roles not only during mammalian embryonic development, but also in response to injury in adults. In injury setting, the various lineages of macrophages play complex roles in injury response and resolution. In the ensuing sections, we will outline the various macrophage lines and their respective roles during development as well as during injury settings.

The first population, known as embryonic macrophages, expresses the *PU.1* transcription factor gene and is derived from hematopoietic stem cells within the yolk sac during embryonic development. Later in development, HSCs migrate from the yolk sac to the bone marrow, which then becomes the main site of hematopoiesis in mammals. The embryonic macrophages function in innate immune protection and regulate fetal architecture by promoting vascularization, clearing apoptotic cells, supplying cellular matrix components (laminin, type IV collagen, and proteoglycans), and providing cues for RBC maturation [103]. Another crucial function for embryonic macrophages is to migrate to sites of developing organs and mature into various types of tissue-resident macrophages, such as the Kupffer cells in the liver. In each organ, resident macrophages have specific roles to maintain the steady state, including clearing cells undergoing apoptosis and engulfing cells to remodel tissue architecture during development. Over the course

of organism's life, resident macrophages self-replenish and carry out immunosurveillance and organ-specific functions [104].

With the onset of injury, the resident macrophage population is aided by the second lineage: the bone marrow-derived macrophages[104]. Both resident and recruited bone marrow-derived macrophages assume different phenotypes over the course of injury to initiate and prolong inflammation, increase phagocytosis, promote other immune cell recruitment, and ultimately resolve injury[104]. The ensuing sections will review known contributions of macrophages in each step of injury and resolution, as well as currently known pathways responsible for each macrophage subtype.

1.4.1.2 Activation during AKI

Much of our understanding of macrophage polarization in the AKI setting has been derived from injury models that recapitulate a few prevalent subtypes of AKI in human population. While various methods converge on damaged and dying RTECs, each source of damage exerts distinct initial damage to the kidney and thus different initial immune response. In IRI-AKI, endothelial cells are the first responders to the injury, immediately displaying signs of vasoconstriction expressing Endothelin-1, Angiotensin II, thromboxane A2, and adenosine [105] [106]. They directly stimulate leukocyte migration to the kidneys by increasing expression of ICAM-1, and the rest of the adhesion cascade, allowing endothelium-leukocyte interaction [38]. In turn, lack of oxygen results in the neighboring RTECs expression of DAMPs and Hypoxia-inducible-factors (HIFs) [107]. The RTEC response accompanied by increased vascular rarefaction results in facilitation of leukocyte migration and the initiation of early inflammatory response in the interstitium within 24hrs of injury [108]. Conversely, nephrotoxic AKI directly targets RTEC. Cisplatin, a widely used chemotherapeutic reagent, can bind to transporters such as Ctr1, OCT2 to translocate into RTECs

and induce DNA damage and inhibit protein synthesis [109]. Cisplatin also plays a direct role in macrophage phenotype even when they are isolated from the kidneys. An *in vitro* study of cisplatin administration on murine peritoneal macrophages significantly increased pro-inflammatory cytokines and nitric oxide (NO) expression via the MAP kinase (MAPK) pathway [110]. While this may explain the high injury severity typically associated with cisplatin-AKI, whether this is true *in* situ and is the cause of high cellular damage has not yet been concluded. Overall, not many studies compare macrophage responses among various models of AKI. Further elucidation of polarization mechanisms may lend insights into repair pathways unique to each subset and improve personalized therapeutics. The ensuing sections cover what is known to date, research mostly conducted in IRI-AKI.

With the onset of injury, damaged RTECs release DAMPs and in sepsis AKI, pathogen-associated molecular patterns (PAMPs), which act as an initial injury signal to sentinel immune cells within the tissue, such as resident macrophages and dendritic cells. Macrophages recognize the initial damage signals through pattern recognition receptors (PRRs), a family of receptors that recognize DAMPs and PAMPs. Recognition of DAMPs and PAMPs via PRRs results in downstream stimulation of macrophage phagocytosis, phagolysosome maturation, antigen presentation, and production of TNFα [111]. These are important factors for further stimulation of innate immune system.

After the initial recognition of injury, resident macrophages further prolong inflammation by recruiting other leukocytes to the site of injury. Among those recruited are neutrophils, bone marrow-derived monocytes and macrophages, and lymphocytes. Macrophage-derived chemokines and cytokines target different stages of leukocyte migration to increase recruitment. For example, TNFα, IL-1β, and histamines stimulate endothelial cells to increase expression of trafficking

molecules (selectins, integrin ligands), whereas chemokines CXC1, CXCL2, and CCL2, directly recruit neutrophils to extravasate from the circulatory system into the interstitium [112]. The initial inflammatory macrophage events are subsequently followed by modulation and then inhibition of the inflammatory response. This phenotypic change, termed as macrophage polarization, occur via tissue-specific, complex pathways and will be delineated in the ensuing sections.

1.4.1.3 Macrophage polarization

The initial tissue macrophage and dendritic cell responses promote further inflammation via recruitment of other pro-inflammatory immune cells such as monocytes and bone marrow derived macrophages. Although derived from the bone marrow, monocytes and macrophages migrate and maintain a stable population in the spleen, a peripheral lymphoid organ that responds to injury signals and readily dispatches immune cells to the site of injury [113]. The recruited monocytes differentiate into macrophages and dendritic cells at the site of injury. The recruited macrophages acquire a wide spectrum of phenotypes, from highly inflammatory to highly reparative and anti-inflammatory, as well as many intermediates. Traditionally, macrophages have been generally categorized into two populations: Inflammatory macrophages, called M1 or classically-activated, and anti-inflammatory macrophages called M2 or alternative macrophages.

At the onset of injury, recruited macrophages become activated by LPS (under sepsis AKI), IFNγ, and GM-CSF released from the damaged microenvironment [114]. In the kidney, M1 specific cytokines increase in expression within the first 24 hrs post injury and significantly decrease at 3 days post injury [115]. Upon activation, M1 macrophages secrete inflammatory cytokines such as IL-1β, TNF, IL-12, IL-18, and IL-23 [116] (Figure 7). As a result of these inflammatory cytokines, the site of injury continues to gain other inflammatory cells, including T helper cells [114]. The M1 macrophages also secrete molecules for destruction of pathogenic particles such as nitric oxide

generated by inducible nitric oxide synthase (iNOS). Once pathogens or damaged cells are cleared, a rapid change in macrophage polarization is necessary to stop further damage to surrounding undamaged cells. Prolonged activation of inflammatory macrophages has negative effects in injury recovery, since the released cytotoxic agents do not discriminate self from pathogenic particles [117,118].

Various experimental models have concluded that prolonged inflammatory macrophage activation imposes negative consequences in injury resolution due to excessive inflammation. A study in the cardiovascular field reported that atherosclerotic lesions with a higher number of inflammatory macrophages correlated with higher likelihood for sudden major cardiovascular ischemia [119]. In the kidney, perdurance of activated macrophages contributes to worse outcome after renal ischemia. Clodronate-induced depletion of all macrophages and then subsequent transplantation of IFNγ-stimulated M1 macrophages prior to renal ischemia resulted in more severe tubular damage [115]. Furthermore, depletion of macrophages before injury reduced blood urea nitrogen levels and post-injury histological markers of tubular injury, whereas depletion during reparative stage resulted in significantly worsened injury markers [120]. Taken together, these studies suggest that while the initial inflammatory response from macrophages is necessary for removal of damaged and pathogenic particles, prolonged inflammatory activity results in further tissue damage, ultimately inhibiting the reparative phase for injury resolution.

M2 macrophages do not become activated until later in the initial injury phase. In an experimental IRI-AKI, an increase in M2 markers is observed at 3dpi, peaking in expression at 7 dpi [115]. M2 macrophages originate from newly recruited monocytes dispatched from the circulatory system, as well as initially recruited M1 macrophages [121]. The phenotypic conversion from monocytes and M1 macrophages to M2 macrophages requires specific cytokine stimulation

and subsequent transcriptional changes. M2 macrophages are activated by macrophage- colony-stimulating factor (M-CSF), IL-4, IL-10, IL-13, and TGF-β [114] (Figure 7). Upon activation, M2 macrophages overexpress mannose receptor (MR), a receptor that will recognize and downregulate high levels of inflammatory glycoproteins previously produced by the inflammatory response [122]. M2 macrophages also produce Arginase, an enzyme necessary to produce ornithine and polyamine, both building blocks for extracellular matrix architecture. Furthermore, M2 macrophages secrete resolvins, lipoxins, TGF-β, and Matrix metalloproteinases that target and cleave chemokines and chemoattractants, resulting in inhibition of inflammatory immune cell activity [112]. Over the past decade, alternative macrophages have been categorized into four subtypes based on their *in vitro* upstream activators and downstream gene expression patterns [123]. M2a are activated by IL-4, IL-13, M2b are activated by IL-1, LPs, M2c are activated by IL-10 and TGF-β, and glucocorticoids, and M2d are activated by IL-6 and adenosine [123]. Currently, only a few studies have investigated the origin of each subset using *in vivo* models and have described each subtype's role in injury resolution.

1.4.2 Neutrophils

1.4.2.1 Origin and function

Neutrophils arise early during development in a process called granulopoiesis. During granulopoiesis, hematopoietic stem cells (HSCs) invade the liver and produce erythro-myeloid progenitors (EMPs), which then differentiate into neutrophils during embryonic development [124]. In later development phase, HSCs and EMPs migrate to bone marrow and continually generate neutrophils and other granulocyte lineages throughout adulthood [125]. During steady state, differentiated neutrophils migrate in the circulation at a steady state of 40μm/s [126]. They will

circulate and phagocytose cellular debris under steady state conditions by generating reactive oxygen species and matrix-modifying granule enzymes [127]. Mammalian neutrophils consist the largest percentage of the white blood cell population, but they turn over quickly as the senescent neutrophils are cleared out by lymphoid organs such as the liver, spleen, and bone marrow [128].

1.4.2.2 Activation in AKI

In steady state, neutrophils travel in a slow-rolling motion in the circulatory system. However, at the onset of injury, they are able to recognize adhesion molecules expressed in endothelial cells during injury. Upon recognition of the injury-related integrins, neutrophils undergo a stepwise cascade of migration, ultimately migrating to the specific site of injury. The four phases must be activated in a stepwise fashion in order for normal neutrophil adhesion and infiltration. First, neutrophils are tethered and begin slow-rolling following interaction with specific selectins expressed by endothelial cells near the site of injury. Neutrophils express P-selectin glycoprotein ligand-1 (PSGL-1), which reduces migration and allows more time for interaction with P-selectin expressed by endothelial cells. Second, upon activation of slow-rolling phase, neutrophils further increase affinity to endothelial cells by increased expression of platelet endothelial cell adhesion molecule (PECAM). This integrin interaction stimulates the firm adhesion of neuthrophils to the endothelial layer, which is required for effective extravasation from the circulatory system into the specific site of injury. Third, the final, neutrophil migration occurs along a gradient of chemokines and cytokines that are secreted by parenchymal and immune cells already present at the site of injury. Tissue-resident dendritic cells and macrophages, produce chemokines and cytokines (CXCL1, CXCL2, TNFα) [129] [130], platelet activating factor, and complement fragments, allowing controlled and localized neutrophil migration [126]. After the final migration step, the neutrophils are activated by a wide panel of factors released by a many cells:

mesenchymal stem cells, T cells, B cells, natural killer cells, macrophages, and dendritic cells. Together, the mesenchymal stem cells and various immune cells release five major types of cytokines: granulocyte-colony stimulating factor (G-CSF), granulocyte-macrophage colony-stimulating factor (GM-CSF), TNF, and Type I and II Interferons (IFN) [131]. Upon activation, neutrophils increase production of effectors such as lytic enzymes, antimicrobial peptides, and neutrophil extracellular traps [131]. Aside from the classically known effectors, neutrophils have recently been described to produce various cytokines that feedback on the other recruited immune cells. They produce CXC-chemokines, CC-chemokines, pro-inflammatory and anti-inflammatory cytokines, immunoregulatory cytokines, CSFs, angiogenic and fibrogenic factors, and TNF superfamily. Interestingly, *in vitro* data suggests neutrophils interact with monocytes and macrophages to inhibit their activation [132,133]. However, *in vivo*, neutrophils may be indirectly stimulating macrophage activation by stimulating other immune cells, such as NK and T cells.

Aside from influencing the function of other immune cells, neutrophils directly control the inflammatory reaction. Outside of the well-known inflammatory activity, recent studies have revealed a passive anti-inflammatory role neutrophil play towards the end of acute injury phase. During the final phases, neutrophils switch from the inflammatory eicosanoid leukotriene B4 biosynthesis to the anti-inflammatory eiconsanoid (lipoxin A4). Neutrophils also synthesize resolvins and protectin D1, which are pro-resolving mediators that block neutrophil transendothelial migration and infiltration [131]. More recent studies have identified neutrophil-derived microvesicles that contain anti-inflammatory cytokines, such as TGF-β. However, these mechanisms are not sufficient for wound resolution- the neutrophil population must remove itself in order for further healing to occur. Neutrophil resolution usually occurs via efferocytosis, neutrophil apoptosis, or reverse track back to circulation [134 135 136] . Inhibition of each of these anti-

inflammatory mechanisms resulted in prolonged inflammation as well as poor injury resolution[137] [138].

Like other wound healing models, neutrophils migrate to the site of damage after AKI in rodents and zebrafish. In various tissue injury settings, high neutrophil infiltration exerts negative consequences in resolving injury [139]. Neutrophil specific secreted factors are correlated with worse prognosis. For example, high urinary NGAL-1 acts as a biomarker for worse prognosis in patients diagnosed with AKI [140]. Recently, various studies focused on targeting neutrophil-associated pathways to inhibit inflammation during AKI and other injury models. For example, targeting factors important for neutrophil migration and activation (TLR2, TLR4, and Myd88) protected renal function and less inflammation in mouse model of sepsis [141]. Neutrophil inhibition to injury sites limits exposure to phagocytosis, degranulation, oxidative burst, and cytokine production. Furthermore, neutrophils are precluded from recruiting further pro-inflammatory innate and adaptive immune cells. Some studies further explored whether improved regeneration is due to lowering neutrophil-derived inflammatory cascade. For example, Kimura *et al*. investigated the effects of neutrophil-derived IFN-γ, a pro-inflammatory cytokine, in repair after cisplatin-induced kidney injury. Mice with neutrophil-specific knockdown of IFN- γ showed improved repair by promoting RTECs autophagocytosis rather than prolonging inflammatory cytokine production [142].

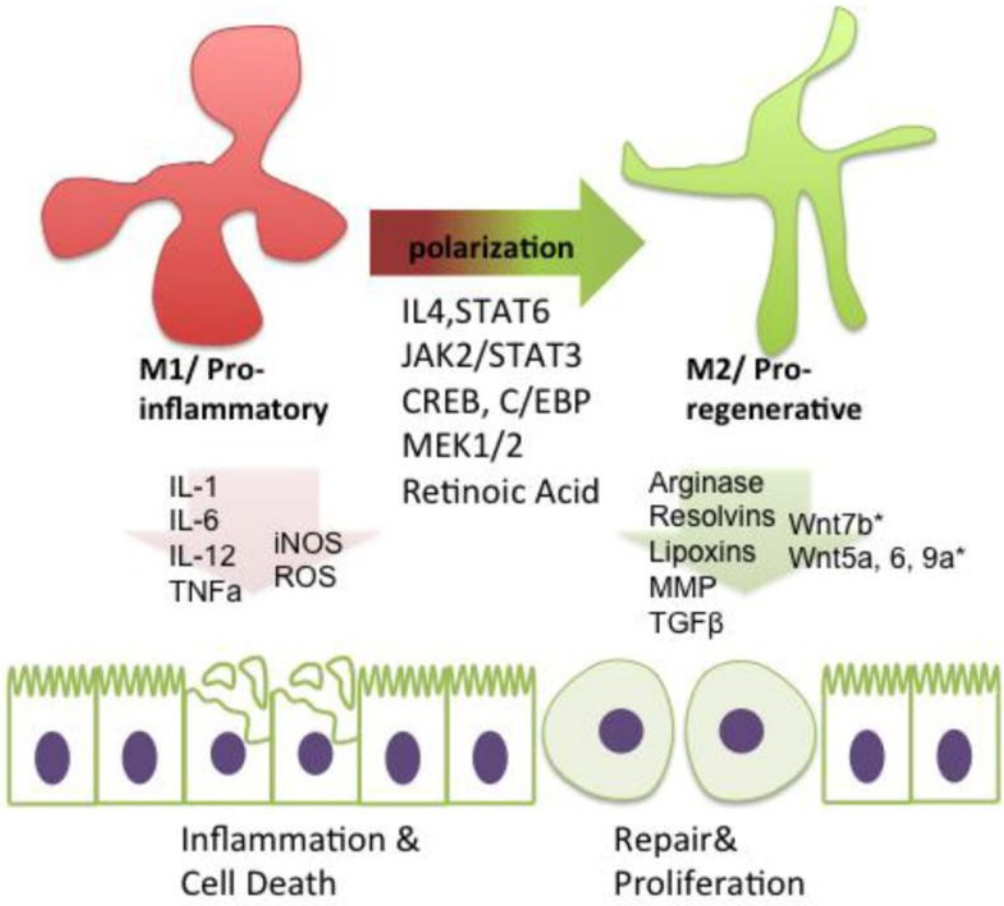

Figure 7 Various pathways identified for macrophage polarization

Experimental studies of several pathways have elucidated critical pathways for driving macrophage polarization from M1 to M2. Among them are IL-4/STAT6, JAK2/STAT3, CREB/C/EBP, and MEK1/2. Each macrophage phenotype has signature expression of certain cytokines and secreted products. M1 macrophages secrete inflammatory cytokines and products and chemoattractants, such as: IL-1, IL-6, IL-12, TNFa, iNOS, and ROS. M2 macrophages secrete anti-inflammatory cytokines and pro-reparative secretions such as: Arginase, Resolvins, Lipoxins, Matrix metalloproteinases, TGF-β, and Wnt ligands. *There seems to be tissue-specificity to types of Wnt ligands secreted, specifically Wnt7b in kidney macrophages and Wnt5a, Wnt 6, and 9a in intestinal macrophages.

M2 macrophage subsets are under scrutiny for both their ability to curtail inflammation before inducing further damage, as well as for their inherent reparative abilities. Saha *et al.* demonstrated that macrophages are crucial for normal repair after an acute injury to the intestines. The post-injury intestinal stem cells required macrophage-derived extracellular vesicles for increased proliferation and repopulation of damaged cells. The Wnt ligands, Wnt5a, Wnt6, and Wnt9a, were the main factors encased in the vesicles driving the repair [143]. In lung injury, MAPK1/2 inhibition resulted in an increased M2 population, leading to better recovery weight and increased macrophage efferocytosis of inflammatory cells [144]. In accordance with the preceding study, post-AKI repair also requires macrophage-derived Wnt for normal kidney repair. Lin *et al.* reported that kidney specific macrophages secrete Wnt7b, a canonical Wnt ligand. In depleting kidney-specific Wnt7b, the study showed Wnt7b is necessary for improved tubular repair, reduced fibrosis, and bypassing G2/M cell cycle arrest [145].

1.5 Zebrafish as model organism

1.5.1 General strengths of zebrafish

The zebrafish (*Danio rerio*) has served as a very powerful tool for studying vertebrate biology, ranging from development, drug screening, to genetics. Over simpler models such as yeast and cell culture, zebrafish offers more complex vertebrate specific organs such as the kidney. With over 70% of the human genome conservation, the zebrafish genome annotation identified more than 26,000 protein-coding genes, as well as conservation of epigenetic processes such as DNA methylation, histone acetylation, non-coding RNAs [146] [147]. In contrast to more complex models

such as mice, the zebrafish offers visual access to *ex utero* development, less space and maintenance requirements, and high fecundity and short developmental time that allows high-throughput studies [148] [149]. Ultimately, zebrafish as a model organism contributed to large forward genetic screens that identified multiple genetic lesions contributing to previously unknown human disease syndromes [149] [150].

Zebrafish, unlike most vertebrate models, are able to regenerate their organ systems more efficiently, which makes them a perfect model for regenerative studies. While most vertebrate models have a few organs with regenerative capacity, the zebrafish can regenerate most of their organs, such as the heart, kidney, liver, fin, and spinal cord [151]. The zebrafish's regenerative capacity along with their genetic conservation to humans open possibilities for discovering mechanisms that can be applied to humans. Finally, the zebrafish community is in a constant move towards development of more advanced genetic tools. Such examples range from microinjection of constructs for successful germline transmission for transgenic fish generation, live cell lineage tracing, tissue-specific transgene expression, targeted cell ablation, heat shock inducible models, GAL4/UAS, CRE/LOXP, TETON/TETOFF, and fluorogen activating proteins technology [151] [149].

1.5.2 Larval zebrafish model of AKI

Not only is the zebrafish kidney developmentally and functionally conserved, but their response to AKI parallels that of the mammalian response. Multiple models of larval zebrafish AKI exist, including injection of nephrotoxins such as gentamicin and cisplatin, mechanical damage, and laser ablation [152]. Nephrotoxin induced AKI consist of about 14-26% of AKI cases and therefore gentamicin-induced AKI (gent-AKI) is a clinically relevant model [153]. Further, molecular hallmarks that occur in mammalian gent-AKI also occur in zebrafish [154] [155] [61]. The

injection of gentamicin into the cardiac venous sinus of 50-70 hpf resulted in edema as well as glomerular and tubular distensions and obstruction due to cell death [154] [155]. Higher number of lysosomes were detected in the RTECs, a common hall mark in mammalian models of aminoglycoside nephrotoxicity [154]. 10kDa dextran, a solute normally transported via RTECs, could no longer be filtered through RTECs post gent-AKI [154].

In addition to RTEC functional changes, our group has shown structural and molecular changes that occur in both mammalian and zebrafish models. After gent-AKI, RTECs show loss of cell polarity, as seen by changes in Na^+K^+ATPase expression pattern and structurally flattened RTECs seen by H&E staining [156]. Cells show increased death as shown by increased terminal deoxynucleotidyl transferase dUTP nick end labeling (TUNEL). Injury accompanies reactivation of developmental genes such as Pax2a and RA response elements (RARE) [157] [158]. The cell cycle was also affected, with injured RTECs showing increased population of cells that incorporate 5-Ethynyl-2′-deoxyuridine (EdU), a thymidine analog that captures cells undergoing the S-phase. This model of AKI results in between 50-80% death after about 7dpi, due to worsening renal function and systematic failure [154]. The larval model of gent-AKI offers a short but clear window of the early injury response. Therefore, this method serves as an excellent model to test candidate drug post-injury and observe their efficacy for early injury prevention.

1.5.2.1 Development recapitulation during injury

As seen in mammals, zebrafish also reactivate renal developmental genes in RTECs during AKI. First, Pax2a, is an important regulator of glomerulus and PT specification [159]. It is a DNA binding, transcription factor required for kidney development [159]. It has been proposed that Pax2 interacts with methyltranferase complexes, such as Ptip (Pax transactivation domain interacting protein) or Grg4 (Groucho-related gene4) to regulate histone methylation and subsequent

expression of various genes necessary for renal development [160] Its earliest expression is detected in the developing renal progenitor cells in the IM [159]. In zebrafish, specifically, it is proposed to inhibit podocyte formation and enhancing proximal segment specification. Lack of *pax2a* results in over-expression of *wt1a* transcripts that results in inhibition of the PT segment [161]. Without *pax2a* expression, the segments fail to become polarized, losing polarity-specific proteins such Na^+K^+ATPase that marks basolateral membrane of RTECs [161].

Another developmental pathway of interest is the RA signaling pathway. RA is important for specification of caudal and rostral segments of the zebrafish pronephros [3]. Genetic or pharmacological disruption of RA signaling in zebrafish embryos result in lack of segmentation, with preferential development of the DT over the glomerulus and PT [16 162]. Conversely, enhanced RA signaling via exogenous treatment results in preferential development of the glomerulus and the proximal tubules over distal segments [162 163 16]. Specifically, in the glomerulus, there is *in vivo* evidence of RA directly affecting its specification by activating RA receptor (RAR) and retinoid receptor (RXR) to induce *wt1a* transcription [164]. Blocking RA signaling results in prevention of two glomerular transcription factors *wt1a* and odd skipped related-1 (*osr1*) [165]. Although the developmental mechanisms and sources of RA are well delineated, the question of how RA affects the kidney regeneration in AKI setting is unclear. RA is enhanced in the PT early on during the nephrotoxin injury model within 12hpi [157]. RA activity is also observed in macrophages that infiltrate the mouse kidney [157]. Mammalian models of AKI have shown that RA treatment attenuates injury and facilitates recovery by inhibiting apoptosis in various models [166 3]. However, the source of synthesis and degradation of retinoids and how and which cell type responds to the final bioavailable RA still remains unknown.

1.5.3 Zebrafish as model organism to study innate immune response

Studies have revealed that both mammalian and zebrafish HSC share conserved mechanisms of myelopoesis during embryonic development. As in mammals, there are two waves of HSC migration and differentiation in the zebrafish, termed primitive and definitive myelopoiesis. The primitive myelopoiesis occurs between 12-48hpf, when various precursor cells initiate differentiation and produce mature cell types from mesodermal tissue along the notochord [167]. The second wave, called definitive myelopoiesis, occurs when HSC migrate and seed in the anterior segment of the pronephros. The migrated HSC remain as the definitive pool of self-renewing cells that continue to produce mature leukocytes from 4dpf larvae to adulthood [167 168]. There are key regulatory factors that are shared between mammalian system and zebrafish that allow macrophage differentiation. For example, *pu.1*, *spi-b*, and *irf8* are required for macrophage development in zebrafish as they are required for mammalian macrophage differentiation [169]

While mammalian and zebrafish myelopoiesis is conserved, very few *in situ* studies have examined zebrafish M1 and M2 macrophage markers. A recent study has shown live imaging of macrophage polarization in fin amputation, using transgenic reporter for *tnfa* and *mpeg1*, a macrophage marker [170]. While additional *in situ* studies are necessary to confirm other markers for zebrafish macrophages, there is evidence that mammalian and zebrafish polarization events are evolutionarily conserved. Many of mammalian markers that appear during macrophage polarization are orthologues upregulated in zebrafish injury settings, like pattern recognition receptors, IFN-γ, iNOS, TNFα, GM-CSF.

Acute immune response is often associated with worsened outcome in human injuries. In studying regeneration to model these injuries in fish, it is imperative to also characterize their immune response. So far, the zebrafish larvae have served an important role in characterizing

macrophage and neutrophil migration, and *in vivo* imaging of macrophage polarization[171] [170]. So far, studies have characterized specific factors required for macrophage interplay with various disease states such as myocardial infarction, fin, and liver regeneration [172] [173] [174]. Furthermore, recent fin amputation studies have demonstrated that macrophage polarization is a conserved phenomenon in zebrafish. Using a transgenic line, Nguyen-Chi *et al.* visualized by *in vivo* imaging activation and subsequent repression of pro-inflammatory (TNFα) gene in macrophages recruited to the site of injury. $TNF\alpha^{+}$ macrophage recruitment was observed as early as 1hr post amputation, while $TNF\alpha^{-}$ macrophage recruitment occurred at approximately 25 hrs post amputation. This study fully captures the advantage of utilizing zebrafish to elucidate unknown questions that have previously been deemed as difficult. The convenience of generating transgenic line paired with powerful imaging tools resulted in tracking macrophages *in vivo*, enabling characterization of M1/M2 velocity, contact frequency, and morphological changes [170]. Taken together, the zebrafish larva has the potential to serve as a good model organism to elucidate the effects of macrophages in repair mechanism.

1.6 4-phenylthiobutanoic acid (PTBA)

1.6.1 Origins of PTBA

Despite advancements in understanding AKI pathophysiology, there is still an unmet need for therapeutics for renal recovery. No targeted clinical treatments can accelerate renal recovery or decrease fibrosis. We previously identified 4-phenylthiobutanoic acid (PTBA), a novel short-chain carboxylic acid class histone deacetylase inhibitor (HDI), which is considered class I HDAC-

specific [148] [175]. The initial screening assay investigated the effect of PTBA in the expansion of embryonic renal progenitor field of zebrafish in the intermediate mesoderm of 10-somite embryos [148] (Figure 2). Upon treatment, PTBA expanded the number of *lhx1a*, *pax2a*, and *pax8* positive cells within 10-somite embryos, persisting to later stages of development after pronephric tubule development [148]. The efficacy of compounds required the presence of actively proliferating cells, as blocking cell division resulted in loss of PTBA-induced proliferation [148]. de Groh *et al.* examined the necessity of the RA pathway in expanding the progenitor cells [148]. Depletion of Rara resulted in loss of *lhx1a* progenitor pool expansion [148]. Overall, early experiments of PTBA during development suggests the compound enhances RPC population in a proliferation dependent manner and requires an intact RA signaling pathway.

1.6.2 PTBA treatment in AKI

The earlier studies on PTBA and its effect on kidney development implicated its potential strength as a therapeutic for post AKI repair. PTBA (UPHD20) was redesigned into prodrugs such as m4PTB (UPHD25), a PTBA methyl ester that is better absorbed and still metabolized into pharmacologically active form after administration [176]. Metabolism studies showed UPHD25 was metabolized into PTBA in the kidney and liver of mice and had the same regenerative capacity [176] (Figure 8). Using prodrugs, histological, functional, transcriptional responses of PTBA were quantified in various models of AKI, both in mice and zebrafish. All studies treated animals with PTBA after AKI has already occurred, a likely scenario in the clinic. Cosentino *et al*. first utilized the larval zebrafish gent-AKI in order to establish the mechanism of repair during PTBA treatment. 2 days after injury, injured fish treated with PTBA showed significantly improved survival [156]. Additional mouse studies gave further insights into long term effects of PTBA treatment. Post

injury treatment with PTBA showed lower renal fibrosis and enhanced renal function, quantified via blood urea nitrogen and serum creatinine levels. At cellular level, PTBA treatment resulted in lower Kim-1 expression, macrophage infiltration, overall reduced inflammation [177] [176].

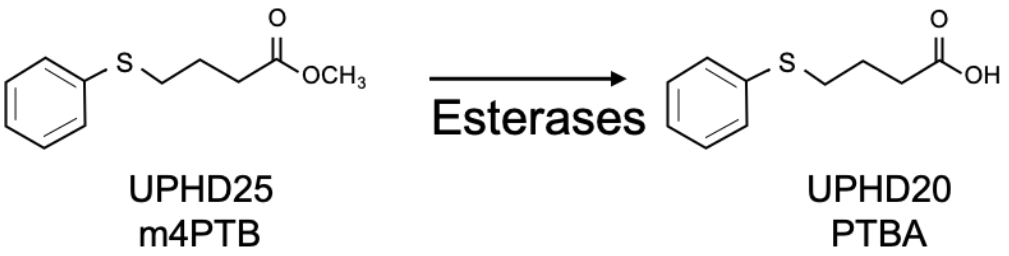

Figure 8 PTBA prodrug metabolism

Upon UPHD25 (m4PTB) treatment, the compond is metabolized by endogenous esterases, therby becoming an active parent compound, UPHD20 (PTBA). UPHD25 acts as a prodrug for more efficient delivery of the parent compound.

PTBA's target has remained elusive, but its structure suggested its role as a class I HDI [178]. PTBA's structure is characterized by: a warhead, the moiety binding zinc and inhibiting HDAC activity; linker and cap, moieties that bind to HDAC amino acid residues to contribute to selectivity [178]. Further function of the compound was validated using *in vitro* and *in vivo* assays to measure hyperacetylation of the histone H4[148] [179]. While the hyperacetylation assay narrowed PTBA's function as an HDI, its target still remained elusive as multiple HDACs affect developmental processes beyond the epigenetic mechanisms. Many HDIs are known to associate with cell cycle changes. Various class 1 HDIs are used to inhibit cell cycle. Some primary examples are Vorinostat, SAHA, class 1 HDIs, used for anti-proliferative and pro-apoptotic activity in cancer metastasis models [180]. The cell cycle dynamics were changed with PTBA treatment. Zebrafish RTECs showed increased EdU-positive cells when treated with PTBA [156]. Novitskaya *et al*. showed PTBA treatment increased the number of actively cycling RTECs and decreased phospho-

histone 3 (pH3) positive cells at 14dpi, suggesting a potential role in decreasing G2/M arrest [177]. A microarray analysis of PTBA-treated mouse kidneys revealed a decrease in cellular metabolism and an increase in cell cycle and microtubule-based processes [177]. While various HDIs are shown to modulate cell cycle, many target multiple HDACs in nonspecific ways, which can cause unwanted side effects [180]. Therefore, it is important to assess each HDAC in class 1 for their role in cell cycle modulation and clearly define their role in disease progression in the context of AKI. Taken together, these studies show PTBA enhances repair after AKI. However, the question still remains to which member of the family class 1 HDAC does PTBA bind and how the inhibition imparts its reparative capacity.

1.7 Histone deacetylase 8

1.7.1 General knowledge

HDACs are categorized into four classes, based on structural similarities, cofactor metals required to activate the enzymes, and cellular localization, ranging from class I, IIA, IIB, III, and IV. Members of class I include HDAC1, 2, 3, and 8. HDACs were originally found to deacetylate lysines of histones, acting as epigenetic modifiers. Gene expression is repressed when HDACs remove an acetyl group from a lysine, a positively charged amino acid, thereby enabling the chromatin to wrap tightly around histones and repressing gene transcription [181] [182]. Recently, HDACs have been scrutinized for their non-histone targets, driving post-translational modifications in a wide range of proteins that affect numerous cellular functions.

HDAC8 is unique in many ways when compared to class I HDACs. In humans, it is a protein of 42kDa, composed of 377 amino acids and is found in multiple organs including the heart, lung, kidney, and pancreas [183]. HDAC8 does not have the conserved c-terminus protein binding domain found in other class I members [180]. Without the conserved c-terminus binding domain, HDAC8 is the only cofactor-independent class 1 member [180]. Another unique property of HDAC8 is its localization to both the cytoplasm and the nucleus. HDAC8 associates with many different proteins, including Structural Maintenance of Chromosomes 3 (SMC3), Estrogen Receptor Related alpha (ERRα), p53, Cortactin, and Alpha tubulin [180 184]. Pathway enrichment of proteins predicted to associate with HDAC8 suggest its downstream roles in chromosomal stability, cell cycle, and cell motility [185 186]. HDAC8 has been recognized for its roles in craniofacial and neural development, and *Schistosoma mansoni* parasite locomotion [187 188 189].

1.7.2 HDAC8 in development and disease

One of the most well studied disease associated with HDAC8 is Cornelia de Lange syndrome (CdLS), a craniofacial neural abnormality attributed to cohesin dysfunction. Multiple genes are attributed to this defective developmental syndrome, including HDAC8, NIPBL, SMC3, SMC1, RAD21, which all play roles in various different aspects of cohesin-associated processes, a ring-like complex that hold sister chromatids together during the cell cycle process [190]. Cohesin is a multi-function complex that affects gene transcription, enhancer-promoter interaction, cell division, cell cycle check points. HDAC related craniofacial development mechanistic studies showed that HDAC8 can also post-transcriptionally repress downstream genes to suppress normal development of skeletal structures [182].

Although the HDAC8 expression was first discovered and characterized in the human kidney, it has recently been gaining attention as a target of interest in the field of AKI [183]. Inhibition of HDAC8 suppresses inflammatory and fibrotic responses in various models of acute injury. One example of the fibrotic response mediated by HDAC8 is AKI-related renovascular hypertension followed by cardiac remodeling, hypertrophy, and fibrosis [191] [192] [193]. Renovascular hypertension has been reported to induce specific HDACs in the left ventricle of the mouse heart, one of them being HDAC8 [191] [193]. HDAC8 expression is associated with genes linked with fibrosis, such as *Tgf-b* and *Ctgf* [191] [193]. When HDAC8 activity is pharmacologically inhibited, fibrosis is significantly lowered in the heart [191] [193] Prolonged epithelial-to-mesenchymal transition has been cited to increase fibrosis in the kidney, which results in increased expression of pro-inflammatory and fibrotic factors such as TGF-β1 and CTGF [194]. HDACs has been implicated in heightening the EMT process to fibrosis. Non-selective class I HDI such as TSA and MS-275 were used to inhibit *Collagen1* and *Fibronectin* expression while maintaining E-cadherin in HK2 cells [192]. Likewise, HDAC8-specific inhibition via siRNA resulted in suppression of mesenchymal phenotypes, Collagen, Fibronectin, and N-cadherin expression, while maintaining of E-cadherin integrity [192]. A recent study showed that RTEC-specific HDAC8 expression as a culprit for renal interstitial fibrosis [195]. In unilateral ureteral obstruction-AKI (UUO) and PT cell culture model, inhibition of HDAC8 resulted in lower fibrosis along with downregulation of EMT, G2/M cell cycle arrest, TGF-β1, Smad3, STAT3, β-catenin, and Snai1 [195].

Although HDAC8 specific mechanisms controlling EMT and fibrosis are not readily understood, pan-class I HDAC inhibitors downregulate E-cadherin by changing epigenetic environment of Id2 and BMP7, genes that are known to antagonize the fibrotic effects of TGF-β1 [196] [197]. In a model of acute LPS-induced neuroinflammation, HDAC8 acts as a culprit in

inflammatory activation. LPS induced expression of pro-inflammatory factors, such as COX-2/ iNOS, TNFα, was negated by a pharmacological inhibition of HDAC8 via WK2-16 [198]. Upstream analysis suggested HDAC8 inhibition suppressed STAT1/3/Akt activation, thereby reducing pro-inflammatory response while enhancing repair response [198].

1.7.3 HDAC8 in cell cycle and beyond

Because HDAC8 is known to have various non-histone protein targets, it would be critical to examine its roles beyond epigenetic targets. One of highly regulated processes after AKI is increased cell cycle progression and check point regulation [199] [75] [65] [95]. There have been many studies pointing to HDACs acting to regulate cell cycle checkpoints, but the exact mechanism still has not been elucidated. A study of global HDAC substrate interactome using affinity purification coupled to mass spectrometry based proteomics found that HDAC8 has a distinct interactome profile when compared to other class I HDACs [185]. HDAC8 is associated with the cell cycle regulators, Structural maintenance of chromosomes 1A (SMC1) [185] [200] [201] [202] (Figure 9).

As HDAC8 strongly interacts with the cohesin complex it is worth scrutinizing the downstream effect the cohesin ring may have on cellular functions. One of the functions of the cohesin complex is to facilitate normal cell cycling. The cohesin complex is comprised of four subunits that form a ring-like complex, SMC3 and SMC1 forming a hinge domain of the ring, and RAD21 cohesin complex component and STAG2 [202] [186] [203] [201]. The assembled ring is then shuttled on and off chromatin throughout the cell cycle via specific enzymatic activities. In G1, the cohesin is loaded onto a 2N chromatid via Nipped-B-Like Protein (NIPBL)/ MAU2 chromatid cohesion factor homolog (MAU-2) complex [186] (Figure 9). During the DNA replicative S phase, the 4N sister chromatids are stabilized by the cohesin ring when it is conformationally locked by

acetylation of SMC3 via Establishment of Sister Chromatid Cohesin n-acetyltransferase2 (ESCO2) [186] (Figure 9). During M, specifically during the separation of sister chromatids (anaphase), the ring must be dissolved by PDS5/Wings apart-like protein homolog (WAPL) mediated conformational change [186](Figure 9). At the end of M, HDAC8 deacetylates the dissociated $SMC3^{Ac}$ to be recycled to the conformationally steady state, unacetylated SMC3 [186] (Figure 9). Dysregulation of cohesin loading results in destabilization of normal cell cycling [186]. SMC3 deacetylation is imperative for recycling of cohesin so that it can be reloaded during interphase for mitotic functions [186]. Pharmacological inhibition of HDAC8 using PCI-34052 resulted in accumulation of $SMC3^{Ac}$ delayed cell cycle progression at G0/G1 and suppressed proliferation [186]. Other studies also confirmed HDAC8 inhibition increases G_0/G1 cell cycle length in HeLa and HEK cells [184].

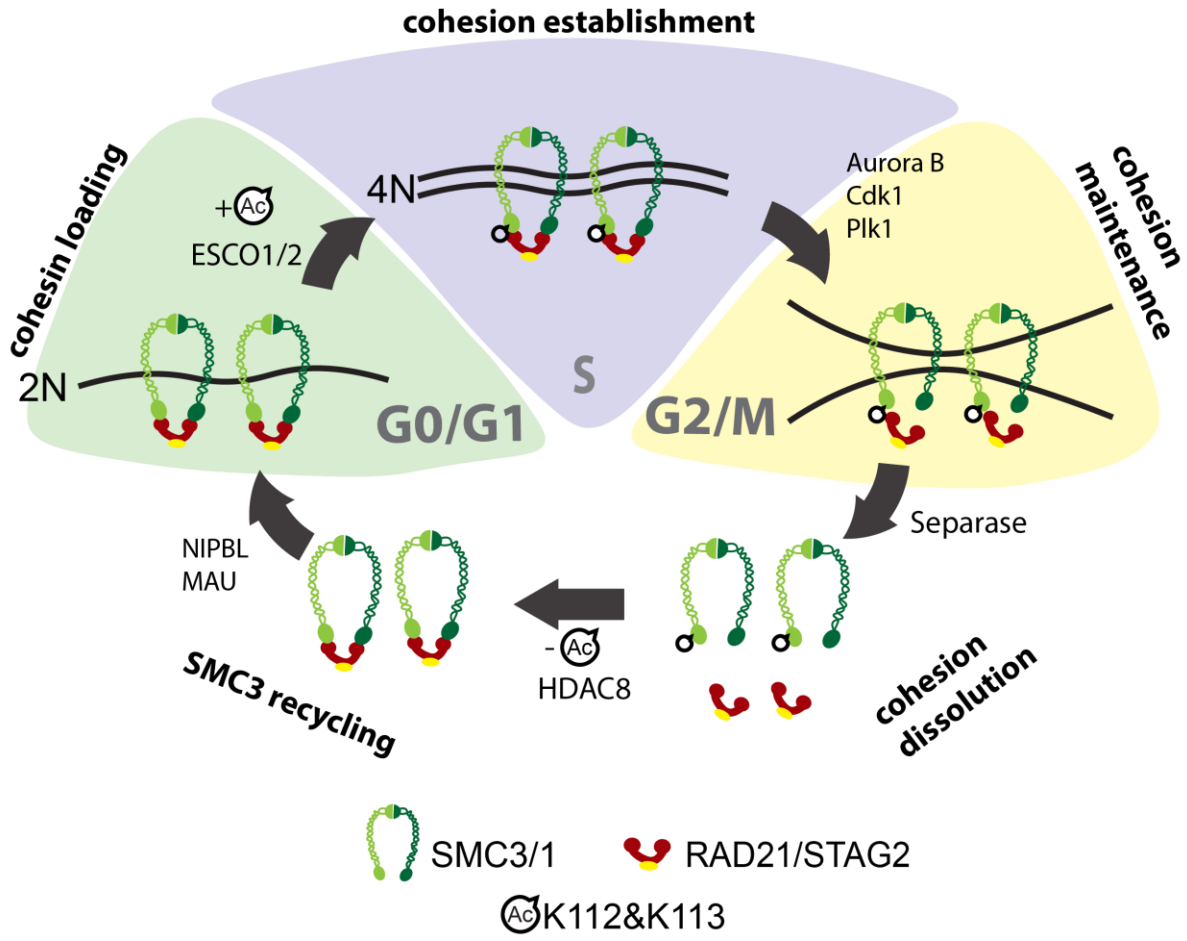

Figure 9 HDAC8 and cohesin complex during cell cycle

Model for HDAC8, SMC3, and cell cycling interaction. Cohesin loading: Cohesin ring is loaded onto 2N during G0/G1 (green) via interphase regulators, NIPBL and MAU. Cohesion establishment: During S-phase (purple), DNA replication occurs. Acetylation of SMC3 is required for cohesion locking to establish sister chromatid cohesion. The acetylation of SMC3 (K112&K113) occurs via acetyltransferase, ESCO1/2. Cohesion establishment: Cohesion continues to be maintained in order to recruit repair proteins in presence of DNA damage up to G2 (yellow). Cohesin dissolution occurs during Mitosis (yellow) via separase in order to separate sister chromatids. The conhesin ring is dissolved into two parts, SMC3/1 and RAD21/STAG2. The freed $SMC3^{AC}$ must be recycled to be used for the next round of cell cyle via HDAC8 removal of acetylation at K112/K113. The newly deacetylated SMC3 is then reused for cohesin loading.

The cohesin ring has multiple roles and is directly implicated in DNA repair as well as transcriptional regulation through various mechanisms. HDAC8 colocalizes with RAD51 and SMC3 at sites of homologous recombination after double stranded breaks in the DNA, suggesting its role in aiding genomic stability after cellular injury [204]. Transcriptionally, the cohesin has diverse mechanisms on regulating gene expression. With its ring-like structure, the cohesin complex can lend dynamic chromatin folds resulting in activation or repression of genes. It can stall RNAPII binding, activate enhancer and promoter looping, V(D) J recombination, and repression through enhanced chromatin looping [205]

Furthermore, the cohesin complex has been shown to be dynamic in locomotion, readily sliding through chromatin, complicating its role in gene regulation [206]. The cohesin complex has been shown in various models to be important for developmentally critical phenomena, EMT and mesenchymal-to-epithelial (MET) transitions. In breast cancer, the cohesin ring loops and isolates TGFβ-1 and ITGA5 transcription start sites, inhibiting RNAPolI from binding and initiating transcription [207]. Without TGFβ-1 and ITGA5 expression, cells are inhibited from initiating EMT. Conversely, knockdown of a cohesin ring component results in high transcriptional activity of EMT-related genes, driving mesenchymal phenotype. Not only is the cohesin complex critical for EMT/MET, it is also critical for transcription important for embryonic development. Zebrafish maternal to zygotic transition of transcription is partially carried out by active cohesin redistribution to active areas of the genome [208].

Material modified and re-published with permission

Han HI, Skvarca LB, Espiritu EB, Davidson AJ, Hukriede NA. The role of macrophages during acute kidney injury: destruction and repair. *Pediatr Nephrol*. 2019;34(4):561-569. doi:10.1007/s00467-017-3883-1

Brilli Skvarca L, Han HI, Espiritu EB, et al. Enhancing regeneration after acute kidney injury by promoting cellular dedifferentiation in zebrafish. *Dis Model Mech*. 2019;12(4):dmm037390. Published 2019 Apr 5. doi:10.1242/dmm.037390

2.0 Elucidating mechanisms of PTBA in enhancing post-AKI recovery

2.1 Hypothesis

In an effort to identify pro-regenerative therapeutics for AKI, de Groh *et al*. utilized developing zebrafish embryos to screen for compounds that allowed expansion of renal progenitor cells within the intermediate mesoderm [148]. The study identified 4-phenylthiobutanoic acid (PTBA), a histone deacetylase inhibitor (HDI), that allowed expansion of renal progenitor cells (RPC) during larvae development [148]. Developmental pathways are often reactivated in the setting of injury. In the kidney, factors necessary for kidney formation such as Pax2 and RA signaling pathway are turned on in RTECs [159 209 210 98 157 16 162]. Compounds that can enhance this development process may also be able to enhance reactivation of such pathways in injury setting. PTBA and its analogs have shown to be effective beyond embryonic development and also enhance survival rates in both zebrafish and mice models of AKI [148 156 177 211]. Further long-term follow-up studies using IRI-, AA-, UUO- AKI collectively showed lower interstitial fibrosis and enhanced renal function, as measured by serum creatinine and blood urea nitrogen levels [176 177 156]. While PTBA enhanced recovery outcomes, none of the cellular mechanisms driving recovery have been elucidated so far. Here, the study focuses on zebrafish AKI assays, as this model organism allows precise delivery of compounds, high throughput screening assays, and heat shock inducible models of interest. I hypothesize that PTBA treatment enhances AKI repair mechanisms via activating renal development processes to increase dedifferentiation and repair of RTECs, thereby attenuating injury.

2.2 Results

2.2.1 PTBA increases dedifferentiation and proliferation post-AKI

We have previously shown that PTBA treatment increases RTEC proliferation in a zebrafish larval model of AKI [156]. To assess whether PTBA increases the population of cells that show AKI mediated reactivation, we examined whether post-AKI UPHD25 treatment increased expression of Pax2a, a critical early developmental transcription factor reactivated in RTEC during AKI [58 212 60 213]. Larvae were injected with gentamicin (gent-AKI) between 78-82hpf, followed by a single-dose of UPHD25 treatment at 2 days post injection (dpi) (Figure 10A). We used the *Tg(PT:EGFP)* line, a transgenic line marking specifically PT of the zebrafish pronephros [156]. In uninjured larvae, UPHD25 treatment had no significant effect on Pax2a reactivation (Figure 10B,C,F). In gent-AKI larvae, Pax2a was reactivated in RTECs within 48hrs after gentamicin injection and expression is maintained in a population of RTECs through at least 3dpi (Figure 10D-F). When gent-AKI larvae were treated with UPHD25, the number of Pax2a-positive RTECs significantly increases in both immunofluorescence assay and in transcript levels (Figure 10D-F, Figure 12). Results suggest that UPHD25 drives dedifferentiation of RTECS exclusively in an injury setting. To demonstrate that Pax2a is expressed in proliferating cells in zebrafish larvae in AKI, as has been shown in murine models, we co-stained for Pax2a and Proliferating cell nuclear antigen (PCNA), which marks cells in S, G2, M-phase, to show increase in cell cycling [212]. Both UPHD25 and DMSO-treated larvae show double positive cells, but UPHD25 treated fish exhibit higher number of double positive cells than DMSO treated fish. (Figure 10G-I). Results suggest that UPHD25 increases RTEC reactivation and proliferation in injury setting.

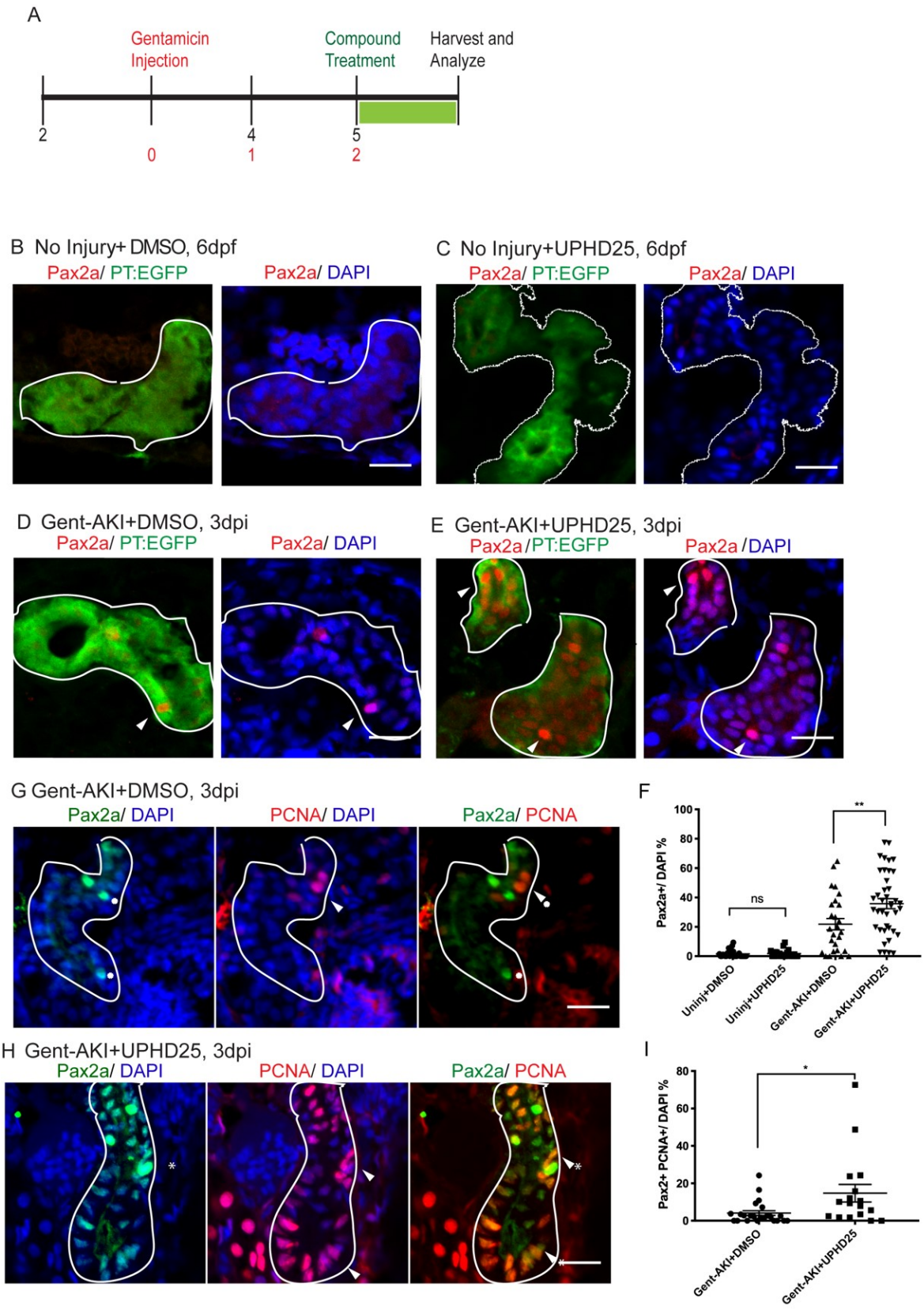
A
Gentamicin Injection
Compound Treatment
Harvest and Analyze
2
4
5
0
1
2
B No Injury+ DMSO, 6dpf
Pax2a/ PT:EGFP
Pax2a/ DAPI
C No Injury+UPHD25, 6dpf
Pax2a/ PT:EGFP
Pax2a/ DAPI
D Gent-AKI+DMSO, 3dpi
Pax2a/ PT:EGFP
Pax2a/ DAPI
E Gent-AKI+UPHD25, 3dpi
Pax2a /PT:EGFP
Pax2a /DAPI
G Gent-AKI+DMSO, 3dpi
Pax2a/ DAPI
PCNA/ DAPI
Pax2a/ PCNA
F
Pax2a+/ DAPI %
ns
**
Uninj+DMSO
Uninj+UPHD25
Gent-AKI+DMSO
Gent-AKI+UPHD25
H Gent-AKI+UPHD25, 3dpi
Pax2a/ DAPI
PCNA/ DAPI
Pax2a/ PCNA
I
Pax2+ PCNA+/ DAPI %
*
Gent-AKI+DMSO
Gent-AKI+UPHD25

Figure 10 PTBA treatment increases Pax2a reactivation and proliferation during AKI

(A) Experiment schematic: *Tg(PT:EGFP)* larvae were injected with gentamicin at 3dpf to induce AKI (gent-AKI). At 2dpi, gent-AKI larvae were treated with 1% DMSO or 1μM UPHD25 for 24hrs (2-3 dpi) then harvested for analysis. (B-E) Immunofluorescence staining of Pax2a (red), proximal tubule (PT, green), and nuclei (DAPI, blue) of age-matched 6dpf no injury+DMSO (B), 6 dpf no injury+UPHD25 (C), 3dpi gent-AKI+DMSO (D), and 3dpi gent-AKI+UPHD25 (E) larvae. Nuclear localization of Pax2a was shown by overlaying with nuclear counterstain, DAPI (blue). PT is outlined in white and Pax2a+ RTECs are marked with arrows. (F) Quantification of Pax2a+ cells. Data pooled from 3 biological replicates are shown expressed as mean+/-SEM. One-way ANOVA (G-H) Immunofluorescence co-stain of Pax2a (green), PCNA (red), and DAPI (blue) in gent-AKI+DMSO (G) and gent-AKI+UPHD25 (H). Nuclear localization of PCNA was shown by overlaying with nuclear counterstain, DAPI (blue). Pax2a+ are marked with asterisks and PCNA+ are marked with arrows. (I) Quantification of Pax2a+ PCNA+ cells. Data pooled from 3 biological replicates are shown expressed as mean+/-SEM. Two-tailed t-test: *$p<0.05$, **$p<0.01$, n.s. = not significant. Scale bar= 20μm.

2.2.2 PTBA increases dedifferentiation and ameliorates injury

To confirm that Pax2a reactivation is associated with dedifferentiation of RTECs, we examined the effect of PTBA on Vimentin expression, an intermediate filament protein that increases in dedifferentiated RTECs after AKI [55]. We treated gent-AKI *Tg(PT:EGFP)* fish with DMSO or UPHD25 at 2dpi and examined co-expression of Vimentin and Pax2a. Uninjured larvae did not show Vimentin nor Pax2a staining, while gent-AKI zebrafish showed Vimentin expression in Pax2a-positive cells (Figure 11A-C). Gent-AKI+UPHD25 zebrafish showed significantly increased Vimentin expression than in gent-AKI+DMSO treated zebrafish in immunofluorescence quantification (Figure 11C-D). As further evidence that dedifferentiation is enhanced with UPHD25 treatment, RNA-seq transcriptome profiling revealed a down-regulation of known epithelial markers and up-regulation of mesenchymal markers with UPHD25 treatment in injury

(Figure 12B,D). Together with an increased expression of Pax2a and Vimentin, this further validates the observation that UPHD25 treatment enhances dedifferentiation in RTECs.

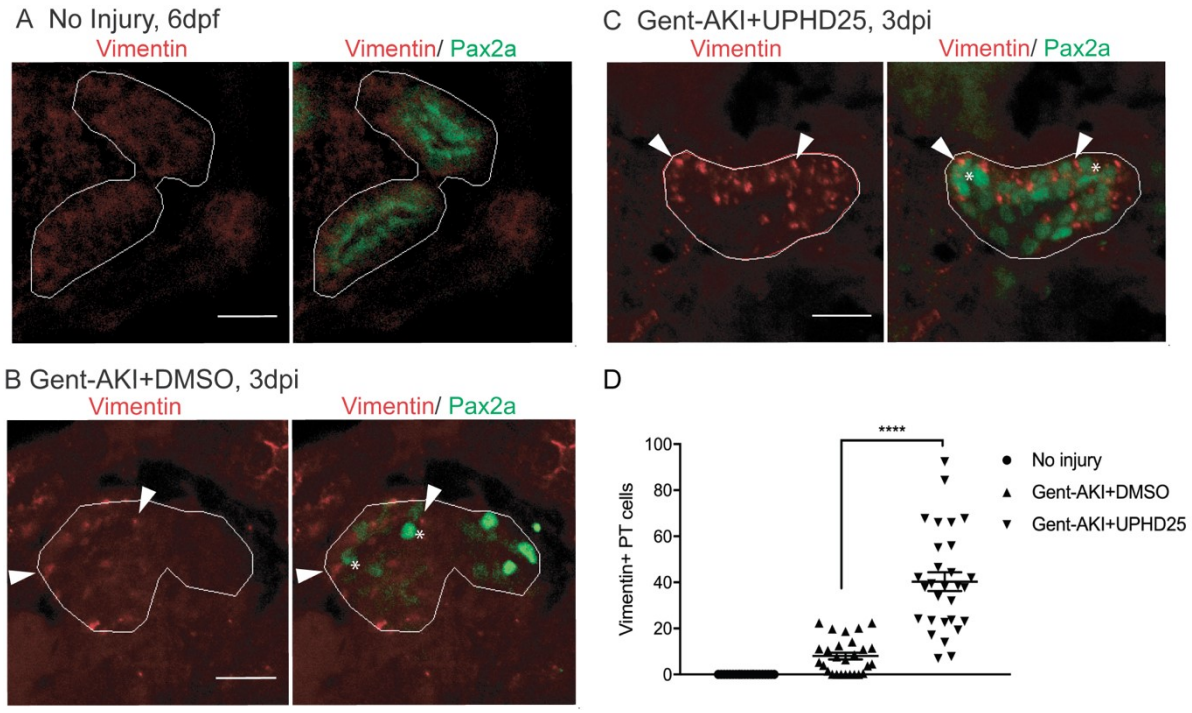

Figure 11 PTBA increases dedifferentiation during AKI

Immunofluorescence co-stain of Vimentin (red, cytosolic) and Pax2a (green) in PT of age-matched 6 dpf no injury (A), 3 dpi gent-AKI+DMSO (B), and 3 dpi gent-AKI+UPHD25 (C). (D) Quantification of Vimentin^{+} RTECs. Pax2a^{+} are marked with asterisks and Vimentin^{+} RTECs are marked with arrowheads. PT is outlined in white. Data pooled from 3 biological replicates are shown expressed as mean+/-SEM. One-way ANOVA: ****$p<0.001$. Scale bar= 20 µm

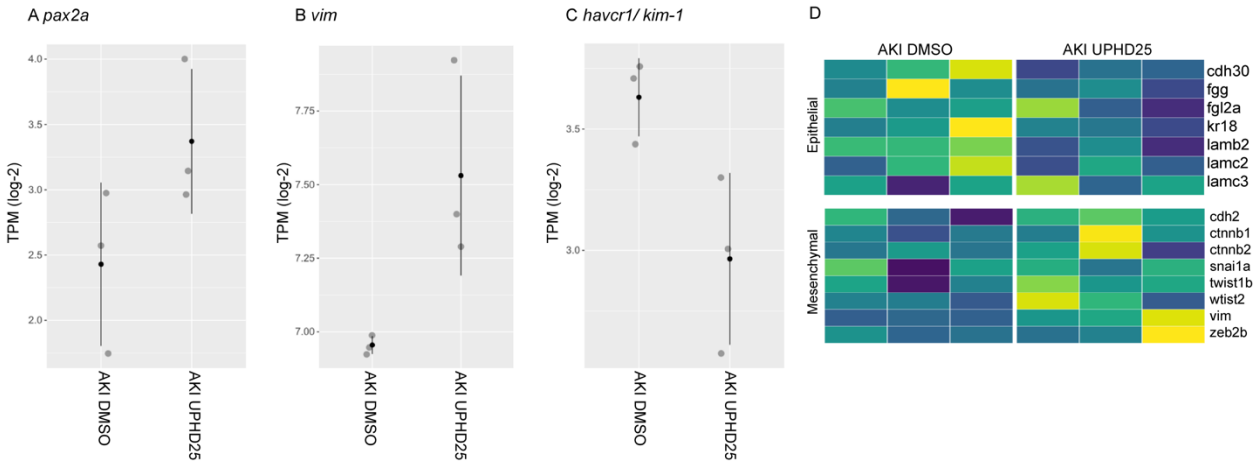

Figure 12 PTBA increases mesenchymal markers and lowers *kim-1* expression

6dpf *Tg(PT:EGFP)* larvae were used to collect 70-100 GFP^{+} pronephros of gent-AKI+DMSO, (AKI+DMSO) and gent-AKI+UPHD25 (AKI+UPHD25) at 3dpi. RNA was extracted then sequenced. Transcript expression for (A) *pax2a,* (B) *vimentin,* (C) *havcr1* (*kim-1*). All graphs were generated using transcripts -per-million (TPM), log2-scale. All treatments were replicated (N=3). Each dot represents a biological replicate (grey) and the mean of total replicates (black). (D) Heatmap of RNA-seq expression levels of a panel of marker genes known to be critical in epithelial-to-mesenchymal (EMT) transition. Each column represents one biological replicate.

Since treatment increases the dedifferentiation and proliferation of proximal tubule cells, we examined the effect of PTBA on levels of kidney injury molecule-1 (Kim-1) expression, which increases in injured RTECs after AKI and also is associated with increased fibrosis and leukocyte recruitment [156 214 215]. Following gent-AKI in zebrafish larvae, robust Kim-1 staining is detectable in injured fish by 2dpi [157]. To quantify Kim-1 protein, we measured the percent area of fluorescence within the tubule as well as the transcript levels, shown by the RNA-seq data (Figure 12C, Figure 13A-D). Compared to gent-AKI+DMSO, gent-AKI+UPHD25 zebrafish showed a lower expression of renal Kim-1 expression at 3dpi (Figure 12C, Figure 13A-D). Collectively, data demonstrate that Pax2a reactivation occurs in dedifferentiated RTECs after gentamicin injury, and that PTBA mitigates cellular injury in RTECs.

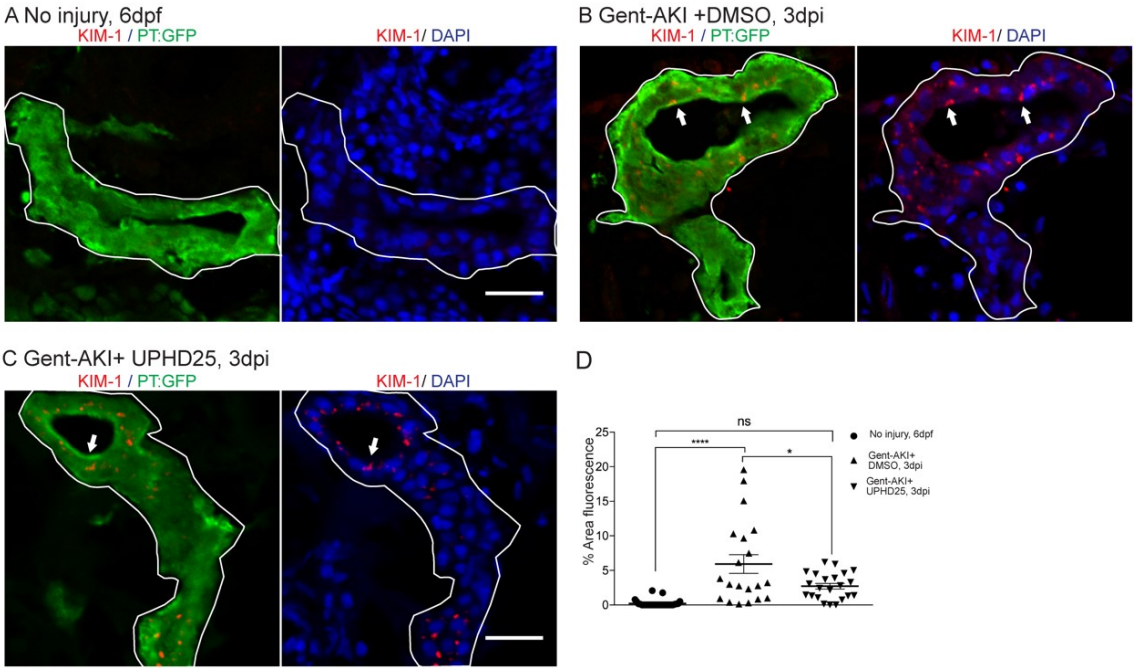

Figure 13 PTBA decreases Kim-1 expression level after AKI

Immunofluorescence of Kim-1 expression in age matched (A) 6dpf uninjured, (B)3dpi gent-AKI +DMSO, (C)3dpi gent-AKI +UPHD25 (C) larvae. Apical localization of Kim-1 was shown by overlaying with nuclear counterstain, DAPI (blue). Histological sectioning poses a challenge to obtaining perpendicular transversal cut to observing Kim-1 at apical localization. See (C) to see an ideal perpendicular transversal section to observe apical expression of Kim-1. PT are outlined in white and RTECs with Kim-1 expression are marked with arrows. (D) Quantification of Kim-1 was acquired via area of Kim-1 expression in PT. Data pooled from 3 biological replicates are shown expressed as mean^{+}/- SEM. One-way ANOVA: *p<0.05, ****p<0.001, n.s.=not significant. Scale bar= 20 µm.

2.2.3 Intact retinoic acid signaling pathway is required for PTBA efficacy

In kidney development, RA concentration gradient is required to stimulate the formation of the proximal tubule specification in the zebrafish nephrogenesis [162] [16]. In mouse kidney development, renal stromal RA signaling is required for ureteric bud branching and nephrogenesis [216] [217] [218]. In rodent IR-AKI model, RA signaling pathway mediates macrophage polarization,

albeit the exact cellular mechanisms are not yet elucidated [157]. Because RA signaling is a critical pathway in PT development, we hypothesized RA may be involved in the increased regeneration during injury. During zebrafish gent-AKI, RA signaling is reactivated within the first 7hpi and remains activated at 25hpi [157] To test whether RA pathway is required for UPHD25 efficacy, I treated gent-AKI *Tg(PT:EGFP)* fish with Ro41-5253 (Ro41), an RAR antagonist that effectively blocks RA signaling in zebrafish larvae [157]. We analyzed proliferation by performing immunofluorescence microscopy and quantifying the number of PCNA-positive RTECs. In DMSO treated larvae, Ro41 did not significantly alter the number of PCNA-positive RTECs compared to untreated larvae (Figure 14A,B,E). UPHD25 treatment increased the number of PCNA-positive RTECs, while co-treatment with Ro41 and UPHD25 significantly decreased PCNA-positive RTECs compared to UPHD25 treatment alone (Figure 14C-E). Therefore, Ro41 effectively blocks PTBA efficacy, suggesting that treatment requires intact RAR signaling to stimulate RTEC proliferation.

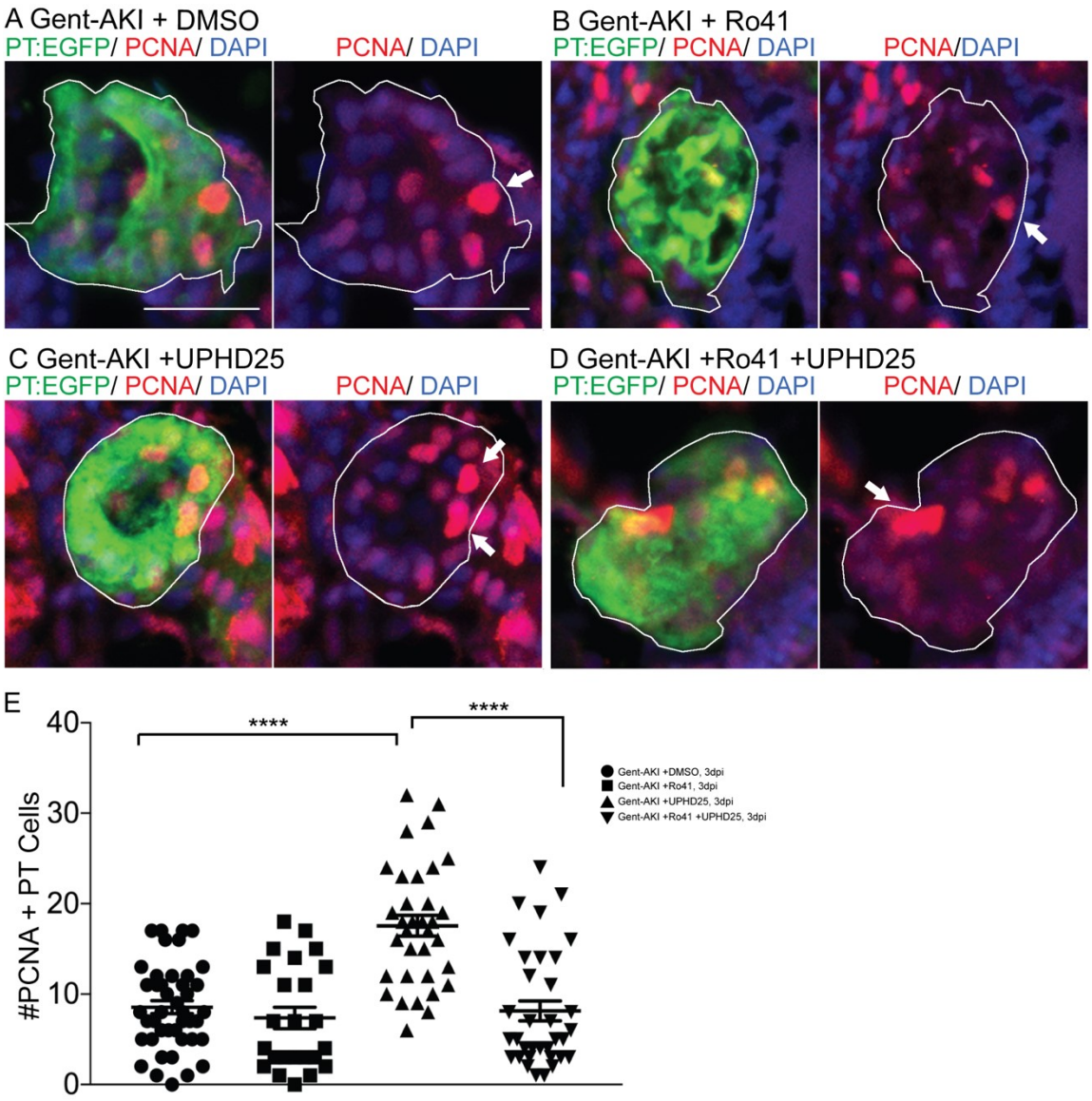

Figure 14 PTBA efficacy requires intact RA signaling

Tg(PT:EGFP) transgenic zebrafish were used to analyze RTEC proliferation. (A-D) Immunofluorescence stain of RTECs actively undergoing S, G2, M-phase marked with PCNA antibody (red) and PT (green) in gent-AKI +DMSO (A), gent-AKI +Ro41 (B), gent-AKI +UPHD25 (C), and gent-AKI +Ro41 +UPHD25 (D). PT is outlined in white and arrows mark $PCNA^{+}$ RTECs. (E) Quantification of $PCNA^{+}$ RTECs in each treatment group. Data pooled from 3 biological replicates are shown expressed as mean+/-SEM. One-way ANOVA: **p<0.01. Scale bar=20 μm. EE contributed to this figure.

To confirm the specificity of Ro41 experiments, we utilized an inducible transgenic zebrafish line *Tg(hsp70l:EGFP-HS-dnRARα)*^{ci1008} in which heat shock stimulates expression of a dominant-negative form of the human RA receptor alpha (DN-RARα) [219] [220] [221]. We previously showed that UPHD25 treatment increased active RTEC proliferation in uninjured larvae [156]. Therefore, we evaluated whether reducing RA signaling in this heat-inducible transgenic model would block UPHD25-stimulated RTEC proliferation. Uninjured *Tg(hsp70l:EGFP-HS-dnRARα)* larvae were heat shocked for 1hr at 5dpf then treated with either DMSO or UPHD25 for 24hrs. We quantified PCNA at 6dpf and compared proliferation to wildtype larvae treated with DMSO or UPHD25 (Figure 15A-E). Proliferation rates were comparable between heat-shocked (+HS) and non heat-shocked (-HS) larvae treated with DMSO (Figure 15A,B). However, UPHD25 -HS treatment showed impaired RTEC proliferation compared to UPHD25 +HS (Figure 15C,D). Therefore, in uninjured larvae, PTBA requires RA signaling to stimulate RTEC proliferation. Similarly, we evaluated proliferation in this transgenic model after AKI at 3dpf. At 2dpi, larvae were heat shocked for one hr and then treated with DMSO or UPHD25 for 24hrs (Figure 15F-J). Overall, gent-AKI larvae showed higher proliferation than the no injury group, suggesting injury results in increased proliferation. Within the Gent-AKI group, proliferation rates were comparable between DMSO +HS and DMSO -HS (Figure 15F,G). However, gent-AKI +UPHD25 +HS showed impaired RTEC proliferation compared to UPHD25 -HS controls (Figure 15H,I). Taken together, both pharmacologic or genetic inhibition of RAR signaling significantly reduces PTBA efficacy. The data indicate that the PTBA mechanism of action requires upstream RA signaling.

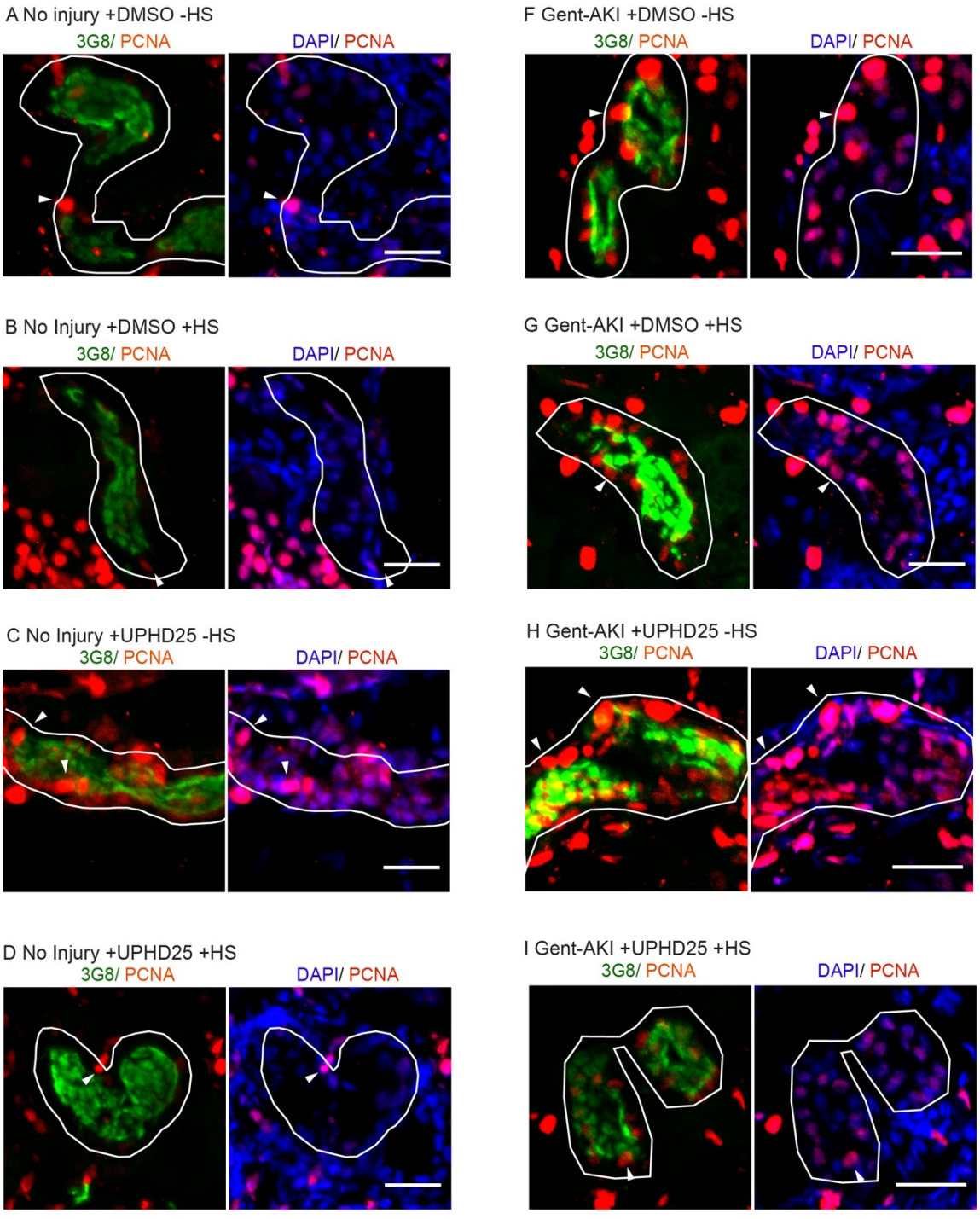
A No injury +DMSO -HS
3G8/ PCNA
DAPI/ PCNA
F Gent-AKI +DMSO -HS
3G8/ PCNA
DAPI/ PCNA
B No Injury +DMSO +HS
3G8/ PCNA
DAPI/ PCNA
G Gent-AKI +DMSO +HS
3G8/ PCNA
DAPI/ PCNA
C No Injury +UPHD25 -HS
3G8/ PCNA
DAPI/ PCNA
H Gent-AKI +UPHD25 -HS
3G8/ PCNA
DAPI/ PCNA
D No Injury +UPHD25 +HS
3G8/ PCNA
DAPI/ PCNA
I Gent-AKI +UPHD25 +HS
3G8/ PCNA
DAPI/ PCNA
E
PCNA+ PT cells
10
8
6
4
2
0
**
No Inj DMSO HS-
No Inj DMSO HS+
No Inj UPHD25 HS-
No Inj UPHD25 HS+
J
PCNA+ PT cells
40
30
20
10
0
*
gent-AKI DMSO HS-
gent-AKI DMSO HS+
gent-AKI UPHD25 HS-
gent-AKI UPHD25 HS+

Figure 15 Dominant negative RARα expression reduces PTBA efficacy

Uninjured (A-E) or gent-AKI (F-J) *Tg(hsp70l:EGFP-HS-dnRARα)* transgenic larvae were heat shocked at 5 dpf to express a dominant-negative form of human RA receptor alpha, which inhibits RA signaling. Larvae were treated with UPHD25 or DMSO then harvested for PT cell proliferation analysis (E, J). (A-H) Immunofluorescence staining for PCNA, marking proliferating cells in S-phase (red), 3G8, marking PT cells (green), and DAPI (blue) in uninjured fish treated with DMSO -HS (A) and +HS (B); uninjured fish treated with UPHD25 -HS(C) and +HS (D); gent-AKI fish treated with DMSO -HS (F) and +HS (G); and gent-AKI fish treated with UPHD25 -HS(H) and +HS (I). PT is outlined in white and arrows mark $PCNA^+$ RTECs. (E) Quantification of $PCNA^+$ RTECs in uninjured treatment groups. (J) Quantification of $PCNA^+$ RTECs in gent-AKI treatment groups.. Data pooled from 3 biological replicates are shown expressed as mean+/-SEM. One-way ANOVA: *p<0.05, **p<0.01. Scale bar=20 μm.

2.3 Methods

2.3.1 Zebrafish husbandry

Studies were approved by the University of Pittsburgh IACUC. Zebrafish were maintained as described [222]In addition to AB wildtype, embryos were used from the following published transgenic lines: *Tg(PT:EGFP)^{nz4}* and *Tg(cdh17:mCherry)^{pt307}* [156] [157]. Both males and females were used for the study.

2.3.2 Gentamicin microinjection

Zebrafish larvae were injected with a single dose of gentamicin at 3 dpf with 7.5ng of gentamicin as previously described[200]. Prior to the gentamicin injection, 3dpf zebrafish larvae were anesthetized in 0.2% tricaine/E3 medium (5mM NaCl, 0.33mM CaCl2, 0.33mM MgSO4, and

0.17mM KCl). Glass capillaries were pulled to produce microneedles and were aspirated with 10µl of 7.5ng/nl gentamicin solution diluted with filtered saline solution (Henry Schein, Cat No.: 1049944). The larvae were injected with 1nl gentamicin solution, delivered via the common cardinal vein. After injection, larvae were incubated in 50µg/ml penicillin/streptomycin diluted in E3 medium.

2.3.3 Compound treatment

All compounds were diluted in E3 medium containing 0.5% DMSO. UPHD25 was synthesized by Enamine and used at a working concentration of 1µM. Larvae were treated with either DMSO or UPHD25 from 2-3dpi or 5-6dpf. For RA inhibition studies, zebrafish larvae were treated with 1 µM Ro41-5253 (Enzo Life Sciences) in 1% DMSO diluted in E3 for 24 hrs from 3 to 4 dpf, and then were washed with several changes of E3.

2.3.4 Heat shock treatment

Tg(hsp701:GFP-dn_Hsa.rarα) transgenic fish were generated by gateway-based Tol2 transposon transgenesis [223]. Constructs were injected into single cell embryos and screened for insertion. Progeny of P_0 founder animals were used to establish the zebrafish transgenic line. Animals were heat-shocked at 37°C for 1hr to induce the expression of human dominant negative RARα under the zebrafish *hsp70l* promoter.

2.3.5 Histological Analysis

Immunofluorescence microscopy was performed on cryosections as described previously [224]. Larvae were fixed in 4% paraformaldehyde and treated with a 10-30% sucrose/PBS gradient before embedding in tissue freezing medium (Ted Pella). Sections were generated at a thickness of 12μm. Slides were blocked with 10% goat serum in PBST (0.1% Tween-20), followed by primary and secondary antibody incubations. Incubation with DAPI (Vector Laboratories) was used to counterstain nuclei. The slides were washed with PBS then mounted with Aqua Polymount (Polysciences). Sections were examined by confocal microscopy (Zeiss LSM 700).

To quantify Pax2a-positive cells in *Tg(PT:EGFP)* fish, we imported serial images into ImageJ 1.46r software (NIH). The ROI tool was used to outline the kidney in the green channel, and "Analyze Particle" function was used to quantify the number of Pax2a-positive cells in the red channel. Background and threshold values were constant between groups for each experiment. Particle size range was 80 to infinity. Per nephron, three images were analyzed. The protocol was used for PCNA immunofluorescence assays. Antibodies used are provided Table 1.

2.3.6 RNA isolation of zebrafish pronephros

6dpf *Tg(PT:EGFP)* larvae were used to collect GFP+ pronephros per treatment (N=70 for no injury ; N=100 for gent-AKI). The larvae were incubated in 10mM DTT in E3 and Tricaine for 1.5-2 hrs at room temperature then with 5mg/ml Collagenase I in HBSS (Sigma Aldrich) for 2.5-3.5 hrs at 32 ºC. The larvae were washed in Minimum Essential Media and 10% fetal calf serum (Gibco). Fine forceps and P10 pipette were used to dissect GPF^{+} pronephros. RNeasy Micro kit (Qiagen) was used for RNA isolation.

2.3.7 cDNA library preparation and RNA sequencing

1µg of total RNA underwent mRNA library preparation using TruSeq Stranded mRNA kit (Illumina), according to manufacturer's protocol. Final libraries were normalized to 10nM, pooled and diluted. NextSeq 500 were seeded with 1.8pM denatured library for automated cluster formation for approximately 30-40 million reads per sample. We used Hisat2 (v2.1.0) [PMID: 25751142] to align paired-end RNA-seq reads to the zebrafish reference genome (UCSC danRer11) and gene-level counts per million (CPM) were calculated using featureCounts and edgeR [225,226]. The RNA-seq data has been deposited in the Gene Expression Omnibus repository with the accession number GSE 126418.

2.3.8 Statistical analysis

Data were analyzed using student t-test, one-way ANOVA, and two-way ANOVA as indicated, and data are reported as mean ±SEM. P-values were considered significant when <0.05. When visible, both nephrons per fish were included.

2.4 Discussion

Upon AKI, RTECs undergo a repair process that starts with reactivation of developmental genes, such as Pax2, then increase proliferation to repopulate the tubular epithelium [98 38]. Our work suggests that the PTBA enhances the endogenous repair process of the kidney. In zebrafish, *pax2a* is required for PT development and specification. It is also activated during injury, suggesting the

innate reparative capacity of the zebrafish pronephric kidney [161 227 228]. More interestingly, PTBA enhances Pax2a and PCNA-double positive RTEC numbers, suggesting PTBA enhanced RTEC cycling and proliferation. This reactivation of developmental genes usually accompanies EMT, in order for the cells to increase its proliferative capacity [228]. We captured the activation of EMT using both immunohistology as well as RNA-sequencing. Both showed a window of upregulated mesenchymal genes as well as Vimentin and downregulation of epithelial genes, such as E-cadherin. PTBA treatment enhances the population of RTECs that undergo EMT, accompanied by enhanced Pax2a expression, repair and re-differentiate into epithelial cells.

We used Kim-1 as an injury biomarker to assess the effect of PTBA in RTEC health. Kim-1 expression was lower in gent-AKI+UPHD25 than gent-AKI+DMSO at 3dpi, suggesting that PTBA attenuates injury. However, the mechanism of PTBA reducing Kim-1 should be carefully assessed: 1) PTBA may prevent RTECs from injury therefore precluding *kim-1* expression during the treatment period; 2) PTBA may reverse RTECs injury, thereby turning off *kim-1* expression during the process of Pax2 and EMT dedifferentiation. Earlier time course and cell-fate experiments can delineate the specific effect of PTBA on enhancing AKI recovery.

Another pathway of interest was the RA signaling pathway, known to be critical for proximal tubule cell specification in the zebrafish pronephros and ureteric branching in the mouse kidney. It is shown to be significantly activated within hrs of AKI in the zebrafish RTECs [157]. RA signaling in injury has a positive effect in repair, as inhibition of RA resulted in worsened survival and lower RTEC proliferation in gent-AKI zebrafish [157]. We hypothesized this pathway will be enhanced with PTBA treatment. Previous results showed PTBA treatment enhances RA response elements [179]. Our work showed that blocking of RA signaling pathway during PTBA treatment abrogated its proliferative effect. Our results suggest that RA activation is a necessary downstream

factor for PTBA mechanism of action. We conclude that PTBA prolongs the window of RA activation, having a positive repair effect by allowing longer window of redifferentiation and repair of the RTECs. The additional RA inhibition via a heat shock inducible model further strengthens our claim that abrogating the RA signaling pathway renders PTBA ineffective. Taken together, this work further characterizes the cellular mechanism of our novel compound PTBA as a promising candidate as an AKI therapeutic.

Additional contributors to the chapter

Ro41 data analysis was performed by Eugenel Espiritu

RNA-seq data analysis was performed by Abha Bais

Material modified and re-published with permission

Brilli Skvarca L, Han HI, Espiritu EB, et al. Enhancing regeneration after acute kidney injury by promoting cellular dedifferentiation in zebrafish. *Dis Model Mech*. 2019;12(4):dmm037390. Published 2019 Apr 5. doi:10.1242/dmm.037390

3.0 Characterizing innate immune system activation in larval zebrafish acute kidney injury

3.1 Hypothesis

One of the hallmarks of AKI is the early immune response, activated by the initial DAMP and PAMP released by RTECs and surrounding damaged tissue. Studies have reported that blocking neutrophil recruitment results in amelioration of AKI [141] [229,230]. Excessive macrophage recruitment and M1 activation lead to increased risk of further deterioration of kidney function and increased fibrosis [231]. Previous study in mouse AA-AKI demonstrated that PTBA treatment decreases the total number of kidney macrophages and lowered inflammatory cytokines [177]. Others have characterized the importance of macrophage polarization in diverging RTECs from undergoing repair or fibrosis [115]. The larval zebrafish has a fully mature and functional innate immune system by 3dpf which is activated via well-conserved pathways, shown in context of fin clip injury model [170]. Although the RTEC component of larval zebrafish AKI has been relatively well characterized, the immune system activation has not yet been investigated. I hypothesize that AKI resulting in cellular apoptosis and necrosis activates the innate immune system in the larval zebrafish model of AKI. PTBA treatment may have an indirect role in reducing leukocyte infiltration by enhancing RTEC repair and precluding DAMPs and leukocyte recruitment. Alternatively, PTBA may directly affect repair by directly changing macrophage polarization to more reparative M2 population.

3.2 Results

3.2.1 Larval zebrafish AKI activates neutrophil migration

PTBA treatment lowered RTEC expression of Kim-1, an AKI biomarker associated with prolonged inflammatory response and fibrosis in mice [39,45,215,232] (Figure 13). Thus, we determined whether PTBA affects the leukocyte response in the zebrafish gentamicin-AKI model. In mammals, AKI results in the rapid influx of neutrophils and macrophages, but these responses have not yet been characterized during AKI in zebrafish [233 234 235 115 236]. Since the innate immune response is functional in zebrafish larvae by 3dpf, we first determined whether neutrophils and macrophages are activated and recruit to the site of injury in the PT [127]. To evaluate the neutrophil response, we performed time-lapse confocal imaging in gent-AKI transgenic fish expressing mCherry driven by the *cadherin*-17 promoter, *Tg(cdh17:mCherry),* a renal tubule marker and enhanced GFP driven by the *lysozyme C* promoter, *Tg(lyz:EGFP),* a marker of neutrophils [237 238 167] (Figure 16A). We captured z-stack images of the PT region over 17hrs beginning at 24 hpi. In uninjured fish, $EGFP^+$ neutrophils migrate rapidly with few cells accumulating near the PT (Figure 16B). In contrast, neutrophils in gent-AKI fish migrate slowly, and several migrated adjacent to the mCherry-positive kidney epithelium (Figure 16B). In order to quantify the response, we acquired samples at several time points and quantified $EGFP^+$ neutrophils adjacent to the PT by examining serial sections (Figure 16C). At 4dpf (1dpi), there was no change in the number of renal neutrophils after gentamicin injection (Figure 16D). However, gent-AKI larvae showed more renal neutrophils at both 5dpf (2dpi) and 6dpf (3dpi), compared to uninjured controls (Figure 16D).

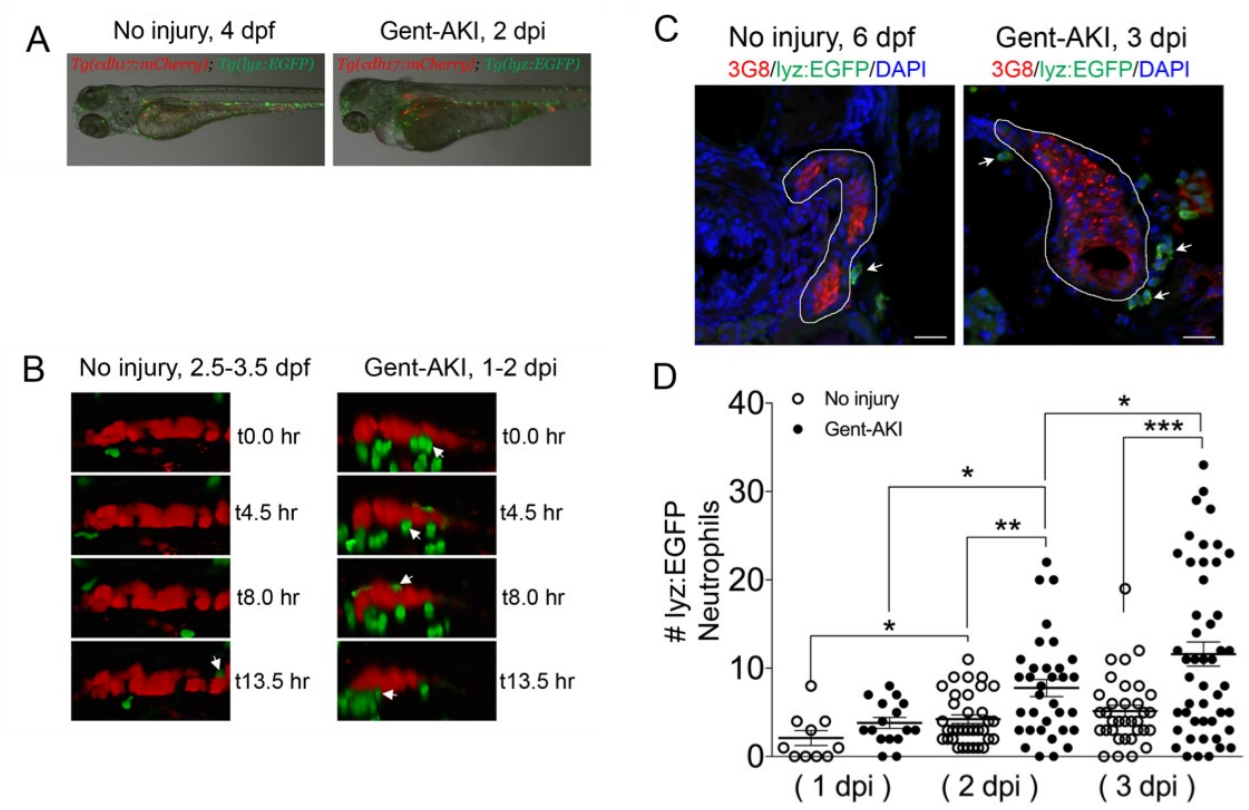

Figure 16 Neutrophil population changes in the kidney field during AKI

Tg(cdh17:mCherry); Tg(lyz:EGFP) transgenic zebrafish were used for neutrophil analyses. (A) Uninjured (left) and gent-AKI (right) at 3dpf and imaged at 2dpi (B) Snapshots of live imaging of lyz:GFP^{+} neutrophils imaged at 1 dpi for 13.5 hrs. Imaged fish were age matched uninjured (left) and gent-AKI (right) (C) Immunofluorescence co-stain of PT (red or green) and neutrophils (green) in no-injury and gent-AKI at 3 dpi. PT is outlined in white and adjacent leukocytes are marked with arrows. (D) Quantification of neutrophil adjacent to PT before and after injury. Adjacent leukocytes were counted for both no injury and gent-AKI at 1, 2, 3 dpi. Data pooled from 3 biological replicates are shown expressed as mean+/-SEM. One-way ANOVA: *p<0.05, **p<0.01, ***p<0.005. Scale bar=20 μm.

3.2.2 Larval zebrafish AKI activates macrophage migration

We also performed imaging and histological studies to evaluate the macrophage response. To visually detect macrophages, we utilized the transgenic reporter line, *Tg(mpeg1:dendra2)* in

which macrophages are green [239]. We performed live time-lapse imaging in *Tg(cdh17:mCherry); Tg(mpeg1:dendra2)* double transgenic fish after gentamicin injection (Figure 17A). Unlike the neutrophils, the macrophages did not increase in recruitment at the early timepoint of 24hpi. Therefore, we captured z-stack images of the PT and macrophage recruitment at a later timepoint, starting at 48hpi, over 20hrs (Figure 17B). Uninjured fish display mpeg:dendra2^{+} macrophages circulating rapidly; however, only a few macrophages made prolonged contact with the PT (Figure 17B). In contrast, gent-AKI fish showed recruitment and retention of many macrophages to the mCherry^{+} kidney epithelium (Figure 17B). To quantify this response, we fixed *Tg(mpeg1:dendra2); Tg(cdh17:mcherry)* double transgenic fish and quantified the number of Dendra2^{+} macrophages adjacent to the PT (Figure 17D). Compared to uninjured fish, gent-AKI larvae showed an increased number of renal macrophages at 3 dpi (Figure 17C,D). Taken together, these data indicate that the gent-AKI zebrafish larvae show a robust innate immune response between 2-3 dpi.

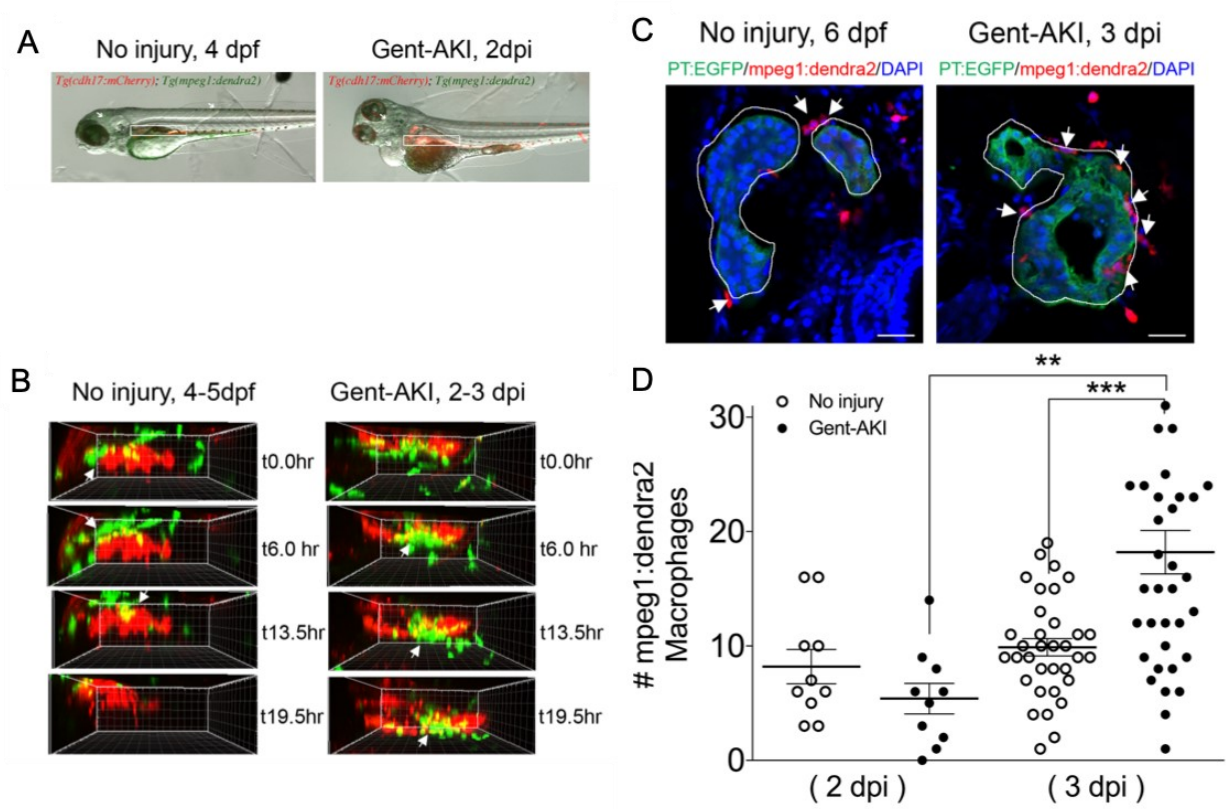

Figure 17 Macrophage population changes in the kidney field after AKI

Tg(cdh17:mCherry); Tg(mpeg1;dendra2) transgenic zebrafish were used for macrophage analyses. (A) Uninjured (left) and gent-AKI (right) at 3 dpf and imaged at 2 dpi . (B) Snapshots of live imaging of mpeg1^{+} macrophages imaged at 2 dpi for 19.5 hrs in no injury and gent-AKI setting. (C) Immunofluorescence co-stain of PT (green) and macrophages (red) in no-injury and gent-AKI at 3 dpi. PT is outlined in white and adjacent leukocytes are marked with arrows. (D) Quantification of macrophage numbers adjacent to PT before and after injury. Data pooled from 3 biological replicates are shown expressed as mean+/-SEM. One-way ANOVA: *p<0.05, **p<0.01, ***p<0.005. Scale bar=20 µm.

3.2.3 PTBA treatment decreases macrophage migration

We have characterized the neutrophil response, which begins within the first 24hrs after injury and remains until 3dpi (Figure 16). Macrophages, however, respond at later time points, starting after 24hpi and reaching their peak at 3dpi (Figure 17). Having characterized the timing of neutrophil and macrophage influx during gent-AKI in zebrafish larvae, we assessed whether PTBA affects the leukocytic immune response. We treated gent-AKI *Tg(lyz:EGFP)* or *Tg(mpeg1:dendra2)* with DMSO or UPHD25, and quantified renal neutrophils and macrophages at 3 dpi (Figure 18A,B). At this time point, there was no change in the number of neutrophils, but there was a small but significant decrease in the number of macrophages between treatment groups. This suggests that PTBA does not affect initial neutrophil recruitment but may decrease the overall number of macrophages that are recruited to the PT (Figure 18C,D).

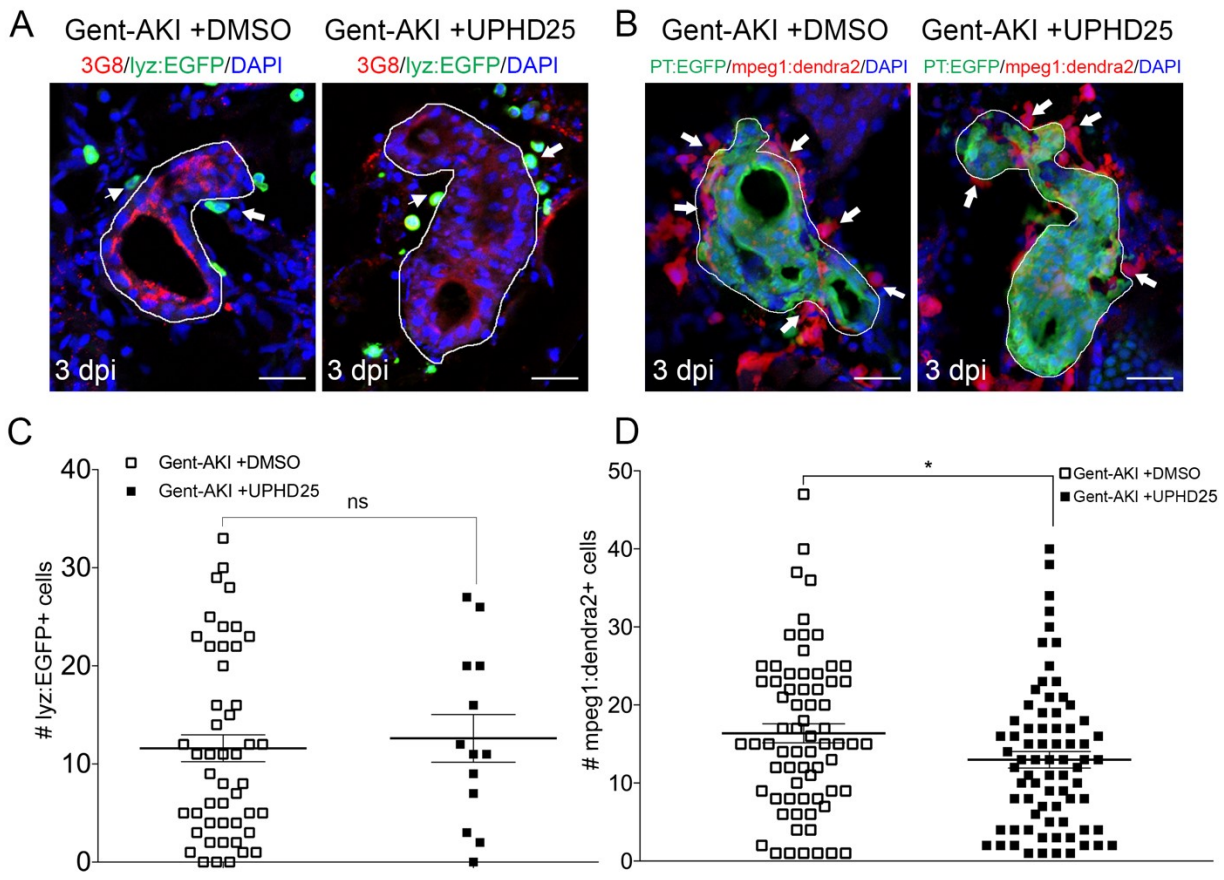

Figure 18 PTBA treatment lowers total macrophage recdruitment during early AKI

(A) *Tg(cdh17:mCherry); Tg(lyz:EGFP)* transgenic zebrafish were used for neutrophil analyses (B)*Tg(cdh17:mCherry); Tg(mpeg1;dendra2)* transgenic zebrafish were used for macrophage analyses. Images of peritubular macrophages after DMSO (left) or UPHD25 (right) treatment Images of peritubular neutrophils or macrophages after DMSO (left) or UPHD25 (right) treatment. Fish were injecdted at 3dpf and treated from 2-3dpi then imaged at 3dpi. PT is outlined in white and adjacent leukocytes are marked with arrows. (C) Quantification of lyz+ neutrophils. (D) Quantification of mpeg1+ macrophages. Data pooled from 3 biological replicates are shown expressed as mean+/-SEM. two-tailed t-test: *p<0.05, ns=not significant. Scale bar=20 μm.

3.2.4 PTBA treatment affects macrophage polarization

We then wanted to determine whether PTBA affected macrophage polarization [235 115 236]. Studies have shown that zebrafish undergo M1/M2 polarization akin to their mammalian counterparts [170 240]. Since the mpeg1 transgenic line is a reporter for all macrophage phenotypes, we stained the *Tg(mpeg1:dendra2)* fish with anti-TNFα antibody, an M1-specific pro-inflammatory cytokine [170]. To quantify M2 macrophages, we utilized a similar staining method, but used an M2 specific marker, anti-Arginase-2 antibody [240]. To validate the specificity of the Arginase-2 antibody, *in situ* hybridization pattern was once again compared to the protein expression (Figure 19). Since other pro-inflammatory cells also express TNFα, we quantified the ratio of cells that co-labelled $TNF\alpha^{+}$/mpeg1:$dendra2^{+}$. In gent-AKI+DMSO treated fish, many M1 macrophages are recruited to RTECs, while gent-AKI+UPHD25 treated fish display fewer M1 macrophages (Figure 20A-C). Comparing gent-AKI+DMSO with gent-AKI+UPHD25 treated fish, we found no change in the number of M2 macrophages in the renal field (Figure 20D-F). Overall, these results suggest that PTBA reduces total macrophage recruitment and the number of inflammatory macrophages to the damaged tubule.

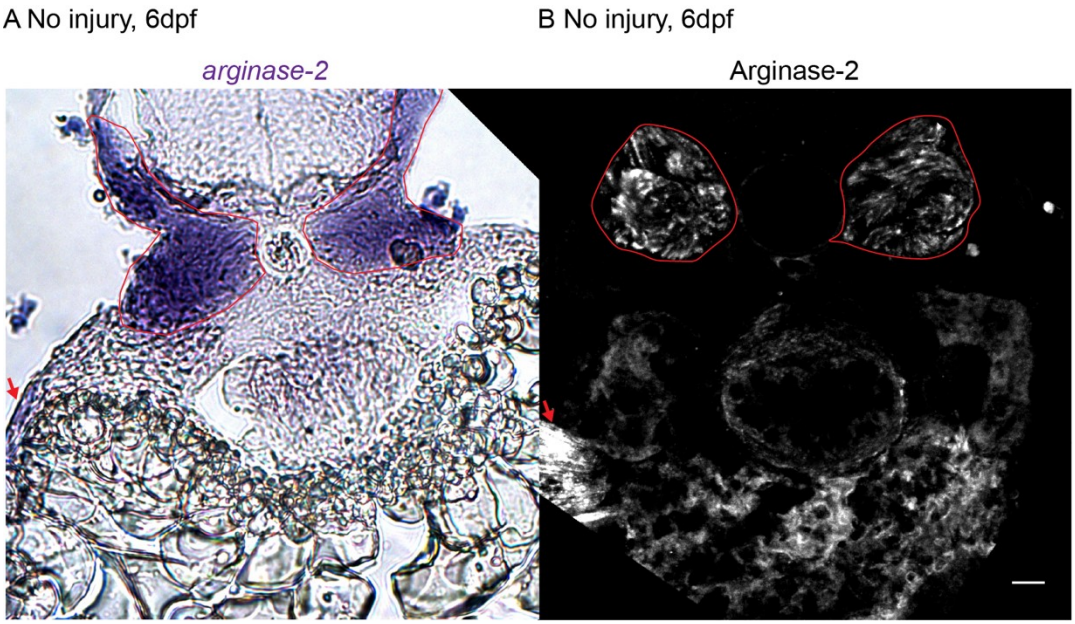

Figure 19 Validation of Arginase-2 antibody via in situ hybridization

To validate the M2 marker Arginase-2, in situ hybridization was used to localize mRNA and compared the expression pattern to immunofluorescence staining with anti-Arginase-2 antibody. (A) In situ hybridization of arginase-2 on frozen section of 6 dpf uninjured larvae demonstrates positive staining in the somites (outlined in red) and pectoral fin (red arrow), consistent with previously reported spatiotemporal expression (Thisse 2004 ZFIN publication). (B) Immunofluorescence staining in uninjured larvae at 6 dpf with anti-Arginase-2 antibody (Thermo Fisher Scientific PA5-27987, 1:100) demonstrates congruent staining pattern, with positive staining in somites (outlined in red) and pectoral fin (red arrow). Scale bar= 20μm.

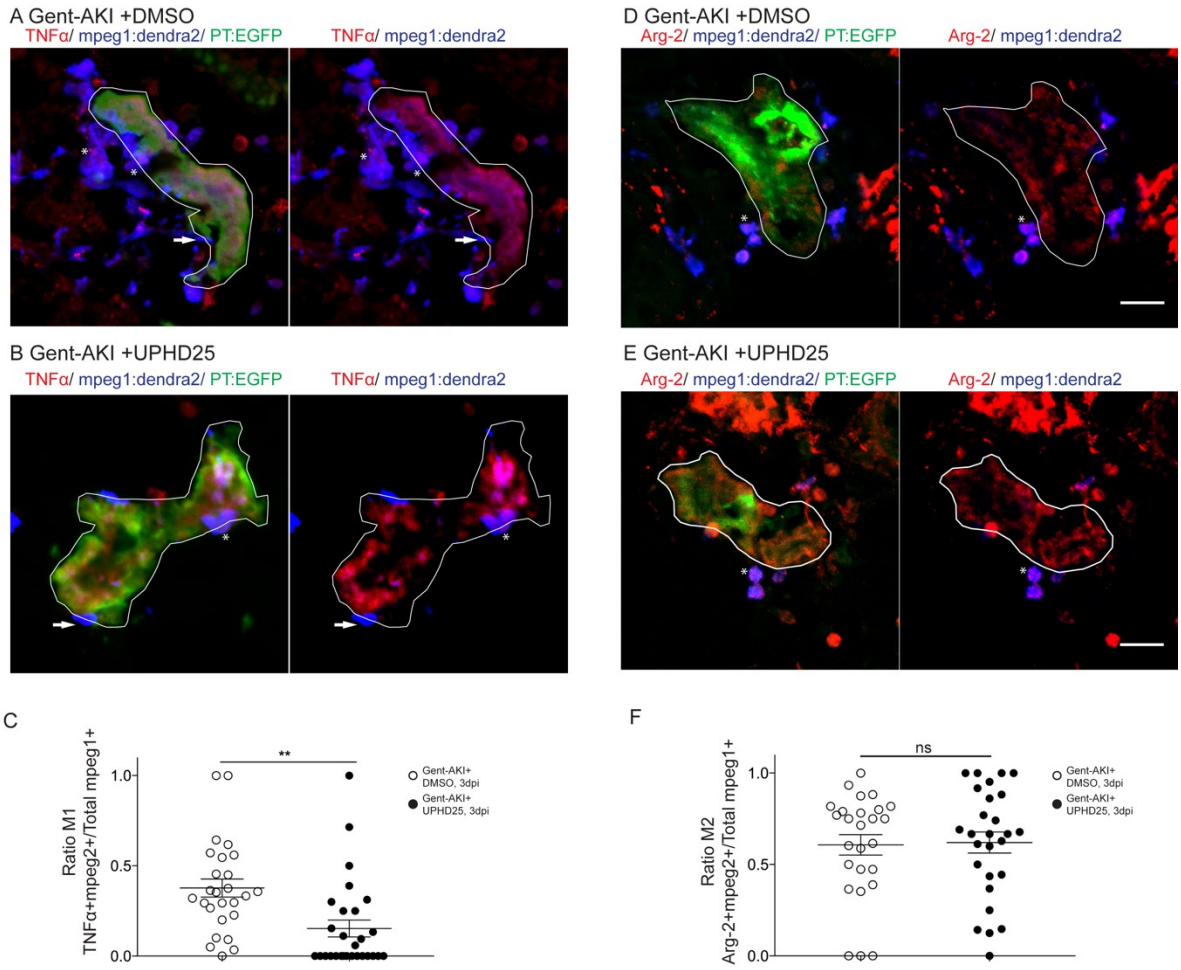

Figure 20 PTBA treatment reduces total M1 macrophage population,

Tg(mpeg1:dendra2); Tg(PT:EGFP) transgenic zebrafish were used for macrophage polarization analysis. (A, B) Immunofluorescence co-stain of TNFα (red), macrophages (blue), and PT (green) in gent-AKI +DMSO (A) and gent-AKI +UPHD25 (B). PT is outlined in white. $TNF\alpha^{+}$/$mpeg1^{+}$ are marked with an asterisk and $TNF\alpha^{-}$/mpeg1 are marked with an arrow. (C) Quantification of M1 macrophage recruitment by counting $TNF\alpha^{+}$/$mpeg1^{+}$ cells adjacent to PT. (D, E) Immunofluorescence co-stain of arginase-2 (red), macrophages (blue), and PT (green) in gent-AKI +DMSO (D) and gent-AKI +UPHD25 (E). $Arg2^{+}$/$mpeg1^{+}$ are marked with an asterisk and $Arg\text{-}2^{-}$/$mpeg1^{+}$ cells are marked with an arrow. (F) Quantification of M2 macrophage recruitment by counting $Arg\text{-}2^{+}$/$mpeg1^{+}$ cells adjacent to PT. Macrophage numbers were normalized by calculating ratio of M1 or M2 over total macrophages; i.e. ($TNF\alpha^{+}$/$mpeg1^{+}$)/total $mpeg1^{+}$. Data pooled from 3 biological replicates are shown expressed as mean+/-SEM. 2-tailed t-test: **$p<0.01$, n.s.= not significant. Scale bar=20 μM.

3.3 Methods

3.3.1 Zebrafish husbandry

Zebrafish husbandry was conducted as stated in Chapter 2

3.3.2 Gentamicin microinjection

Gentamicin microinjection was conducted as stated in Chapter 2

3.3.3 Compound treatment

Compound treatment was conducted as stated in Chapter 2

3.3.4 Live two-photon confocal imaging

24hrs after gentamicin injection, *Tg(cdh17:mCherry);Tg(lyz:EGFP)* larvae were anesthetized in tricaine, embedded in a thin layer of 0.5% low-melt Sea Plaque agarose (Cambrex), and covered with E3 medium / 0.003% PTU to prevent pigment development. Image stacks were acquired using a Leica TCS SP5 multiphoton microscope (Leica Microsystems) with an HCX IRAPO L 20X/0.95 water immersion objective, non-descanned detectors and a custom-built motorized stage (Scientifica). Sequential stack scanning was performed bidirectionally with a resonant scanner (16000 Hz, phase set to 1.69) with 32x line averaging and a zoom of 1.7x. EGFP and mCherry were excited with a Mai Tai DeepSee Ti:Sapphire laser (Newport/Spectra Physics) at 900 and 561 nm, respectively. Using the “Mark and Find” function, (x,y) coordinates and z-

series parameters (step size 1.48μm) were defined for individual larvae. Images were captured every 27 mins for 17hrs. Maximal projections were compiled in series to generate time-lapse movies using LAS AF Version: 3.0.0 build 8134 and Metamorph software.

48hrs after gentamicin injection, *Tg(cdh17:mCherry);Tg(mpeg1:dendra2)* larvae were processed for imaging using the protocol above. Image stacks were acquired using Nikon Eclipse Ti confocal microscope (Nikon Instruments) with a 20X dry objective, and a motorized stage. Stacks were captured with 40 optical sections, with 5μm step size. Dendra2 and mCherry were excited with 488nm and 560nm lasers, respectively. Dendra2 is photoconvertible with 488nm and UV but maintains its original green fluorescence emission (509nm) when imaged under laser power between 2-7%. Experiments utilizing *Tg(mpeg1:dendra2)* maintained low laser power to inhibit photoconversion from green to red. Using the "Mark and Find" function, (x,y) coordinates and z-series parameters (5μm) were defined for individual larvae. Images were captured every 90 mins for 24hrs. Maximal projections were compiled in series to generate time-lapse movies using Imaris image analysis software (Bitplane).

3.3.5 Histological analysis

Histological analysis was conducted as stated in Chapter 2. Antibodies used are provided Table 1. As with Chapter 2, similar ImageJ analysis was performed in *Tg(PT:EGFP); Tg(mpeg1:dendra2)* fish to quantify macrophage cell size. For these images, there was no background removal, mpeg1:dendra2 channel threshold was 53 to 255, and particle size range was 60 to infinity.

3.3.6 *In situ* hybridization

The *arginase-2* clone was synthesized and cloned into pEX-K248 with Sp6 promoter to drive the reverse transcription (Eurofins). The *arg-2* clone was synthesized and cloned into pEX-K248 with Sp6 promoter to drive the reverse transcription (Eurofins). The digoxigenin (DIG) probe for *arg-2* targeted 500bp of 3' end of coding region and 500bp of 3'UTR. 6dpf larvae were fixed in 4% PFA/PBS overnight at 4°C. Larvae were washed in PBS. Larvae were dehydrated in of MeOH and then moved to -20°C for 1hr. Larvae were transferred to acetone for 10min at -20°C. Larvae were rehydrated in PBS and treated with 100µg/ml Proteinase-K in PBS/0.2%BSA/0.1%Tween-20 (PBTw) for 30min at RT. Larvae were again fixed in 4% PFA for 20min. Larvae were incubated with the *arg-2* probe overnight at 65°C. Larvae were incubated in 1:2000 anti-DIG Alkaline Phosphatase antibody (Roche) overnight at 4°C. The larvae were stained with BM purple (Roche) RT. The reaction was stopped with 4% PFA. Larvae were then cryosectioned at 25µm and imaged using a 20X objective on an Axiovert 40 CFL brightfield scope (Zeiss). Images were captured using Axiovision Rel v4.8 software (Zeiss).

3.4 Discussion

While the zebrafish leukocyte system has been relatively well studied, its activation in the context of zebrafish AKI had not been elucidated [103,137,170,241]. Here, we demonstrated leukocyte activation in real-time during AKI, which has never been described in literature. In addition, we applied our knowledge of leukocyte activity to further characterize PTBA's role in modulating this immune environment.

Results of the neutrophil assays suggest that the larval zebrafish AKI model is comparable to mammalian AKI models, in that neutrophils serve as the first line of defense. Neutrophils are seen in the live imaging as early as 24hpi, reaching the peak of infiltration at 2 and 3dpi. No change in neutrophil numbers are observed when treated with PTBA. Given that neutrophils are the first responders within the first day of injury, it is expected that the later PTBA treatment window should not affect its infiltration. The assay of neutrophil population at 3dpi suggests that neutrophil dissolution is not affected by the compound treatment. Results show that while neutrophils are activated by AKI, PTBA has no effect on driving their infiltration or their resolution.

Results of initial macrophage recruitment assays suggest that the larval zebrafish AKI model is comparable to mammalian AKI models. As seen in mammalian AKI models, macrophage infiltration occurs following the neutrophil activation, presumably due to neutrophils conferring macrophages via chemokines and cytokines, such as G-CSF, GM-CSF, INF-γ, IL-8, MIP-1α, Type I IFNs, and Type II INF [242]. The real time imaging reveals a larger population of macrophages that are recruited to cdh17^{+} PT that are undergoing phagocytosis from 2-3dpi. PTBA treatment slightly decreases tubular macrophage infiltration when observed at 3dpi. This could be attributed to lower initial infiltration due to a healthier environment, less expression of DAMPs, thus fewer recruited macrophage. Alternatively, PTBA may play a direct role in macrophage recruitment. Time course experiments to measure RTEC-specific cytokines and chemokines may lend insight into whether the damage associated cytokines are resolved prior to recruiting macrophages.

Interestingly, macrophage polarization was altered with UPHD25 treatment. We saw a significant decrease in TNFα^{+}/mpeg1:dendra2^{+} or M1 macrophages in gent-AKI UPHD25 fish. However, we did not see a significant increase in Arg2^{+}/mpeg1:dendra2^{+} or M2 macrophages. The lack of M1 macrophages may be an indirect consequence of healthier, repaired RTECs expressing

lower inflammatory cytokines and chemokines. Conversely, PTBA may have a direct, cell-autonomous impact on polarization through modulating the RA signaling pathway. Chiba *et al*. have shown a paracrine and autocrine RA signaling interplay between two cell types: macrophages and RTECs [210]. Macrophage-derived production of RA to lower M1 population in the interstitium of the kidney. In RTECs, intact RAR expression is required to convert M1 to M2 in the interstitium to increase M2 macrophages. Furthermore, it has been shown that RA treatment inhibits the production of inflammatory cytokines and also increases of tolerance to cytokines [243]. Retinoid treatment inhibits production of IL-12 in LPS-activated macrophages by competitive inhibition of RXR and NF-kB process [244]. Vitamin A deficient mice fail to convert tissue resident macrophages during infection, leading to deregulated inflammatory response [245]. RA is anti-inflammatory effect as exogenous RA administration in diabetic nephropathy and ulcerative colitis resulted in decreased inflammatory marker via suppressing TLR-4 activation and NF-kB nuclear localization [246] [247]. Taken together, the modulation of RA pathway via PTBA may have a direct impact on macrophage transcriptional activity of inflammatory cytokine production. Taken together, this study demonstrates the very conserved nature of the leukocytic response between the larval zebrafish and mammalian AKI models. Taking advantage of the conserved nature of innate immune response, we have characterized the interaction between PTBA and the immune system.

Additional contributors to the chapter

Lauren Skvarca contributed to initial neutrophil and macrophage recruitment experiment

Material modified and re-published with permission

Brilli Skvarca L, Han HI, Espiritu EB, et al. Enhancing regeneration after acute kidney injury by promoting cellular dedifferentiation in zebrafish. *Dis Model Mech*. 2019;12(4):dmm037390. Published 2019 Apr 5. doi:10.1242/dmm.037390

4.0 *hdac8* knockout results in enhanced repair after acute kidney injury

4.1 Hypothesis

Various HDACs are expressed in the kidney and they play a complex role in development and disease progression [178]. Studies have reported confounding results due to the complexity of cellular interactions that occur during an AKI event [248] [185]. One of the challenges of HDAC inhibition studies is the nature of selectivity. Treatment with pan-HDIs results in inhibition of multiple HDACs whereas selective-HDIs inhibit one or two specific HDACs [249]. The broad inhibitory effect of most HDI is not ideal, since individual HDAC have diverse functions under physiologically different scenarios [249]. Previously, we published that PTBA, an HDI, enhances regenerative capacity in various models of AKI [155] [177] [176]. However, its direct binding target and downstream pathways have yet to be elucidated, both required knowledge to translate PTBA into a human therapeutic. In this chapter we first utilized *in vitro* and *in vivo* selectivity assays to identify HDAC8 as the target of PTBA. Then, we utilized *hdac8* mutant zebrafish to assess its roles in post-AKI repair using various assays to measure overall survival, RTEC cell cycle dynamics, transcript analysis, and bulk RNA-sequencing. I hypothesized that *hdac8* knockout zebrafish will result in enhanced repair after AKI, by affecting the acetylation state of HDAC8's downstream target that may be important for RTEC cell cycle progression.

4.2 Results

4.2.1 PTBA selectively binds to HDAC8

Based on its classic cap, linker, warhead structure, our pro-regenerative compound PTBA was identified as a class I HDI [158] [178] [148]. HDAC specificity is important to minimize unwanted binding and potential side effects. Therefore, we used cellular thermostability assay (CETSA), to assess PTBA binding to class I and class II HDAC members (Figure 21). While traditional thermostability assays uses a single protein of interest grown and isolated in culture, CETSA uses the cellular contents [250]. Because HDACs can be found in large complexes, with multiple co-factors and other proteins, we used CETSA to determine the binding specificity of PTBA to different HDACs [251]. CETSA uses the inherent thermodynamic properties of a protein's structure to determine the amount of kinetic energy required to melt the protein [252]. Each protein has a specific melt temperature (T_m), the temperature at which half of the protein is in the folded soluble form and the other half insoluble aggregate [253]. When a protein (HDAC) binds to a selective ligand (PTBA), additional energy is necessary to overcome the biophysical interactions within the protein/ligand for the protein to unfold. This results in an increase in the T_m of the HDAC/PTBA complexes compared to the unbound HDAC [254]. HEK293T cells were transfected with plasmids of specific HDACs containing an N-terminus HALO tag, then the cell lysates were incubated with 10μM PTBA, or DMSO. The samples were subjected to the thermostability gradient, visualized by Western blot, and fitted to the Boltzman constant sigmoidal curve to calculate the T_m. HDAC8 and PTBA increased the T_m compared to DMSO control by 3.43°C [255] (Figure 21A). Modification to the CETSA experiment known as isothermal dose response curves (ITDR) uses the known T_m for the protein and a concentration gradient of compound to calculate the IC50 [256]. Results showed

an IC50 of 17nM for HDAC8 (Figure 21B). Other class I HDACs did not show increased stability with PTBA (Figure 21C).

To validate that our CETSA experiment demonstrated that PTBA was binding to HDAC8, we performed CETSA on a known HDAC8 selective inhibitor, PCI-34051[257]. PCI-34051 increased the T_m by 3.46°C (Figure 21D). Further validation with ITDR for HDAC8 identified the IC50 of 8.4nM (Figure 21E). Taken together, the *in vitro* data suggests PTBA selectively binds to HDAC8 over other class 1 and class2 HDACs.

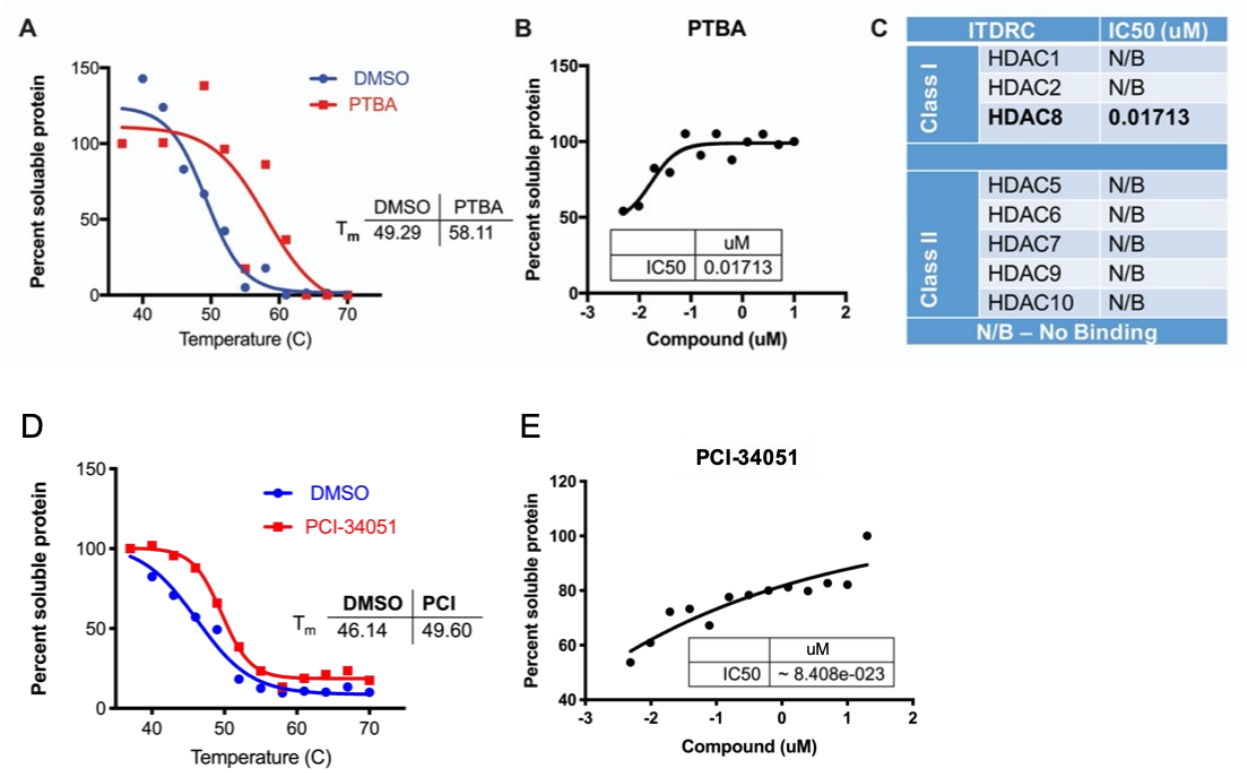

Figure 21 PTBA selectively binds to HDAC8

(A) CETSA curves of HEK297T cell lysates transfected with HDAC8-HALO tag. The lysates were incubated with 10μM PTBA or 0.1% DMSO. T_mDMSO=49.25°C. T_mPTBA=58.11°C. (B) ITDR curves of HDAC8 using log-fold concentration gradient of PTBA, incubated at 58.11°C. (C) ITDR of class I and class II HDACs were calculated using the method presented in (B). Only HDAC8 had a detectable IC50 of 17.13nM. (D) CETSA curves of HEK297T cell lysates transfected with HDAC8-HALO tag. The lysates were incubated with 20μM PCI-34051 or 0.1% DMSO. T_mDMSO=45.32°C. T_mPCI-34051=64.70°C. 3 biological replicates were performed. (E) ITDR curves of HDAC8 using log-fold concentration gradient of PCI, incubated at 49.60°C.

4.2.2 *hdac8* loss of function mutants show enhanced survival after AKI

To confirm the selectivity of PTBA against HDAC8, we used a hdac8 mutant zebrafish line, *hdac8*^{sa14948}, a T → A point-mutation resulting in an early stop codon at exon 5Figure 22A) [258]. Further amino acid alignment of the mutant allele predicted a truncation of the translated

product from 378aa to 154aa (Figure 22B). Both heterozygous (*hdac8*$^{-/+}$) and homozygous (*hdac8*$^{-/-}$) larvae were embryonically viable and reached maturity. This viability in loss-of-function organism is also observed in humans and mice. For example, adult human patients with Cornelia de Lange Syndrome (CdLS), a developmental defect due to mutations in *hdac8* showed undetectable levels of HDAC8 [187]. In mice, HDAC8 loss of function mutants showed sub-Mendelian levels of viability, and displayed a failure to thrive and usually died with 4-6hrs after birth [182]. Upon postmortem analysis, *HDAC8*$^{-/-}$ mice revealed no visible defects in the kidney, liver, heart, lung, intestine, and bladder but showed brain and skull development defects [182]. In our zebrafish larvae model, we performed transcript analyses of *hdac8*$^{-/-}$ fish using both qPCR and *in situ* hybridization at multiple timepoints, showing a distinct absence of *hdac8* mRNA, suggesting that the mutants undergo nonsense mediated decay and result in no translated protein (Figure 22C,D).

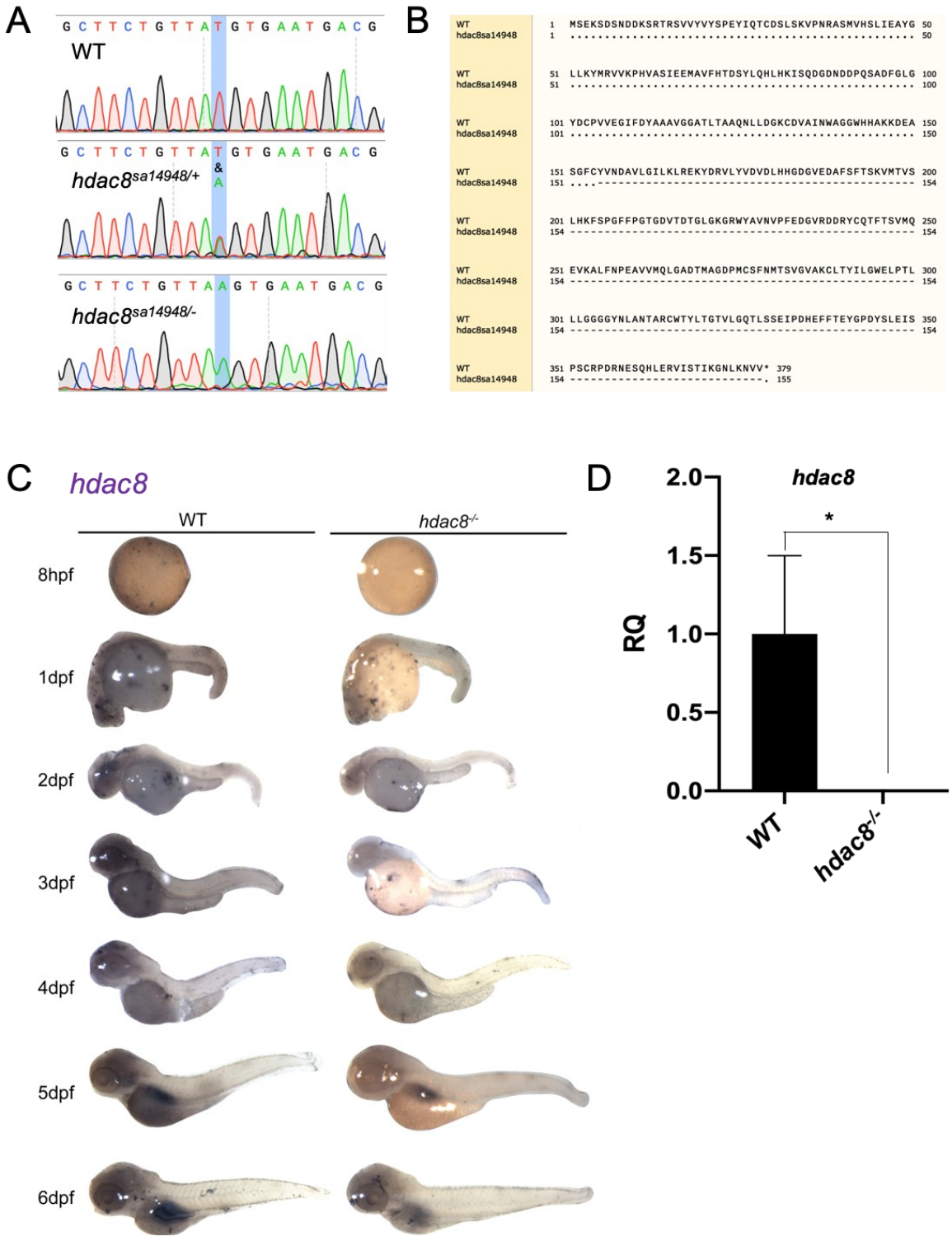

Figure 22 Characterization of *hdac8*^{sa14948} larval zebrafish

Sanger sequencing chromatogram of *hdac8*^{sa14948} site of lesion. Wildtype (WT), heterozygous *hdac8*$^{sa14948/+}$, and homozygous *hdac8*$^{sa14948/-}$. Nonsense mutation from T to A (peaks highlighted in blue) resulting in an early stop

codon at exon 5 (B) Amino acid alignment of WT HDAC8 (378aa) and predicted *hdac8*^{sa14948} HDAC8 (154aa) using Needleman-Wunsch method. • represents identical aa, - represents different aa, * represents stop codon. (C) Whole mount zebrafish *in situ* hybridization to visualize *hdac8* transcripts localization. Both WT and *hdac8*$^{-/-}$ were analyzed at various timepoints from 8hpf,1-6dpf. (D) RT-PCR of hdac8 transcript quantification of WT and *hdac8*$^{-/-}$ 2mo old adult fin clips. Student's t-test was used.

To examine whether homozygous fish were embryonically viable, *hdac8*$^{-/+}$ were in-crossed, and the resulting clutch of embryos were reared until adulthood then genotyped. The clutch showed the expected Mendelian pattern (Figure 23A). We observed a low penetrance of craniofacial deformity of 1% in all homozygous adults similar to craniofacial deformities observed both in mice and humans lacking HDAC8 [188,190] [182] (Figure 23B,C).

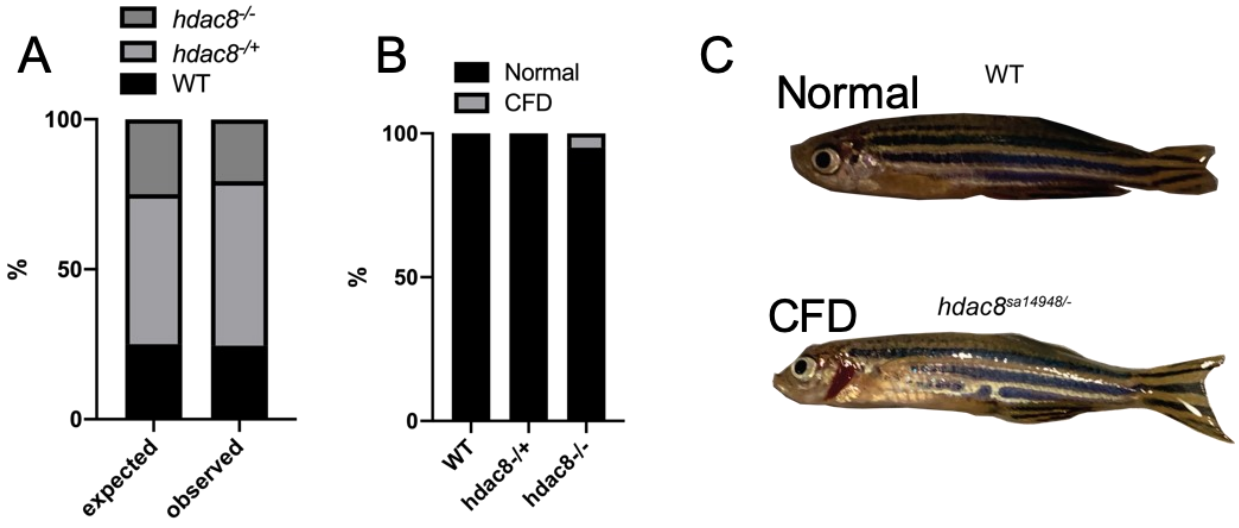

Figure 23 Characterization of *hdac8*^{sa14948} adult zebrafish

(A) Expected and observed Mendelian ratio of heterozygous in-cross to examine hdac8 mutation survivability. (B) Analysis of craniofacial deformity (CFD) frequency. Frequency of CFD was counted in 3 independent clutches. 1% of homozygous mutants displayed craniofacial deformity (C) Images depict normal (top) and CFD (bottom) phenotypes. 3 independent clutches were reared to adulthood, with total of N=102 adult fish examined.

Since we demonstrated that PTBA is a selective HDAC8 inhibitor, and the *hdac8*$^{-/-}$ were viable, we compared the survival response in WT, *hdac8*$^{-/+}$, and *hdac8*$^{-/-}$ larvae in our nephrotoxin AKI model [156] (Figure 24A). A cohort of wildtype and heterozygous and homozygous mutants were injected with gentamicin to induce gent-AKI and then observed for the rate of survival until 7dpi. *hdac8*$^{-/-}$ fish showed significantly enhanced survival compared to WT and *hdac8*$^{-/+}$ fish (Figure 24G). This data suggests the loss of HDAC8 function enhanced survival in our nephrotoxin larval zebrafish model.

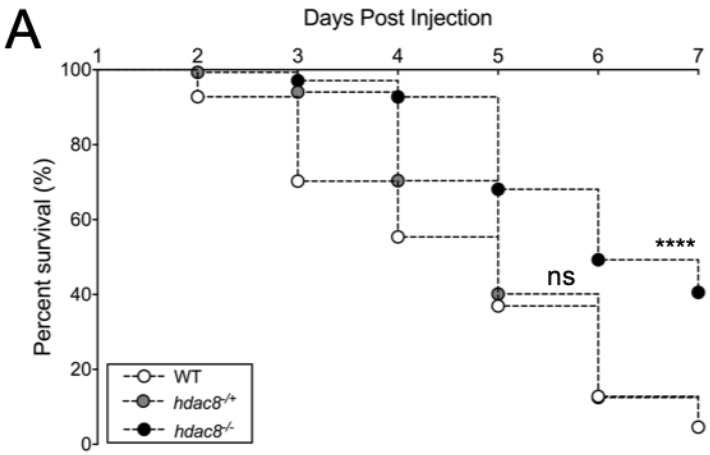

Figure 24 *hdac8* loss of function results in enhanced post-AKI survival

(A) Survival curves of gent-AKI zebrafish of WT, *hdac8*$^{-/+}$, and *hdac8*$^{-/-}$. A cohort of larvae were given gent-AKI then recorded from 1-7dpi for survival. Log-rank (Mantel-Cox) test was used compare survival to the control (white circle). 3 biological replicates were conducted. ****p<0.0001. n.s.=not significant.

4.2.3 *hdac8* is required for PTBA efficacy

Having shown PTBA selectivity to HDAC8 *in vitro*, we aimed to show PTBA selectivity to HDAC8 i*n vivo*. To confirm *in vivo* selectivity of PTBA, we assessed efficacy of the compound

with suboptimal or lack of *hdac8* expression. If PTBA selectively binds to and inhibits HDAC8 to enhance repair, then PTBA treatment in the absence of HDAC8 should result in a loss of PTBA efficacy. Zebrafish larvae treated with PTBA analog UPHD25 showed a significantly increased survival when compared to vehicle treated larvae (Figure 25A). As a known selective inhibitor of HDAC8, PCI-34051, was also used to test if pharmacological inhibition of HDAC8 would result in enhanced post-AKI survival. Gent-AKI fish treated with PCI-34051 showed an improved survival when compared to the vehicle treatment (Figure 25B). We then wanted to test the requirement of HDAC8 in PTBA efficacy. If HDAC8 inhibition is required for PTBA's efficacy, then absence of HDAC8 should render the compound ineffective, since there is no functional protein to inactivate. We first determined a suboptimal dose of UPHD25 by performing survival assays of various concentrations. Compound efficacy on survival was concentration dependent, with the highest dose (4μM) resulting in the highest survival (Figure 25C). At 1μM PTBA, survival was not significantly affected but has been previously shown to enhance cellular response to AKI (Figure 25C). Therefore, 1μM was determined as a suboptimal concentration, the lowest dosage still beneficial with minimum possibility of nonselective binding to other targets. We treated WT, *hdac8*$^{-/+}$*, and hdac8*$^{-/-}$ with 1μM UPHD25 to test if HDAC8 is required for PTBA efficacy. WT expressing functioning HDAC8 showed increased survival as expected (Figure 25D). *hdac8*$^{-/+}$also benefited from the suboptimal dose of the compound, suggesting one intact copy of *hdac8* is sufficient for PTBA to bind, inhibit, and impart benefits to post-AKI recovery (Figure 25D). However, *hdac8*$^{-/-}$ fish showed significantly lower survival compared to the siblings (Figure 25D). While unexpected, the lower survival in *hdac8*$^{-/-}$ may stem from non-specific binding of PTBA to other proteins in the absence of HDAC8, rendering the PTBA treated-*hdac8*$^{-/-}$more vulnerable to injury response.

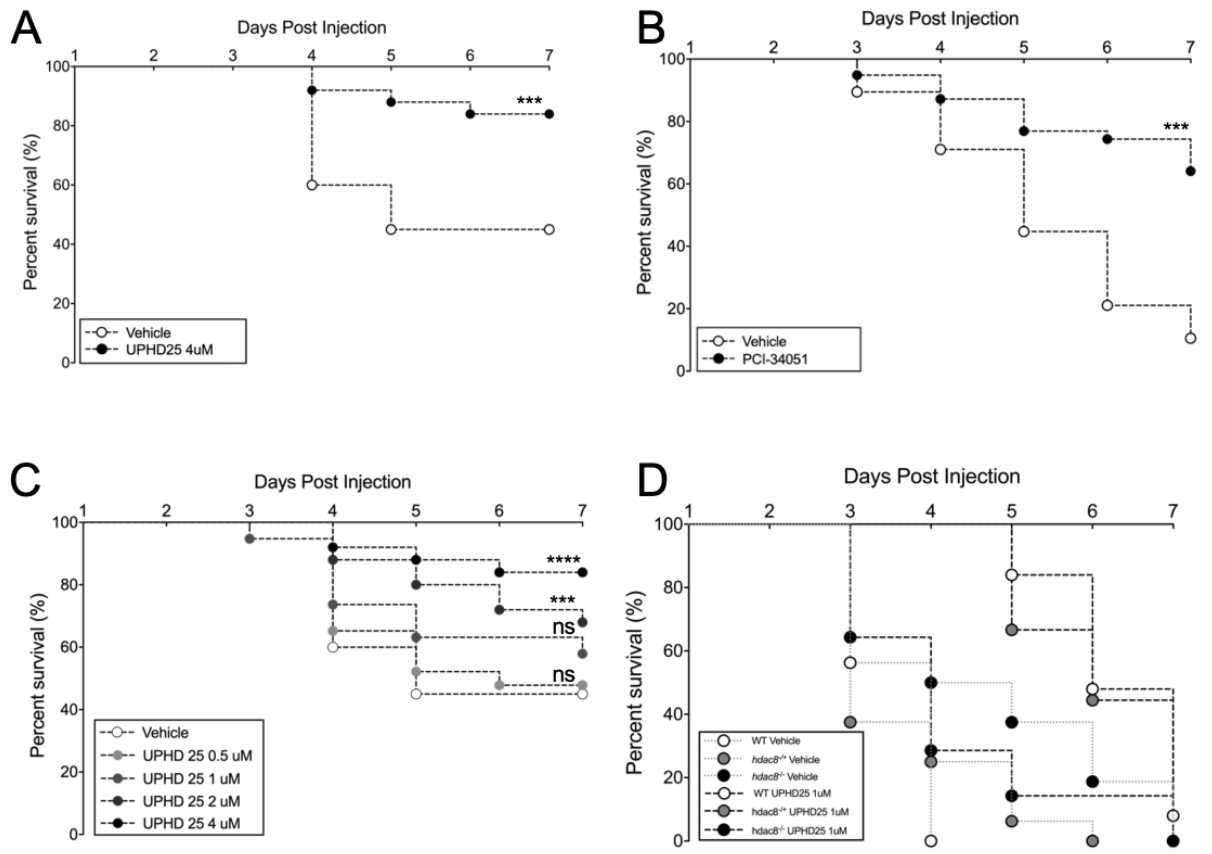

Figure 25 HDAC8 expression is required for PTBA efficacy

(A) WT fish survival curves of UPHD25 and vehicle (0.5%DMSO). (B) WT fish survival curves of known HDAC8 inhibitor, PCI-34051, and vehicle (0.5%DMSO) (C) WT fish survival curves of UPHD25 concentration gradient of 0.5μM, 1μM, 2μM, 4μM and vehicle (0.5%DMSO) to identify the suboptimal dose. A cohort of larvae were given gent-AKI then recorded from 1-7dpi for survival. Log-rank (Mantel-Cox) test was used compare survival to the controls (white circle). 3 biological replicates were conducted.*p<0.05, **p<0.01, ***p<0.001, ****p<0.0001. n.s.=not significant. (D) Survival curves of WT, *hdac8*$^{-/+}$, and *hdac8*$^{-/-}$. treated with suboptimal dose of UPHD25 (1μM) and vehicle (0.5%DMSO) 1 biological replicate was conducted.

4.2.4 *hdac8* loss of function results in cell cycle delay

Next, we examined cellular hallmarks of injury in *hdac8*$^{-/-}$. Classic hallmarks of AKI are increased RTEC cell cycling, cell cycle arrest, and proliferation, which must occur in fine balance

to achieve adaptive repair [199] [75] [65] [95]. In larval zebrafish model of AKI, RTECs show an increase in proliferation in the days following an AKI event [156] [158]. We assessed whether there is a change in the cell cycle dynamics, as HDAC8 deacetylates cell-cycle related factors, such as SMC3 [186] [201] [259] [260] [185]. We treated fish with 5-Ethynyl-2'-deoxyuridine (EdU), a thymidine analog, for 24hrs prior to harvesting, to capture the population of RTECs cells undergoing S-phase at 3 and 4dpi. At 3dpi, *hdac8*$^{-/-}$AKI had a higher population of S-phase RTECs than WT AKI (Figure 26A,B). At 4dpi, *hdac8*$^{-/-}$ AKI again showed a higher population of S-phase RTECs than in WT AKI (Figure 26A,B). To assess whether other cell cycle phases follow a similar trend, we stained with phospho-Histone3 (pH3), a marker of cells undergoing G2/M [261] [262] [263]. At 3dpi, *hdac8*$^{-/-}$ AKI showed no change in pH3 expression than WT AKI, an opposite trend than the increase in S-phase RTECs in *hdac8*$^{-/-}$ AKI (Figure 26C,D). At 4dpi, *hdac8*$^{-/-}$AKI showed a higher number of pH3^{+} than WT AKI (Figure 26C,D). At 3dpi, *hdac8*$^{-/-}$ RTECs show an increase in S-phase cell numbers but no change in G2/M. At 4dpi, *hdac8*$^{-/-}$ RTECs show an increase in S-phase cell numbers as well as well as an increase in G2/M cell numbers. Data suggests that *hdac8*$^{-/-}$ fish show a delay of cell cycle at 3dpi but allows cell cycle recovery and subsequent cell division at 4dpi.

To validate this claim, we harvested early to late (1-4dpi) RTECs and searched for indications of cellular delay and recovery. We used qPCR to quantify the expression cellular arrest marker, *cdkn1a* or *p21a*, a checkpoint inhibitor [264] [265] [266] (Figure 26E). During DNA damage, an upstream DDR response will cascade into increased expression of *p21* to arrest cells at either G1/S or G2/M [78](Figure 5, Figure 6). After injury is resolved at G1/S, *p21* expression declines to recover cell cycle progression whereas injury at G2/M is likely to result in irreversible arrest and mitotic catastrophe [78] [267](Figure 5, Figure 6). In our model, WT and *hdac8*$^{-/-}$ fish have differential expression of *p21a*. In *hdac8*$^{-/-}$AKI, *p21a* expression increases steadily from 1dpi to 3dpi then

decreases at 4dpi (Figure 26E). This correlates with the EdU and pH3 immunofluorescence data, which suggests slowing of division at 3dpi followed by recovery of cell cycling and increased RTEC division at 4dpi (Figure 26A-D). Conversely, in WT AKI *p21a* level continues to increase from 1dpi to 4dpi, which indicates irreversible cell cycle arrest and thus decline of RTEC health [20] [199] [75] (Figure 26E). Data suggests that *hdac8*$^{-/-}$ contributes to cell cycle delay up to 3dpi then recovery at 4dpi to increase in RTEC proliferation.

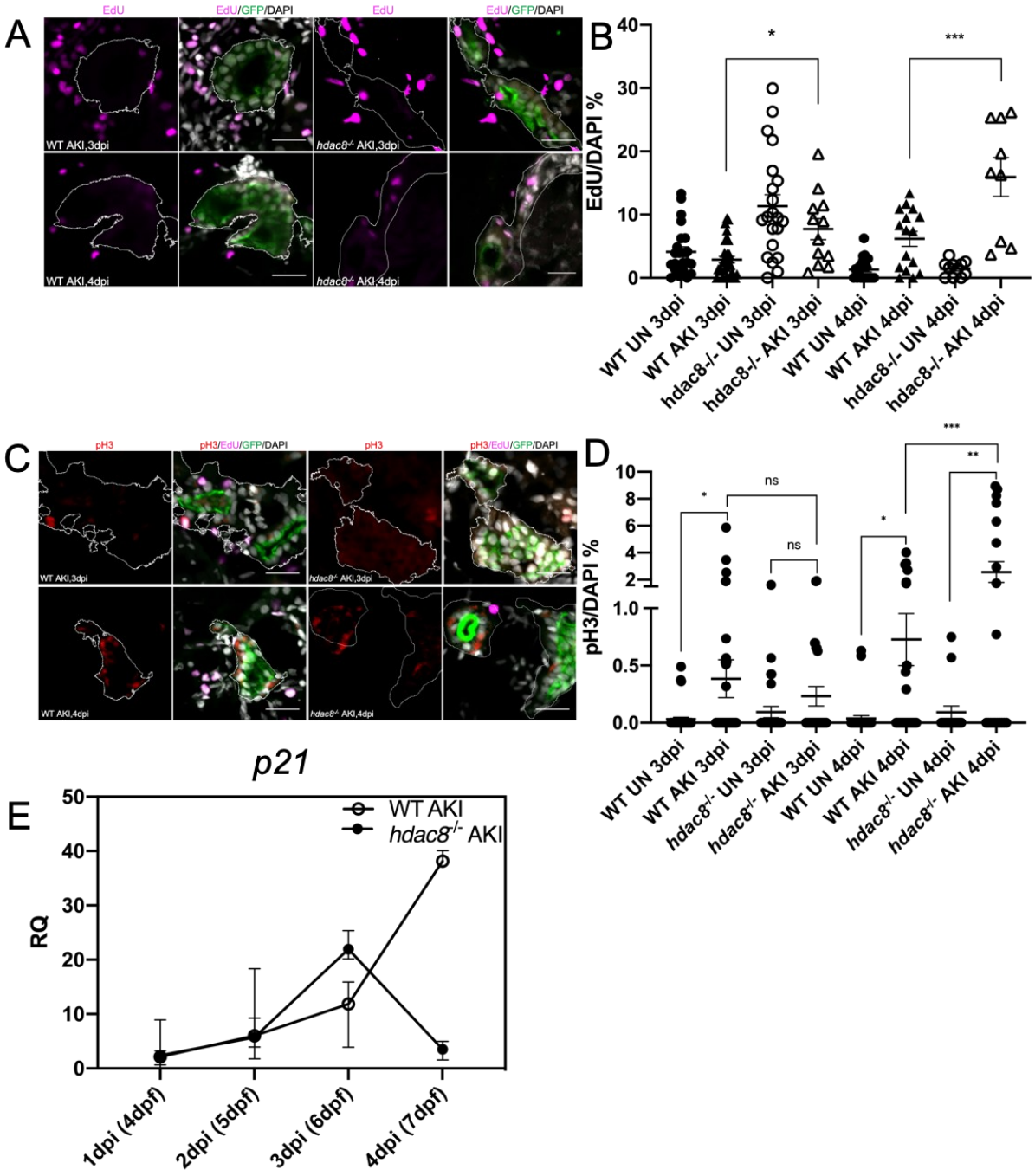

Figure 26 *hdac8* loss of function results in changes in cell cycle dynamics

(A) Immunofluorescence of EdU pulse chase to quantify S-phase cells. EdU was treated for 24h before harvesting. PT of WT AKI 3dpi, WT AKI 4dpi, hdac8-/- AKI 3dpi, hdac8-/- AKI 4dpi are captured. EdU (magenta) marks S-phase cells, GFP (green) marks PT, DAPI (grey) marks nuclei. PT are outlined in white. Scale bar= 20μm. (B) Quantification of EdU cells in PT. 3 biological replicates were conducted. 3 biological replicates were conducted.

One-way ANOVA was used for statistical analysis. Results represented as Mean +/- SEM. **p<0.01 (C)Immunofluorescence of pH3 to quantify G2/M-phase cells. PT of WT AKI 3dpi, WT AKI 4dpi, hdac8-/- AKI 3dpi, *hdac8*$^{-/-}$ AKI 4dpi are captured. pH3 (red) marks G2/M cells, GFP (green) marks PT, DAPI (grey) marks nuclei. PT are outlined in white. Scale bar= 20μm. (D) Quantification of pH3 cells in PT. One-way ANOVA was used for statistical analysis. 3 biological replicates were conducted. Results represented as Mean +/- SEM. *p<0.01 n.s.=not significant. (E) RT-PCR of *p21a* transcripts from PT cells collected from 1dpi (4dpi) to 4dpi (7dpf). White dots represent WT AKI. Black dots represent *hdac8*$^{-/-}$ AKI. RQ represents relative quantification.

To identify mechanism underlying this cell cycle change, we looked at an HDAC8 target that plays a role in cell cycle dynamics. Structural maintenance of chromosome 3a (SMC3a) is a well characterized target that acts as an essential subunit in the cohesin ring required for cell cycling, chromosome stability, DNA repair, and transcription regulation [268] [188] [269] [260] (Figure 9). The cohesin ring is loaded onto 2N chromosome at G1[200] [270]. During the replicative S phase, the resulting sister chromatids stay together via the "locked" cohesin ring [200] [270]. The "locked" conformation change is possible when N-acetyltransferase Establishment of cohesion 1 homolog 2 (ESCO2) acetylates SMC3, thereby stabilizing the sister chromatin [200] [270]. During the G2 phase, sister chromatids are maintained until mitosis when the two daughter cells undergo anaphase [200] [270]. In order to free sister chromatids, the enzyme Separase dissolves the cohesin ring and frees the individual components, including the previously acetylated SMC3^{Ac} [200] [270]. In the ensuing cell cycle, the SMC3^{Ac} must be deacetylated to allow it to bind to the 2N chromosome at G1[200] [270]. It will not be loaded onto the 2N chromosome unless it is in the deacetylated conformation [200] [270] [202] [201] [187]. HDAC8 deacetylates and changes the acetylation state from SMC3^{Ac} to SMC3 [202] [201] [187]. Without functional HDAC8, there is a higher ratio of SMC3a^{Ac} /SMC3 [186]. This higher concentration of SMC3a^{Ac} delays the efficient loading of unacetylated SMC3 onto the chromatin, thereby resulting in inefficient cell cycling and delay [184] [186]. We hypothesized that the cell cycle

delay in *hdac8*$^{-/-}$ may be attributed to an abundance of SMC3^{Ac}. To test this hypothesis, we quantified the Smc3a^{Ac} using western blot. Results showed a 2-fold increase SMC3a^{Ac} /SMC3 ratio in *hdac8*$^{-/-}$ fish compared to WT fish (Figure 27A,B)

To test our hypothesis that a cell cycle delay at 3dpi is sufficient to enhance repair, we used a pharmacological inhibition of CDK4/6, cyclin dependent kinases crucial for G1/S progression, but is a different mechanism than SMC3/HDAC8 mediated cell cycle delay. We induced gent-AKI in larval zebrafish and treated with Abemaciclib, a known G1/S cell cycle inhibitor, and observed the survival rate [271]. A cohort of wildtype fish were treated with Abemaciclib or UPHD25 for positive and vehicle for negative control. Fish treated with Abemaciclib showed a significant increase in survival over the DMSO control (Figure 27C). These results suggest that slowing the cell cycle during AKI events will promote functional repair. It is possible that *hdac8*$^{-/-}$enhance survival by using Smc3a^{Ac} as a mechanism to slow down cell cycle and drive cellular self-repair, before cellular division at 4dpi, whereas wildtypes commence division during injury without this cell cycle delay.

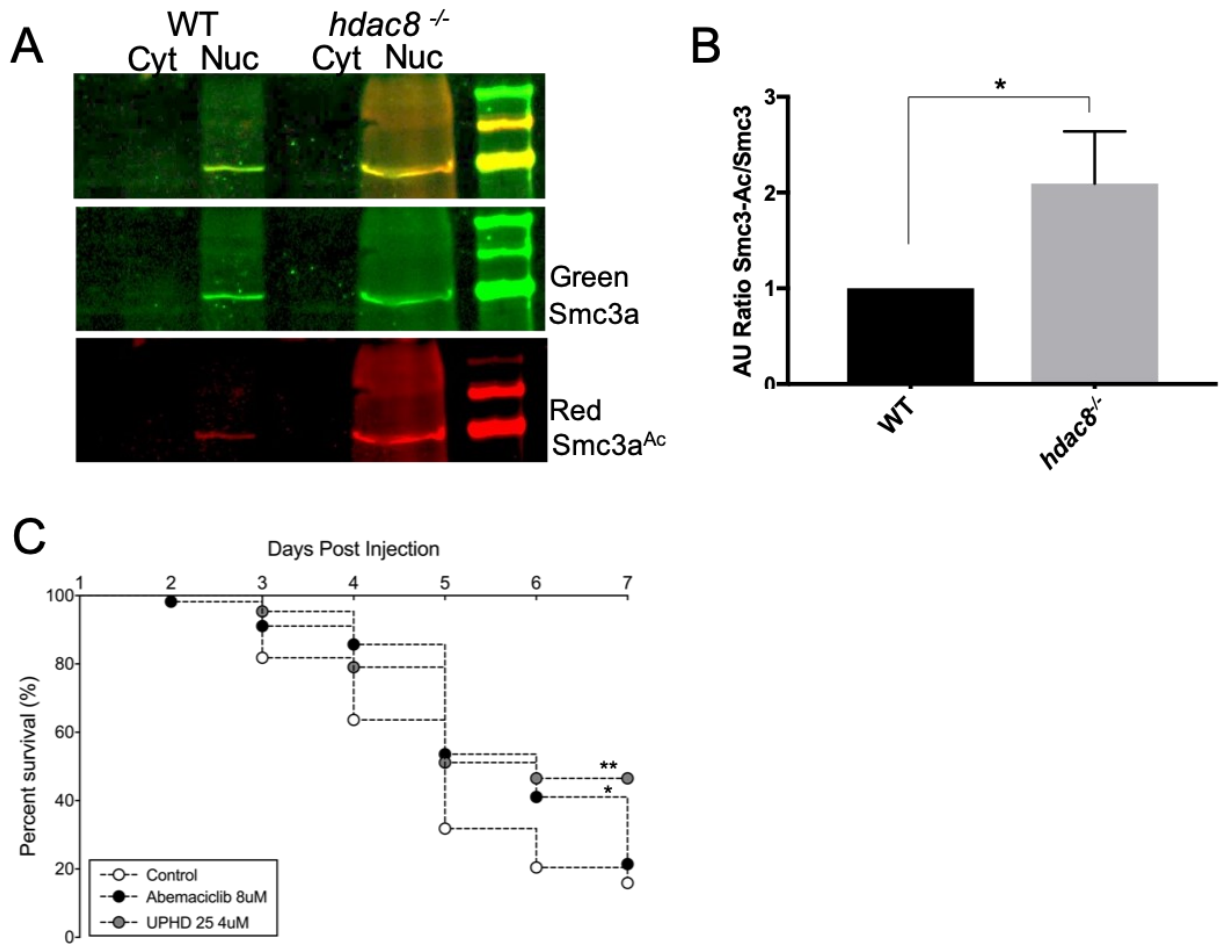

Figure 27 *hdac8* loss of function results in higher SMC3^{Ac}

(A)Western blot comparing WT and *hdac8*$^{-/-}$. Cytoplasmic and nuclear fractions were ran to identify Smc3a cellular localization. Green represents Smc3a. Red represents Smc3a^{Ac}. Yellow represents colocalization of both proteins at 130kDa. (B) Quantification of the WB. 3 biological replicates were conducted. Student's t-test was used. *$p<0.05$. (C) Survival curves of larvae treated with 8μM Abemaciclib, 4μM UPHD25, or vehicle (0.5%DMSO). Log-rank (Mantel-Cox) test was used compare survival to the control (white). 2 biological replicates were conducted.*$p<0.05$, **$p<0.01$.

4.2.5 *hdac8* loss of function reduces RTEC injury

We have demonstrated loss of *hdac8* increases survival after gent-AKI, which is associated with a pronounced cell cycle delay. However, the question remained of how the cell cycle delay is protecting against injury. Two potential hypotheses were: 1. Absence of HDAC8 function prevents damage from occurring; 2. Absence of HDAC8 function enhances repair more efficiently. To test these hypotheses, we collected PT cells of injured larvae from early to late (1-4dpi) phases of injury to establish the baseline and the progression of injury. To collect pure PT cells, we crossed *hdac8*$^{-/-}$ and WTs to *Tg(gtshb:gfp)*, a PT reporter and used FACS isolation of GFP^{+} PT RTECs [272]. 500 GFP+ PT cells were sorted from a pool of 60 larvae per condition. Using cDNA synthesized from the sorted cells, we quantified *kim-1* transcript levels, a marker of RTEC injury. In WT UN, *kim*-1expression was set at baseline during 1-4dpi. WT AKI showed 15-fold increase in expression at 1dpi and continues to decrease to 2-fold (A). *hdac8*$^{-/-}$UN had a low baseline *kim-1* expression (Figure 28A). *hdac8*$^{-/-}$AKI also had a low, baseline *kim-1* expression comparable to *hdac8*$^{-/-}$ UN (Figure 28B). In comparing WT AKI and *hdac8*$^{-/-}$AKI, we found that WT AKI had higher *kim-1* expression than *hdac8*$^{-/-}$ AKI from1-3dpi (Figure 28B). At 4dpi, WT AKI and *hdac8*$^{-/-}$AKI showed no difference (Figure 28B).

The time-course of *kim-1* expression suggested that loss of *hdac8* is protective against injury. However, *kim-1* is a downstream marker of RTEC injury. Prior to *kim*-1 transcription, many upstream damage and repair programs are activated. Upon the initial injury, cellular damage releases ROS, resulting in DNA breaks [273] [274]. This DNA damage recruits and activates ATM and ATR to the site of damage then increases *Chk* expression. CHK1 then phosphorylates STAT3 and activates the transcription of *kim-1* [275] (Figure 28C). We hypothesized the cell cycle delay mechanism alters more upstream mechanisms, leading to the resolution of damage of RTECs.

Therefore, we analyzed the expression of upstream damage response, *chk1* or *chek1*, the zebrafish homolog. The expression of *chek1* RNA-seq data showed that *hdac8*$^{-/-}$ had a 40x lower expression of *chek1* transcripts (Figure 28D), explaining lower expression of *kim-1*. Results suggest that *hdac8*$^{-/-}$ are not completely protected from injury but may have more efficient repair mechanism that resolves injury thereby preventing progression to a worsened outcome.

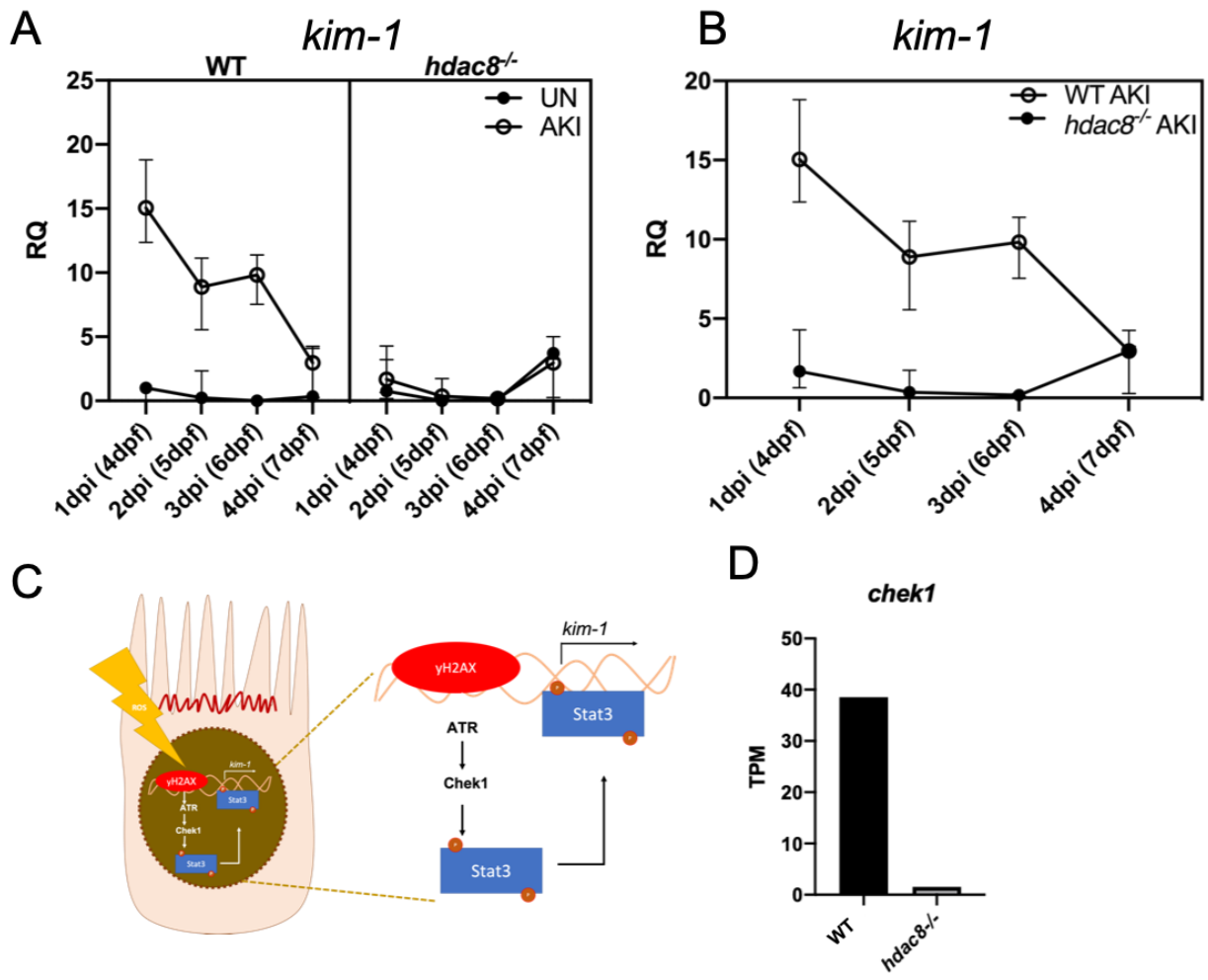

Figure 28 *hdac8* loss of function results in reduced *kim-1* expression

(A) RT-PCR of kim-1 transcripts from PT cells collected from 1dpi (4dpi) to 4dpi (7dpf). Left panel represents WT UN (black dots) and AKI (white dots). Right panel represents *hdac8*$^{-/-}$UN (black dots) and AKI (white dots). (B) RT-PCR of kim-1 transcripts from PT cells collected from 1dpi (4dpi) to 4dpi (7dpf). Comparison of WT AKI and hdac8-/- AKI. of White dots represent WT AKI. Black dots represent *hdac8*$^{-/-}$AKI (C) Proposed pathway of *kim*-1 expression by Ajay *et al.* [275]. ROS results in DNA damage and recruits yH2AX. It then triggers a cascade of DDR, starting with ATR activation, *CHEK1* expression, phosphorylation of STAT3, and ultimately transcriptional activation of *Kim-1*. (D) RNA-seq quantification of chek1 from WT AKI and *hdac8*$^{-/-}$AKI. Reads are quantified in transcripts per million (TPM).

4.2.6 *hdac8* loss of function epithelial polarity and reactivation

To further understand the extent of damage acquired in *hdac8*$^{-/-}$ fish, we looked at another marker of injury, Na^+K^+ATPase. Na^+K^+ATPase is an electrogenic transmembrane ATPase, expressed in basolateral membrane in steady state PT cells [276]. However, upon injury, the epithelial polarization is one of the first markers to be disrupted, driving RTECs to lose basolateral Na^+K^+ATPase expression [276] [72]. Injured RTECs undergo EMT process as repairing cells lose epithelial polarity, gain mesenchymal phenotype, dedifferentiate, proliferate, then re-establish epithelial polarity [72] [20] [98]. We assessed RTEC epithelial polarity via immunostaining with Na^+/K^+ATPase to assess polarity. We looked at 2 and 3dpi, in uninjured and injured WT and *hdac8*$^{-/-}$ to assess the changes in polarization over time. A semi-qualitative analysis was used score RTEC polarization in one of three states: Polarization (intact basolateral expression), partial polarization (maintains basal polarization but no distinct lateral expression), or mispolarization (complete loss of polarity) (Figure 29A-E). Results showed that at 2dpi 100% WT UN show normal basolateral polarity while 100% WT AKI fish show severe loss of polarization of Na^+/K^+ATPase (Figure 29A,B). 100% *hdac8*$^{-/-}$ UN also showed normal basolateral polarity (Figure 29C). Interestingly *hdac8*$^{-/-}$ AKI showed varying degree of RTEC polarization, with 40% of analyzed tubules showing intact polarization (Figure 29D) while 50% showed partial polarization (Figure 29E) and 10% mispolarization (Figure 29C-F). By 3dpi, *hdac8*$^{-/-}$AKI showed ameliorated RTEC health, as there was an increase in intact polarity at 60% and lower percentage of partial (30%) and mispolarized (10%) tubules (Figure 29F). Conversely, WT AKI continued to display a high percentage of mispolarized tubules at 80% and slight recovery of polarized tubules (20%) (Figure 29F). Results suggest *hdac8*$^{-/-}$ may lead to more efficient EMT and redifferentiation

to regain the polarized epithelial phenotype whereas WT further remain in mesenchymal state resulting in deterioration of cellular health.

We then quantified Pax2a, a developmental renal specification gene, which becomes reactivated during injury and contributes to new proliferating cells [158] [60] [98]. Since we observed *hdac8*$^{-/-}$ fish with less *kim-1* and better polarization, we hypothesized that Pax2a would be enhanced to repair and repopulate the epithelium. Using immunofluorescence, we quantified Pax2a counts at 3dpi, a known time point that has shown an increase in Pax2a in WT AKI as outlined in the previous chapter (Figure 10). Results showed that injury increased Pax2a expression in both WT and *hdac8*$^{-/-}$ (Figure 29G). *hdac8*$^{-/-}$AKI shows a significantly higher Pax2a than WT AKI (Figure 29G,H). Overall, results suggest that *hdac8*$^{-/-}$still accumulates injury, as indicated by a change in Na^+K^+ATPase polarity. However, mutants are protected from further progression of injury, as indicated by the lower expression of *chek1* and *kim-1*. Moreover, there is higher expression of epithelial genes and lower expression of mesenchymal genes in the mutants, suggesting *hdac8* loss of function results in more efficient EMT and repolarization of RTECs. The injury is reversed more efficiently in the mutants, as seen in the increase expression of Pax2a in the mutant RTECs.

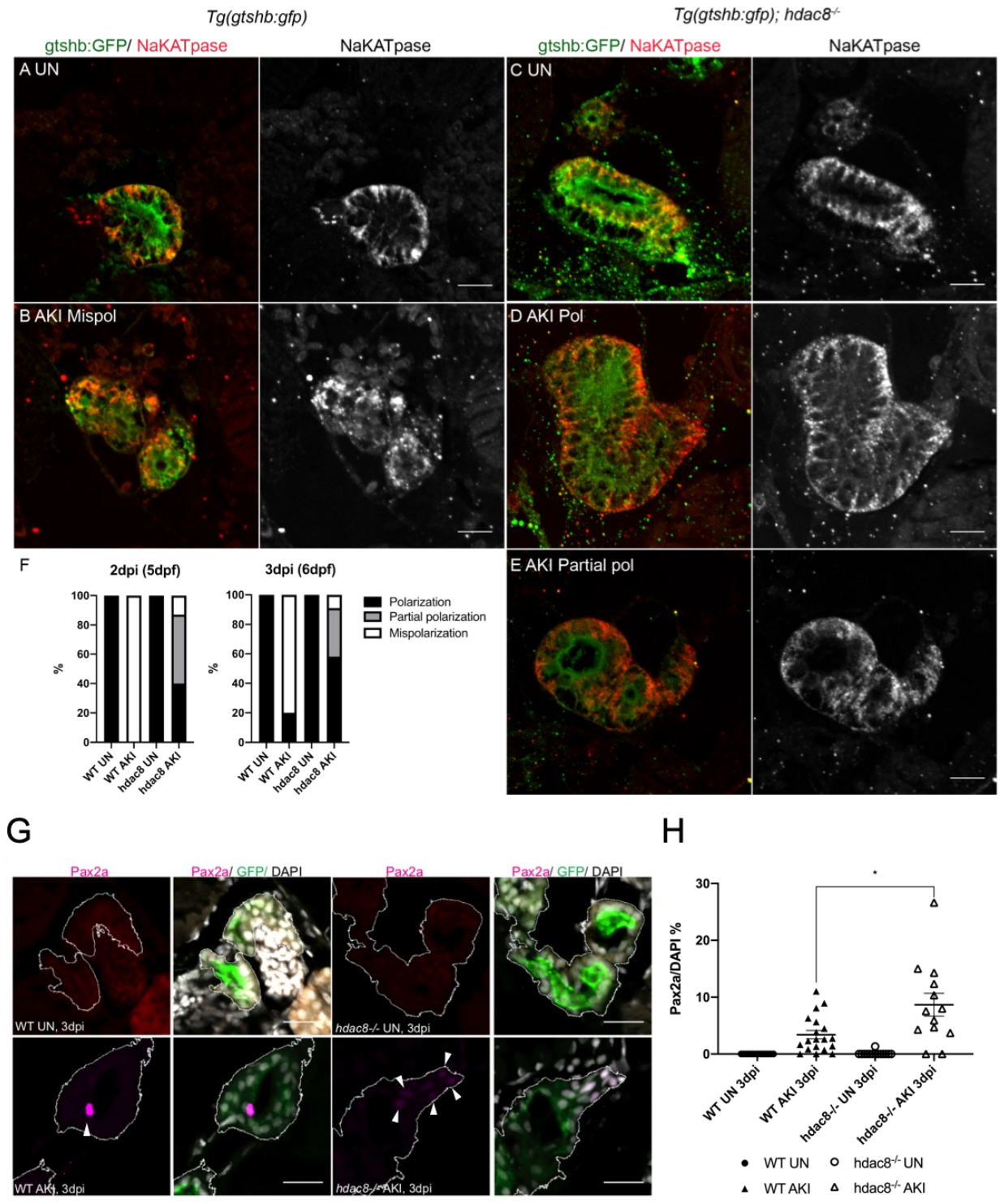

Figure 29 *hdac8* loss of function enhances Na^+K^+ATPase polarity and Pax2a expression

(A-F) Immunofluorescence staining of Na^+K^+ATPase to quantify polarization of RTECs. PT of WT UN 3dpi, WT AKI 3dpi, *hdac8*$^{-/-}$UN 3dpi, *hdac8*$^{-/-}$AKI 3dpi are captured. Na^+K^+ATPase (red and grey) marks polarization state,

GFP (green) marks PT. PT are outlined in white. Scale bar= 20μm. (F) Semi-qualitative quantification of Na^+K^+ATPase. Each tubule is scored from 1 of 3 categories: Polarization (black), Partial Polarization (grey), and Mispolarization (white). Polarization state was quantified for 2dpi and 3dpi fish. (G)Immunofluorescence staining of Pax2a (magenta) RTECs. PT of WT UN 2dpi, WT AKI 2dpi, *hdac8*$^{-/-}$ UN 2dpi, *hdac8*$^{-/-}$AKI 2dpi are captured. Pax2a (magenta), GFP marks PT (green), and DAPI marks nuclei (grey). PT are outlined in white. Pax2a are marked with white arrows Scale bar= 20μm.(H) Quantification of Pax2a+ RTECs. One-way ANOVA was used for statistical analysis. Tukey's multiple comparison test was used for post-hoc. Data pooled from 3 biological replicates are shown expressed as mean+/-SEM. *$p<0.05$.

4.2.7 *hdac8* loss of function results in enhanced DNA damage response and lower apoptosis

We have shown that AKI in *hdac8*$^{-/-}$ larvae result in RTEC mispolarization but not a concomitant increase in *kim-1* expression (Figure 28, Figure 29). This may be due to repair of damage upstream to *kim-1* while the cell cycle is arrested. Others have also demonstrated that the cell cycle delay can be a beneficial repair mechanism since it can allow enough time for resolution of genotoxic stress via various DDR mechanisms before mitosis [277 278 279 280]. Without proper DDR, mitosis causes genome instability, resulting in necrosis and apoptosis [280 278]. To test if *hdac8*$^{-/-}$ mutants showed enhanced upstream DNA repair process, I used immunofluorescence assay to quantify phospho-gamma H2AX (p-H2A.X), the earliest indicator of DDR [281 277 279]. Results show that WT UN and *hdac8*$^{-/-}$ UN both have low expression of p-H2A.X$^+$ RTECs (Figure 30A,B). However, in AKI setting, *hdac8*$^{-/-}$ have higher p-H2A.X expression than WT AKI, suggesting more damage is being recognized by the DDR complexes. Upon DNA damage, cells undergo complex fate determination leading to DNA repair and cell cycle recovery, or apoptosis [78].

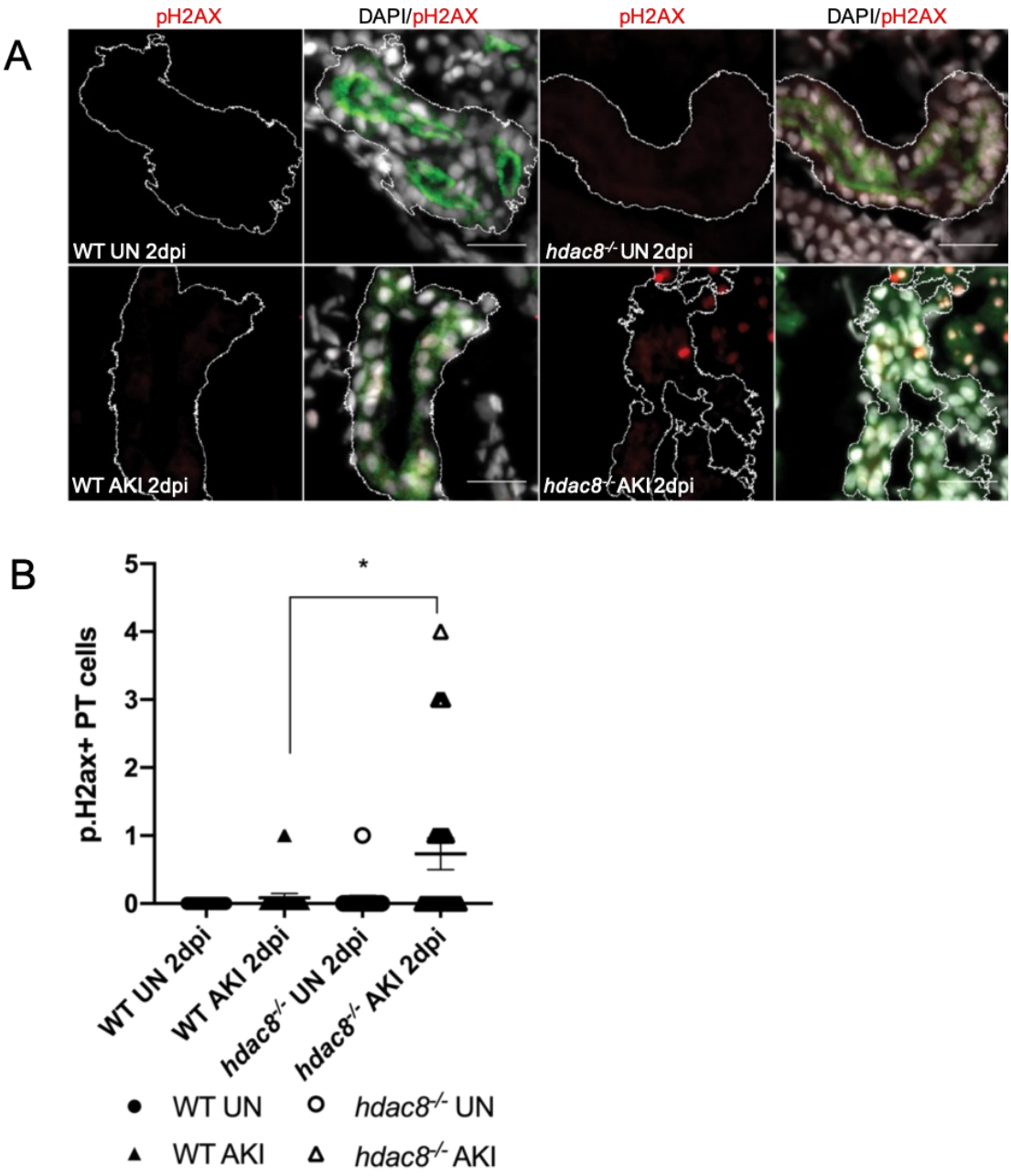

Figure 30 *hdac8* loss of function results in enhanced DNA damage response

(A) Immunofluorescence of p-H2A.X to quantify DNA damaged RTECs. PT of WT AKI 2dpi, WT AKI 2dpi, hdac8-/- AKI 2dpi, hdac8-/- AKI 2dpi are captured. p-H2A.X (red) marks DNA damaged cells, GFP (green) marks PT, DAPI (grey) marks nuclei. PT are outlined in white. Scale bar= 20μm. (B)Quantification of p-H2A.X cells in PT. One-way ANOVA was used for statistical analysis. Tukey's multiple comparison test was used for post-hoc. Results represented as Mean +/- SEM. *$p<0.05$

To test if *hdac8*$^{-/-}$ increase in p-H2A.X are fated to be repaired or undergo apoptosis, we utilized terminal deoxynucleotidyl transferase dUTP nick-end labeling (TUNEL) to quantify apoptotic RTECs. Results showed that WT UN and *hdac8*$^{-/-}$ UN both had a low expression of TUNEL+ RTECs (Figure 31A,B). However, in AKI setting, WT AKI and *hdac8*$^{-/-}$ AKI had increased apoptosis compared to WT UN and *hdac8*$^{-/-}$ UN, respectively (Figure 31A,B). WT AKI showed a significantly higher expression of TUNEL+ RTECs than in *hdac8*$^{-/-}$AKI (Figure 31A,B). Overall, these results suggest that *hdac8*$^{-/-}$show increased DDR while preventing RTEC apoptosis. The early DDR mechanism may protect the downstream *kim-1* expression and prevent further damage.

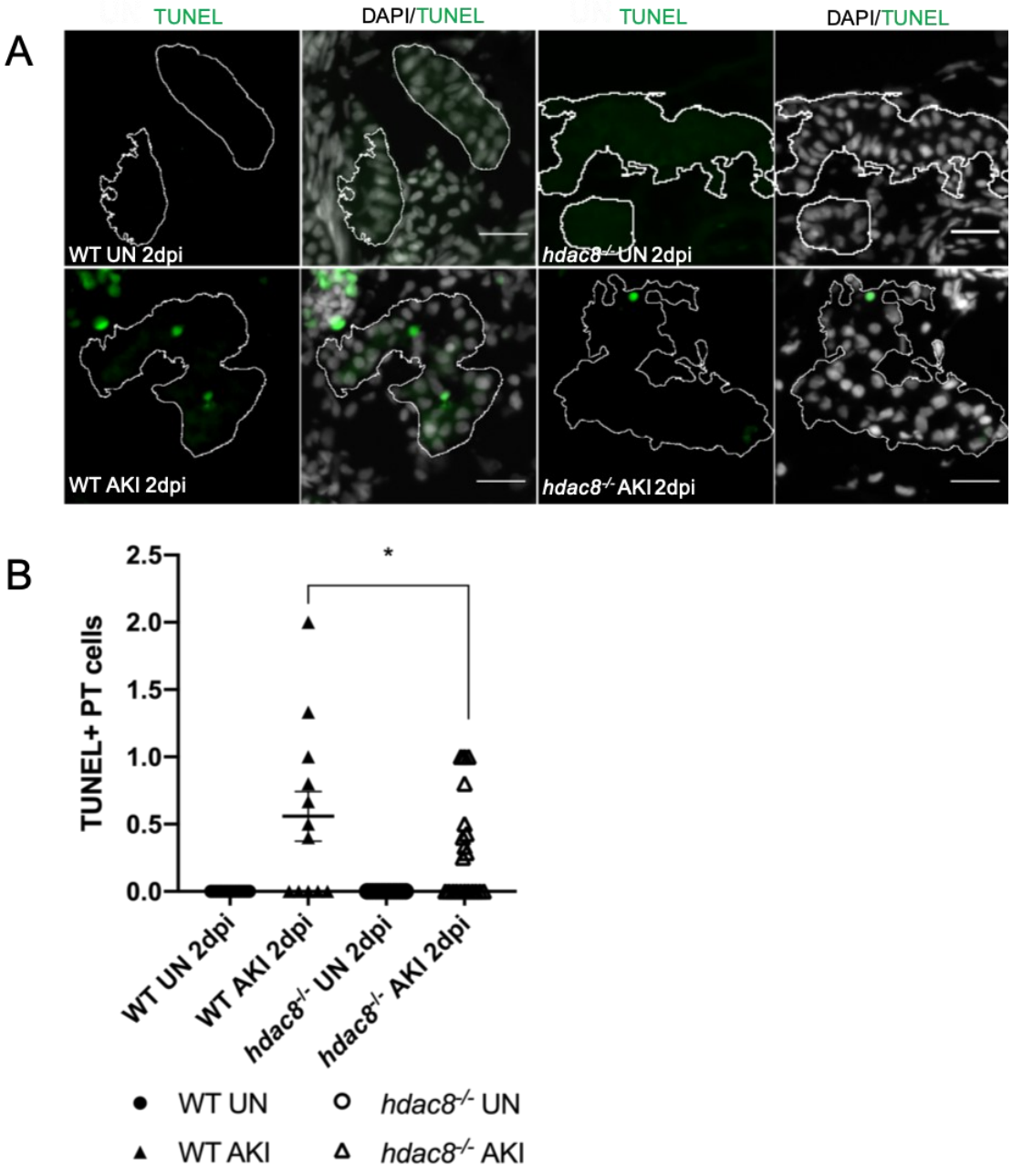

Figure 31 *hdac8* loss of function results in lower apoptosis

(A) Immunofluorescence of TUNEL to quantify apoptotic RTECs. PT of WT UN 2dpi, WT AKI 2dpi, *hdac8*$^{-/-}$UN 2dpi, *hdac8*$^{-/-}$AKI 2dpi are captured. TUNEL (red) marks apoptotic cells, GFP (green) marks PT, DAPI (grey) marks nuclei. PT are outlined in white. Scale bar= 20μm. (B) Quantification of TUNEL+ cells in PT. One-way ANOVA was used for statistical analysis. Tukey's multiple comparison test was used for post-hoc. Results represented as Mean +/- SEM. *$p<0.05$

4.2.8 RNA-seq shows EMT and cell cycle delay in *hdac8* loss of function mutants

We performed bulk RNA-sequencing with 3dpi fish to identify pathways that activate prior to and responsible for the subsequent cell cycle recovery at 4dpi. We crossed *hdac8*$^{-/-}$ mutants and WTs to *Tg(gtshb:gfp),* and sorted as explained previously [272]. Four conditions and two biological replicates were collected and sequenced: WT UN, WT AKI, *hdac8*$^{-/-}$ UN, *hdac8*$^{-/-}$ AKI (Figure 32A). In order to validate the RNA-seq data, we compared transcripts of *kim-1* and *p21,* two genes previously quantified by RT-PCR (Figure 32B,C). *kim-1* was lower and *p21* was higher in *hdac8*$^{-/-}$ AKI than in WT AKI*,* both in agreement with the previously reported RT-PCR results (Figure 26, Figure 28). In addition, we analyzed EMT-related genes, as previous Na^+K^+ATPase polarity data suggested *hdac8*$^{-/-}$ AKI mutants show enhanced epithelial polarity at 3dpi. Along with *atp1a1a*, the subunits that heterodimerize to form Na^+K^+ATPase, we also quantified genes that have been cited to be involved in EMT transition in RTECs [72] [73]. Trends suggest WT AKI had more mesenchymal gene expression while *hdac8*$^{-/-}$ AKI had more epithelial gene expression (Figure 32D). We then generated a list of genes that were highly upregulated between WT UN and WT AKI but downregulated between *hdac8*$^{-/-}$UN and *hdac8*$^{-/-}$AKI (Figure 32E). The list of genes were processed through g:Profiler to acquire a list of enriched pathways, specific to the zebrafish genome [282]. At 3dpi, *hdac8*$^{-/-}$ showed lower expression of genes related to innate immune system recruitment, sister chromatid cohesion, mitotic spindle checkpoint (Figure 32F). Results suggested that genes specifically downregulated in *hdac8*$^{-/-}$ AKI are genes associated with cell divisions and sister chromatid cohesion, which further validates our hypothesis that cell division is halted via downregulating SMC3a (Figure 27). Moreover, the results also present candidate mechanisms to study in the future in context of HDAC8 and the innate immune system. Results show *hdac8*$^{-/-}$AKI show lower immune system response, which parallels with our previous finding that PTBA lowers

macrophage recruitment, as well as a reduction of the M1 inflammatory macrophages [158](Figure 18, Figure 20). Taken together, the RNA-seq results not only further validate the previously explored results but also allows us to further investigate potential genes and pathways of interest in the future.

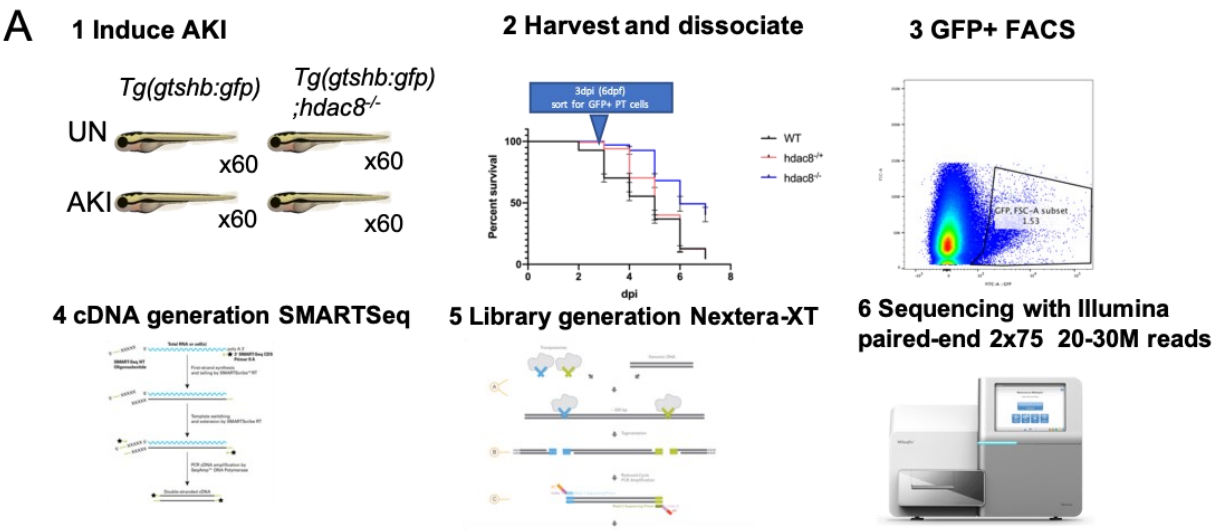

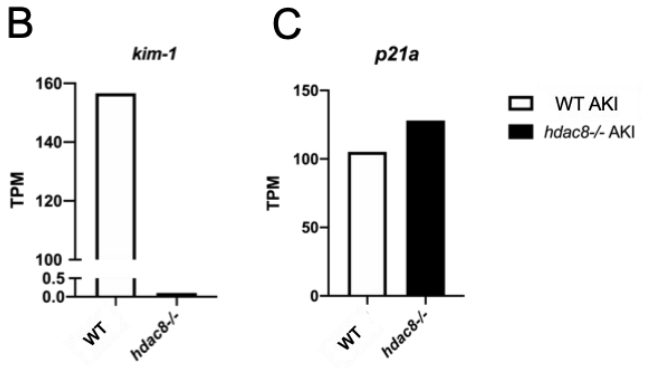

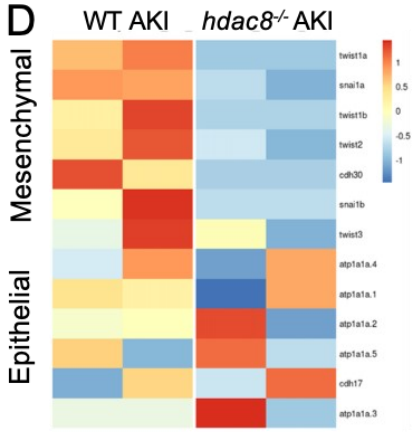

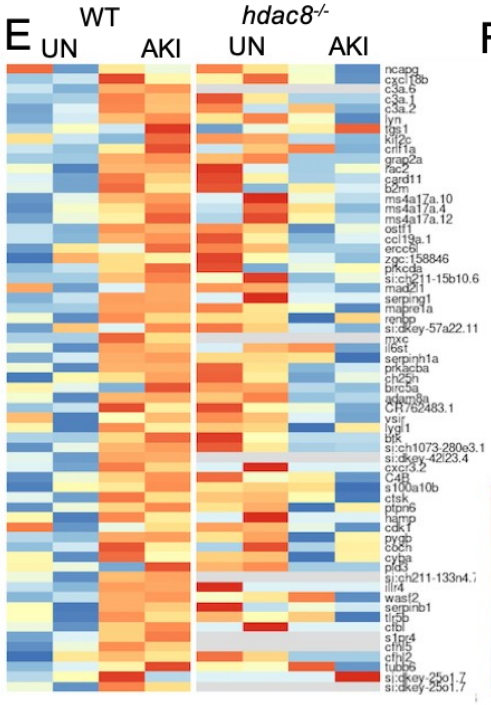

F

Term name	Term ID	Padj	−log10(Padj)
RHO GTPase Effectors	REAC:R-DRE-1...	1.120×10^{-5}	
Innate Immune System	REAC:R-DRE-1...	5.198×10^{-4}	
Signaling by Rho GTPases	REAC:R-DRE-1...	8.585×10^{-4}	
Immune System	REAC:R-DRE-1...	3.256×10^{-3}	
Resolution of Sister Chromatid Cohesion	REAC:R-DRE-2...	6.251×10^{-3}	
RHO GTPases Activate NADPH Oxidases	REAC:R-DRE-5...	1.194×10^{-2}	
Amplification of signal from the kinetochores	REAC:R-DRE-1...	1.240×10^{-2}	
Amplification of signal from unattached kinetochores vi...	REAC:R-DRE-1...	1.240×10^{-2}	
Mitotic Spindle Checkpoint	REAC:R-DRE-6...	2.867×10^{-2}	

Figure 32 RNA-seq reveals *hdac8* loss of function mitigates EMT, immune response, and cell cycle delay. **(**A) Experimental schematic of RNA-sequencing. *Tg(gtshb:gfp)*, PT specific reporter line, was crossed to both WT and *hdac8*$^{-/-}$. WT UN, WT AKI, *hdac8*$^{-/-}$UN, and *hdac8*$^{-/-}$AKI were used for RNA-seq. 60 fish per group were pooled and dissociated. 500 GFP+ PT cells were isolated using FACS. SMARTSeq HT was used to generate cDNA and Nextera-XT was used for library generation. Illumina was used for paired-end 2x75bp to generate 20-30M reads per sample. Experiment was done in 2 biological replicates and all samples were sequenced on the same day to reduce batch effects. (B-C) Transcripts per million of *kim-1* (B) and *p21a* (C) from RNA-seq data. WT AKI (white) and *hdac8*$^{-/-}$AKI (black) were quantified .(D)Heatmap of mesenchymal and epithelial genes from the RNA-sea data. Each column represents a biological replicate. (E) Heat map of genes upregulated in WT AKI and selection of genes with opposite response in *hdac8*$^{-/-}$ AKI. Differential expression analyses of WT and *hdac8*$^{-/-}$ were carried out independently then qualitatively identified based on the opposite expression pattern. In WT and *hdac8*$^{-/-}$ comparisons, genes represented were filtered to meet the criteria of FDR p<= 0.05. Each column represents one biological replicate (F) List of enriched pathways with the list of genes generated (E) using g:Profiler. Selected pathways of interest, immune system, sister chromatid cohesion, mitotic checkpoint, are selected (red).

4.3 Methods

4.3.1 Zebrafish husbandry

Zebrafish husbandry was performed as in Chapter 2

4.3.2 Gentamicin microinjection

Gentamicin microinjection was performed as in Chapter 2

4.3.3 Survival assays

After gentamicin injections at 3dpf, each larva was placed in a well of a 48-well plate. The larvae were incubated in E3 medium with 50μg/ml penicillin/streptomycin. A cohort of 20-30 larvae were observed for death every day up to 7dpi.

4.3.4 Compound treatment

Compound treatment was performed as stated in Chapter 2

4.3.5 CETSA

4.3.5.1 CETSA intact cells

HEK293T cells were transfected with plasmids of specific HDACs containing an N-terminus Halo tag. Cells were gently washed with TBS three times. 2.5ml of CETSA buffer (TBS+Halt protease inhibitor cocktail), (Thermo Fisher Scientific, Cat No.: 78430) was added to the plate and gently pipetted up and down to remove the intact cells. The cell suspension was then and pipetted into 5ml tube. 620ml of cell suspension was transferred to a 1.5ml centrifuge tube and treated with compound to a final concentration of 10μM. The same volume of DMSO was added to separate aliquot for the negative control. Cells were incubated at 37°C for 1hr. Then, 45ml of cell suspension and compound were aliquoted into 12 PCR tubes. Each individual sample was heated to a single temperature on a gradient ranging from 37-70 in 4°C increments for 5mins, followed by 1min at 4°C before cooling on ice. The samples were flash frozen in liquid nitrogen followed by thawing at room temperature three times.

4.3.5.2 CETSA cell lysates

HEK293T cells were transfected with plasmids of specific HDACs containing an N-terminus Halo tag. Cells were gently washed with TBS three times. 2.5ml of CETSA Lysis buffer (TBS+ Halt protease inhibitor cocktail, 0.80% NP-40), (Thermo Fisher Scientific) was used to scrape cells off the plate. Cell lysis was incubated on ice for 30mins followed by sonication for 30secs at 10% intensity for 0.5secs pulsing. Cell lysates were then spun for 10mins at 4°C at high speed to pellet insoluble components. Supernatant was removed and aliquoted into 620µl in1.5ml centrifuge tubes and treated with compound to a final concentration of 10µM.The same volume of DMSO was added to separate aliquot for the negative control. Lysates were incubated at 37°C for 1hr. Then, 45µl of lysates and compound were aliquoted into 12 PCR tubes. Each individual sample was heated to a single temperature on a gradient ranging from 37-70 in 4°C increments for 5mins, followed by 1min at 4°C before cooling on ice

4.3.5.3 Isothermal dose response curve

Cell lysates or intact cells were prepared as in the CETSA assays above. 45µl samples were aliquoted into 12 PCR tubes and treated with 1:1 dilution series of compound with 10µM as the highest concentration. Samples were incubated at 37°C for 1hr followed by incubation at 45°C for intact cells and 52°C for cell lysates for 5mins followed by cooling at 4°C for 1min before cooling on ice.

4.3.5.4 CETSA/ITDR Western blot

The samples were the run on a Sorval RC-6 centrifuge with a microplate rotor for 30mins at 4000xG. 25ml of supernatant was removed mixed with 5ml 5x loading buffer (bromophenol

blue (0.25%) DTT (dithiothreitol; 0.5M)glycerol (50%) SDS (sodium dodecyl sulfate;10%) Tris-Cl (0.25M, pH 6.8). The samples were heated at 95°C for 5mins followed by 1min at 4°C. Samples were spun on a small tabletop centrifuge for 3secs. 25µl of the samples were separated on a 10% SDS-acrylamide gel, and transferred to a 0.45µm MilliporeSigma™ Immobilon™-FL PVDF Transfer Membranes (Thermo Fisher Scientific, Cat No.: IPVH00010) and probed with 1:1000 dilution of mouse anti-HaloTag antibody (Promega, Cat No.: G9211). Infrared dye-conjugated secondary antibodies (Li-COR) were used according to the manufacturer's specifications. Antibody staining intensity was quantified using an Odyssey CLX system. The percent soluble protein was normalized to 37°C for all samples and was fit to the Boltzmann constant sigmoidal curve using GraphPad Prism (GraphPad Software, La Jolla California, v7)

4.3.6 Fin clip and genotyping

Adult fish were placed in tricaine until gill movement slows and becomes erratic. The 1/3 of the caudal fin was cut with a clean scalpel and placed in PCR tube. To PCR tube containing fin, 50µl DNA lysis buffer (10mM Tris pH8.4/ 50mM KCl/ 1.5mM MgCl2/ 0.3% Tween-20/ 0.3% NP-40) was added to each fin clip. The wells were incubated for 20mins at 94ºC and cooled to 55ºC. Using the repeat pipette, 5µl 10mg/ml proteinase K was added per tube and incubated for 1hr at 55ºC followed by 94ºC for 20 min.

To genotype *hdac8*^{sa14948}, a custom Taqman SNP genotyping assay was designed at the site of SNP (Thermo Fisher Scientific; Cat No.: 4332077, Assay No: AN7DPND). Reaction was mixed using 2.5µl of 2x TaqMan Genotyping Master Mix (Thermo Fisher Scientific, Cat No.: 4371355), 0.25µl 20x Taqman SNP genotyping assay, 1.75µl H2O, and 1µl of DNA. The assay was ran in a

384-well plate and the Genotyping Assay function was used in QuantStudio 12K Flex Real-Time PCR system (Thermo Fisher Scientific, Cat No.: 4471090).

4.3.7 Histological analysis

Samples were stained as Chapter 2. Antibodies used are provided Table 1.

4.3.8 EdU incubation

Fish were treated with 500μM EdU (diluted in 1%DMSO and E3) for 24hrs capture cells undergoing cell cycling for 24hrs prior to collection. Sections were fixed and sectioned as described in Chapter 2. Protocol was slightly adjusted from Click-iT Plus EdU Cell Proliferation Kit for Imaging, Alexa Fluor 647 (Thermo Fisher Scientific, Cat No.: C10640). Cryosectioned samples are washed using PBS 3 times. Freshly made 1x buffer additive was made for each assay by diluting 10x buffer additive with water. For each slide, 130μL of the reaction cocktail was made (111.8μL 1x Click-IT buffer, 5.2μL CuSO4, 0.321μL Alexa fluor 647 azide, and 13μL 1x buffer additive). Slides were incubated for 1hr at room temperature. Slides were then washed using PBS 3 times.

4.3.9 TUNEL assay

Cell death was detected using *In Situ* Cell Death Detection Kit and the provided protocol was adapted for zebrafish tissue (Millipore Sigma, Cat No.: 11684795910). Sections were fixed and sectioned as described in Chapter 2. Slides were washed with PBS 3 times. Permeabilize

sections with sodium citrate buffer (10mM sodium citrate, 0.05% Tween-20, pH 6.0) for 10mins at 95°C and cool for 1min. Remove 100uL Labelling solution for negative control. For positive control, incubate slides with 30U/ml DNase for 10mins at RT prior to Enzyme and Labelling solution mixture incubation. Add Enzyme solution to 450μL Labelling solution. Mix via pipetting and keep on ice. Incubate slides with Enzyme and Labelling solution mixture at 37°C for 1hr. Wash with PBS 3 times. Stain nuclei with DAPI as described in Chapter 2.

4.3.10 Na^+K^+ATPase staining and embedding

4.3.10.1 Fixation and staining

10-15 fish at 5-7dpf were fixed using 1ml Dent's (80% MeOH, 20% DMSO) for 4hrs at RT. They were rehydrated using MeOH/ PBT (PBS with 0.5% Tween20) series from 75%, 50%, 25% MeOH, each wash for 20mins. Fish were washed with PBT for 20 mins, careful not to expose them in air. Fish were incubated in blocking solution (PBS with 1% DMSO, 0.5% Tween20, 10% normal goat serum) for 3hrs at 4 °C on a nutator. Fish were incubated with mouse anti-Na^+/K^+ATPase antibody at 1:25 (Developmental Studies Hybridoma Bank, a6F) with incubation solution (PBS, 1% DMSO, 0.5% Tween20, 2% Normal goat serum) overnight at 4°C on a nutator. Samples were washed with incubation solution for 30 mins, three times. Fish were incubated with secondary antibody (Goat anti-mouse Alexa fluor 594, Abcam, ab150116) at 1:500 using incubation solution (fixation and embedding will give off autofluorescence at FITC channel). Samples were washed with PBT for 30 mins, three times.

4.3.10.2 Embedding

Stained tissues were dehydrated using EtOH/PBT series from 50%, 75%, 100% EtOH. JB-4 embedding solutions were prepared (Polysciences, 00226-1): Solution1 Infiltration solution: 25mL of solution A and 0.25g of plasticized benzoyl peroxide; Solution2 Embedding plastic: 35µL of solution B per 1mL of Infiltration solution. Fish were incubated with the pre-made infiltration solution for 30min at room temperature. Infiltration can be stored in 4°C for up to 1 month. Molding was labeled and filled with 2ml prepared embedding plastic. Working in small volumes (5-10mL) will reduce the exothermic reaction of the catalyst and will slow down the polymerization process and allow longer time to embed samples. 5-10 samples were mounted per mold. EBH-2 Block Holders (Polysciences, 15899) were used as a chuck for samples. For proper polymerization, the mounted samples were stored in a vacuum overnight at room temperature.

4.3.10.3 Sectioning

The mounted and polymerized samples were sectioned at 4µM transversally using a Shandon Finesse microtome (Thermo Fisher Scientific). Sections containing pronephros were collected on glass slides over DI water. Slides containing sections were incubated on 45°C slide warmer and stored until completely dry. Sections were cover slipped and imaged using confocal microscopy as described in Chapter2.

4.3.11 Zebrafish larvae homogenization

The protocol was adapted from Bresciani *et al* [283]. Dissociation mix was using 460µl 0.25% trypsin-EDTA + 40µl Collagenase 100 mg/ml. DMEM-10% FBS was prepared. They were made from fresh aliquots each time. The solutions were pre-heated at 30°C. The rest of the protocol was

carried out at room temperature with as little delay as possible to maintain cell survival. 30 zebrafish larvae of age 4-7dpf were anesthetized using tricaine and washed with PBS and replaced with 500µl pre-heated dissociation mix. Fish were mechanically dissociated via harsh pipetting using P1000. Samples were pipetted swiftly 100 times, for about 5mins. To stop dissociation, 800µl DMEM-10% FBS was added. The sample was mixed and centrifuged 5mins at 800g at room temperature. The supernatant was discarded. The pellet was resuspended with 1ml of PBS and centrifuged at 800g at room temperature. The samples were then resuspended in 1ml of DMEM-10% FBS. Cells were passed through 40µm filter in order to reduce debris and cell aggregates. Depending on downstream application, such as fluorescence activated cell sort, resuspend the cells in 500µl of 1X propidium iodide (PI, in 1X PBS) to stain for live and dead cells (Abcam, ab139418).

4.3.12 Fluorescence Activated Cell Sort

Live, single cell suspension of PT reporter zebrafish line, *Tg(gtshb:gfp)*, was used to isolate GFP^+ PT RTECs [272]. For each experimental group, 60 zebrafish larvae were pooled and homogenized using the previously mentioned protocol [283], in 500µl 1X PI. To differentiate auto-fluorescent cells during gating, age-matched, wildtype embryos were prepared along with experimental samples. Samples of nonfluorescent embryos were used to set sorting gates. Cells were sorted at the Rangos Flow Cytometry Core (Pittsburgh, PA) using LSR II Flow Cytometer (BD Biosciences). Gating varies from samples and instruments. Briefly, single cell suspension was gated using SSC-A and FSC-A to isolate cells from debris. Then, FSC-W and FSC-H were used to gate and isolate single cells. FSC-A and PE-Texas Red-A was used to isolate live single cells

(PI^-) from dead cells (PI^+). FIT-C channel was used to isolate GFP^+, only gating those that do not overlap with wildtype GFP^- control, at 10^3 fluorescence unit. For each experimental group, total of 500 cells were collected into 96-well plate filled with Smart-Seq HT sorting buffer for downstream protocols

4.3.13 RT-PCR

Zebrafish larvae at 1-4 dpi (4-7dpf) were homogenized and sorted as stated above. For each timepoint, four conditions were collected: WT UN, WT AKI, *hdac8*$^{-/-}$ UN, *hdac8*$^{-/-}$ AKI. Due to the low GFP+ PT cell count, a low-sample cDNA generation kit was used to directly amplify cDNA from sorted cells. 500 isolated GFP+ PT cells were collected in Smart-Seq HT kit sorting buffer in 96-well plate (Takara Bio USA, 634455). Per Smart-Seq HT kit manual, the one-step first-strand cDNA synthesis and quantification was performed carried out at the Health Sciences Sequencing Core at Children's Hospital of Pittsburgh (Pittsburgh, PA). cDNA was quantified using Qubit. The generated cDNA for all samples were diluted to a working stock of 1ng/µl. The primers were diluted to working stock of 10µM. SYBR Green RT-PCR was performed out in a 10µl reaction (3.6µl SYBR Green PowerUp 2X, 3.6µl RNase-free H2O, 0.8µl 1:5 cDNA, 4.4µl 1:10 reverse and forward primers) (Thermo Fisher Scientific, A25742). Each reaction was run in triplicates. Primer sequences are provided in Table 2.

4.3.14 cDNA library preparation and RNA-sequencing

Zebrafish larvae at 3dpi (6dpf) were homogenized and sorted as stated above. For each timepoint, four conditions were collected: WT UN, WT AKI, *hdac8*$^{-/-}$ UN, *hdac8*$^{-/-}$ AKI. cDNA

synthesis, quantification, library preparation, and sequencing were performed as stated above and carried out at the Health Sciences Sequencing Core at Children's Hospital of Pittsburgh (Pittsburgh, PA). Nextera XT kit was used to generate unstranded, mRNA-specific enriched library according to the manufacturer's protocol (Illumina, FC-131-1096). Final libraries were normalized to 10nM, pooled and diluted. NextSeq 500 (Illumina) was seeded with 1.8pM denatured library for automated cluster formation for approximately 30- to 40- million reads per sample.

4.3.15 RNA-seq analysis

Hisat2 (v2.1.0) [284] was used to align paired-end RNA-seq reads to the zebrafish reference genome (UCSC danRer11) and gene-level counts per million (CPM) were calculated using featureCounts [225] and edgeR [226]. Pathway analysis was performed by inputting list of differentially expressed genes from the said analysis. g:Profiler was used for pathway enrichment, selecting *Danio rerio* as the host organism (Elixer, Estonia).

4.3.16 Statistical analysis

Data were analyzed using Student's *t*-test, one-way ANOVA, two-way ANOVA, and Log-rank (Mantel-Cox) as indicated, and data are reported as mean±SEM. *P*-values were considered significant when <0.05. For immunofluorescence studies in zebrafish larvae, Each dot on graphs reflects the number of pronephros included in the analysis per group. When visible, both nephrons per fish were included.

4.4 Discussion

We have identified HDAC8 as the target of PTBA and elucidated the role HDAC8 plays in progression of AKI. Various HDIs have been used to enhance regenerative capacity of the kidney in the past. However, the non-selective nature of various pan-HDIs has confounded the underlying reparative mechanisms conferred by these drugs. Here, we were able to use CETSA to show the selective binding of PTBA to an HDAC class I member, HDAC8. We also demonstrated *in vivo* selectivity by treating WT and *hdac8*$^{-/-}$gent-AKI zebrafish larvae with PTBA analog, UPHD25 and showing *hdac8*$^{-/-}$ mutants results in no compound efficacy. We demonstrated that PTBA's efficacy depends on the presence of HDAC8.

Since PTBA was validated as a selective HDAC8 inhibitor, the next step was to assess the effect of genetic deletion of HDAC8 in AKI. While homozygous mutants were viable until adulthood, 1% developed craniofacial deformities. HDAC8 is one of the mutations identified in CdLS patients, but does not result in embryonic lethality unlike other class I HDAC knockouts. In mice, HDAC8 loss of function results in embryonic viability, but shorter lifespan, due to craniofacial and brain deformities. A more in-depth developmental and cognitive characterization through embryonic to adult stages may be an interesting question to those interested in the role HDAC8 plays in CdLS. For our purpose, however, we focused our attention on AKI progression. In *hdac8*$^{-/-}$ there was a significant increase in survival compared to WT, which phenocopies PTBA's efficacy in increasing survival rate of zebrafish after AKI.

During AKI, more cells undergo cycling to eventually repopulate lost RTECs. In WT zebrafish, RTEC proliferation occurs at 3dpi, as seen by an increase EdU/pH3 staining. However, in *hdac8*$^{-/-}$ the RTEC completion of the proliferation response does not occur at 3dpi, but rather delayed at 4dpi. At this later timepoint, both EdU and pH3 both are significantly higher than WT

AKI. This delay in cycling was further supported by the *p21a* qPCR quantification. As EdU and pH3 expression go up, *p21* expression is lowered. This is concomitant to cell cycle recovery, with lowering of checkpoint inhibitor and progression from G1/S to G2/M [78]. This cell cycle delay can possibly be explained by HDAC8 association with SMC3a, a member of the cohesin ring. Without HDAC8, SMC3a cannot be recycled into the next cell cycle, therefore cycling cells progress more slowly [186,202]. Because there is a freshly translated SMC3a, cell cycle continues to occur but it is theorized to be achieved at a slower rate [186,190]. This hypothesis that slower cell cycling may be beneficial for damaged cells undergoing repair was supported when we treated fish with Abemaciclib, a CDK4/6 inhibitor [271]. Inhibition of cell cycle increased survival of larval zebrafish with gent-AKI. This is hypothesized to be due to prolonged DDR response prior to S and G2/M phase, which is more error-prone and therefore likely to lead to genomic instability. This is in line with past AKI studies that have shown that careful modulation of cell cycling, for example with other pharmacological inhibitors of CDK4/6, will lead to enhanced AKI recovery [81-83].

We looked at DDR response and apoptosis, to see if HDAC8 and its delay in cell cycle is leading to more efficient and enhanced repair response. In *hdac8*$^{-/-}$, RTECs showed higher pH2ax expression of at 2dpi, during the period of delay. The p-H2A.X was also accompanied by lower TUNEL^{+} staining. Increased pH2ax expression in *hdac8*$^{-/-}$ suggests that mutants are indeed injured by gent-AKI as p-H2A.X levels indicate first signs of DDR. Lower cell death, however, suggests that the damage is repairing and preventing downstream apoptotic response. There are multiple pathways that can be activated downstream of p-H2A.X. For example, DDR proteins (MRE1/NBS1/RAD50, MDC1, 53BP1, BRCA1) can colocalize with p-H2A.X and activate ATM [281]. P-H2A.X also associate with checkpoint phosphorylation, chromatin remodeling, cohesin recruitment, which all result in further cell repair mechanisms [281].

Further analysis of the *hdac8*$^{-/-}$ mutants revealed that EMT-related genes were differentially expressed between WT and *hdac8*$^{-/-}$. A very recent study is in concurrence with our findings, also citing HDAC8 inhibition results in less EMT and less cell cycle arrest [195]. During injury, damaged RTECs undergo EMT and reactivate developmental genes, such as *pax2* and *sox9*, as a mechanism to proliferate and repopulate the damaged proximal tubule[98]. However, prolonged mesenchymal state has also been associated with damage and cellular senescence, as those cells increase in pro-fibrotic factors [67,72,73]. Analysis of earlier timepoints at 2 and 3dpi, suggests that *hdac8*$^{-/-}$ fish undergo EMT, but lower than in WT. Even though there is a change in dynamics of EMT, the reactivation gene Pax2a is still expressed in the mutants. It would be interesting to test if the mesenchymal cells are the source of Pax2a expression in *hdac8*$^{-/-}$ RTECs. As prolonged mesenchymal state results in further inflammation and profibrotic response, it would be interesting to see if *hdac8*$^{-/-}$-mediated efficient EMT occurrence results in less fibrosis in a long-term study. Mice and human organoids will be both accessible and serve as more translatable models to study long term effects of *hdac8* deletion. One caveat of the study was the universal deletion of *hdac8*$^{-/-}$. By utilizing a global knock out of *hdac8*$^{-/-}$, we still have not teased apart the effect HDAC8 on specific tissues and its potential negative effects it may have in other cycling cells. There are other known targets of HDAC8, such as ERRα, cortactin, and p53. It would be worthwhile to conduct proximal tubule specific acetylomics to understand a wide range of targets that exist that may contribute to this enhanced repair process.

Overall, this study not only identified HDAC8 as PTBA target, but more importantly we were able to characterize the role of HDAC8 in isolation from other class I HDACs in a zebrafish AKI model. We have demonstrated that genetic deletion of *hdac8* results in cell cycle delay due to hyper-acetylation of Smc3a. This *hdac8*$^{-/-}$-driven cell cycle delay during injury serves as a

beneficial phenomenon. The delay is associated with prevention of irreversible damage: enhancing DDR response and preventing *kim-1* expression and apoptosis. The extent of damage may be less severe in delayed RTECs, allowing EMT and redifferentiation to fully polarized epithelial cells to be established. HDAC8, unlike its class I family members, does not impart developmentally lethal conditions. HDAC8 may be playing a role as a bimodal regulator to independently regulate two pathways: to delay cell cycle as well as reducing EMT. This study demonstrates that HDAC8 is a promising candidate for selective pharmacological inhibition, as it may result in an accurate and targeted repair response without conferring critical off-target and side effects. This work demonstrates a potential target of interest for AKI and a novel mechanism of cell cycle delay to achieve enhanced damage response via HDAC8 inhibition.

Additional contributors to the chapter

Amanda Crunk and Christina Crana performed CETSA and Western blots

Michael McDaniels performed survival assays

Abha Bais performed RNA-seq analysis

5.0 General discussion

Collectively, our finding furthers PTBA's mechanism of action as well as identifying a novel target and mechanisms involved in the progression of AKI. We've determined that PTBA enhances RTEC dedifferentiation, reduces cellular injury, and requires intact RA pathway for efficacy. We've characterized the zebrafish leukocyte activation during AKI and its changes under PTBA administration. Lastly, we identified the target of PTBA, HDAC8, using in *vivo* and *in vitro* methods. Using mutant zebrafish, we validated that genetic ablation of *hdac8* results in enhanced survival, RTEC cell cycle delay, decreased injury, efficient EMT, and overall better repair than WT (Figure 33).

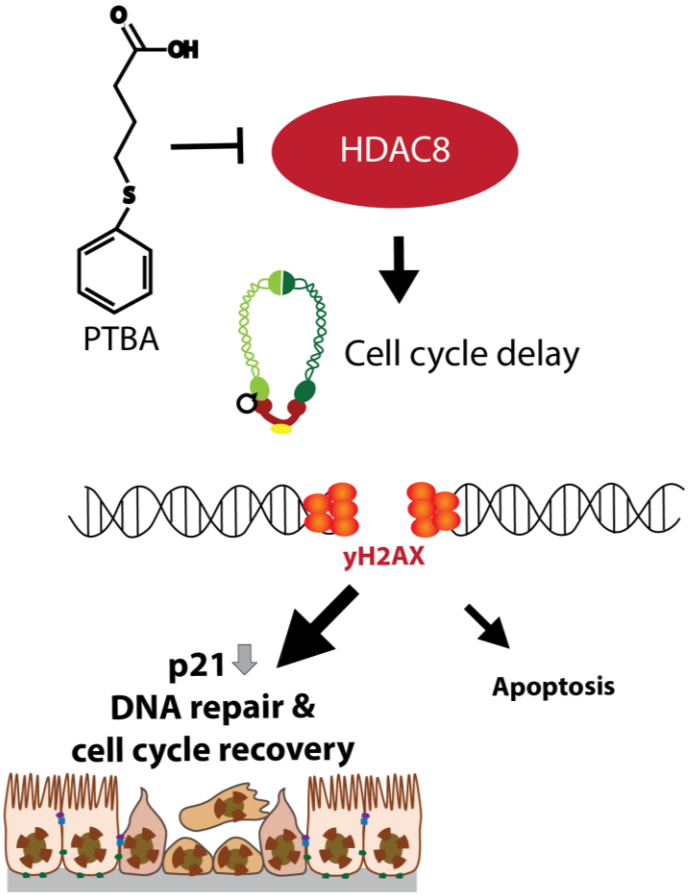

Figure 33 HDAC8 inhibition results in enhanced repair

PTBA selectively binds to HDAC8. HDAC8 is implicated in cell cycle progression via deacetylating SMC3 (green). When HDAC8 is inhibited, cell cycle delay and recovery occurs in actively dividing RTECs. This delay and subsequent recovery allows longer time for DNA repair prior to cell division, as supported by increased number of γH2AX-positive RTECs and enhanced RTEC epithelial polarity.

Perhaps the most exciting finding is the identification and further characterization of HDAC8's role in AKI injury response. We first wanted to validate the claim that PTBA enhances repair by inhibiting HDAC8. We've identified many reparative phenotypes consistent with *hdac8*$^{-/-}$ mutants and PTBA treatment in wildtype fish. *hdac8*$^{-/-}$ and PTBA treated WT similarly displayed enhanced survival, increased cell cycling, enhanced reactivation of Pax2a, and reduced *kim-1* expression, and reduced apoptosis [156]. Earlier experiments validated that PTBA enhances

proliferating PCNA^{+} RTEC population. However, PCNA is a wider marker of cell cycle phases (S, G2, and M) and therefore cell-cycle specific staining and the use of FACS will further characterize the cell cycle dynamics in detail. The newly identified repair mechanisms in *hdac8*$^{-/-}$ are cell cycle delay, increased epithelial polarity, and enhanced p-H2A.X. These are characterizations in *hdac8*$^{-/-}$ fish that should also be repeated for PTBA treated fish.

There are other phenomena which diverge between PTBA and *hdac8*$^{-/-}$. In PTBA treated fish, we see enhanced EMT, a phenomenon required for dedifferentiation and proliferation of RTECs. In *hdac8*$^{-/-}$, the EMT process is less pronounced, with the RNA-seq results showing more epithelial genes and protein expression. EMT, however, is a multifaceted physiological that also presents problems during maladaptive repair. Maladaptive RTECs, along with mesenchymal factors, can co-express pro-inflammatory cytokines and pro-fibrotic factors [194]. To parse out whether EMT is serving as a regenerative dedifferentiation or injury, the RNA-seq data was analyzed for expression of pro-inflammatory and pro-fibrotic factors. Both AKI+UPHD25 wildtype fish and *hdac8*$^{-/-}$ AKI fish expressed lower levels of *tgfb*, *tnfa*, *mmp*, *col,* and *ils* compared to their AKI+DMSO or WT AKI controls, respectively (data not shown). Results suggest that EMT serves a regenerative purpose to drive dedifferentiation, not fibrosis, in our experimental models.

Overall variable results between PTBA and *hdac8*$^{-/-}$ likely due to the differences in of HDAC8 inhibition. PTBA serves as a temporary HDAC8 inhibition, treated after the injury response is occurring, and the compound is metabolized and rendered ineffective within 6hr of treatment. [176] [156]. This contrast in HDAC8 inhibition dosage may affect the results and phenotypes we observe. A recent study by Wen *et al.* has shown treatment time and dosage is critical in drawing optimal PTBA efficacy [211]. This may be due to the time-sensitive nature of other signaling

pathways that are activated and crosstalk with PTBA. Previous work in the lab has shown RA response occurs in RTECs within the first 7hrs of gent-AKI [157]. p21 activity during early phases of injury is beneficial, whereas prolonged p21 activity leads to worsened outcome in mouse models [84,85 273]. It would be critical to identify and treat patients at the right window of disease progression. It will be important to assess efficacy of inducible, tissue-specific *hdac8* knockout model. This would enable further delineation of HDAC8 function at different timepoints of injury progression.

Certain mechanisms explored in the PTBA study are yet to be explored in the *hdac8*$^{-/-}$ model. In our current work and past studies, intact RA signaling pathway is necessary for PTBA efficacy as well as conferring regenerative effects in AKI setting [157 166 247 246]. We suspect *hdac8*$^{-/-}$ mutants will enhance the endogenous RA response in injury setting. Others have shown links between HDAC8 and RA signaling pathway. Cotreatment of HDAC8 inhibitor, PCI-34051, and exogenous RA treatment showed a positive synergistic effect in differentiating neuroblastoma cells [285]. HDAC8 and RA pathways converge at pCREB (phospho-cAMP-response element-binding protein), necessary for cellular proliferation during organ repair setting and kidney dedifferentiation [286 287 288 289]. RA positively regulates pCREB activation while HDAC8 negatively regulates pCREB [285 290]. Inhibition of HDAC8, along with endogenous increase of RA activity in the kidney, pCREB may become synergistically activated thereby conferring regenerative effect in the kidney.

Another system yet to be explored in the *hdac8*$^{-/-}$ model is the immune system. Studies have shown HDAC8 inhibition shows anti-inflammatory effect as well as modulating macrophages transcriptional response to toxins [191,193,291]. Overall, HDAC8 inhibition has shown decline in inflammatory response in various injury models [191,193]. Studies have also shown a direct link between HDAC8 and cortactin, a key regulator of actin cytoskeleton responsible for f-actin

polymerization [292,293]. Cortactin is a known substrate of HDAC8 deacetylase activity and is implicated in cellular motility, especially migratory cells such as leukocytes and osteoclasts [294,295] [293]. Our current RNA-seq data further validates decrease of innate immune response in *hdac8*$^{-/-}$ model. With the techniques optimized throughout this study, more in-depth studies are now accessible. Macrophage infiltration and polarization dynamics can be studied in *hdac8*$^{-/-}$ fish using real time 2-photon confocal imaging and FACS.

In developing therapeutics, cell type specificity of a candidate drug is important [296]. The next step in PTBA development is to identify its main cellular target Generation of PT-specific or macrophage-specific inducible *hdac8* knockout models will delineate the answer. Another method will be to analyze the effect of PTBA in an isolated kidney setting, using organoids, in which human iPCS is differentiated to tubules, blood vessels, and interstitium [297]. Preliminary studies in our group have shown organoids can serve as a model for interstitial fibrosis (unpublished). Utilizing the human-derived organoids will serve as a partner to our zebrafish model, validating the current findings and assessing long-term effects such as interstitial fibrosis [298]. The Hukriede lab is currently in the process of establishing *hdac8* knockout organoids to understand the role of HDAC8 in a more translationally relevant setting.

Overall, this study shines light on the zebrafish, in conjunction with cell-based assays, as an enduring model of AKI to continue PTBA characterization. In the past, the Hukriede lab first initiated the search to fulfill the lack of AKI therapeutics by using zebrafish embryos to perform large phenotypic screening to identify our candidate compound [148]. Then, our lab transitioned to take advantage of the conserved nature of the zebrafish pronephros and their injury response to gent-AKI [155,156]. Our current study used these past studies as a stepping-stone to further our understanding of PTBA efficacy, biomarker response, as well as target identification, both *in vitro*

and *in vivo*. In doing so, we have identified HDAC8 as a novel target and its mechanisms underlying the enhanced repair response. This work provides an insight on cellular repair mechanisms and one more step on finding a cure for acute kidney injury.

Appendix A Antibodies used for histology

Table 1 Antibodies and antigen retrieval protocol for histology

Primary antibodies						
Antigen	**Source**	**Cat#**	**Host species**	**Dilution**	**Tissue**	**Antigen retrieval**
3G8	DSHB	3G8.2C11	Mouse	1:200	Frozen	None
Pax2a	GeneTex	GTX128127	Rabbit	1:200	Frozen	Citrate
GFP	Aves Labs	GFP-1020	Chicken	1:300	Frozen	None/Citrate
Kim-1	R&D Systems	MAB1817	Rat	80µg/ml	Frozen	None
Dendra2	Origene	TA180094	Mouse	1:200	Frozen	None
TNFα	AnaSpec	AS-55383	Rabbit	1:100	Frozen	Citrate
Arginase2	Thermo Fisher	PA5-27987	Rabbit	1:100	Frozen	Citrate
PCNA	Sigma	P8825	Mouse	1:3000	Frozen	Citrate
E-Cadherin	BD Biosciences	610182	Mouse	1:200	Frozen	Citrate
Vimentin	Milipore	MAB3400	Mouse	1:100	Frozen	Trypsin
p.H2A.X (phospho Ser139)	GeneTex	GTX127342	Rabbit	1:200	Frozen	Citrate
p-Histone H3 Ser	Cell Signaling	9701	Rabbit	1:100	Frozen	
Na+K+ATPase	DSHB	a6F	Mouse	1:25	JB4 embedded	None

Table 1 continued

Secondary antibodies						
Antigen	**Source**	**Cat#**	**Host species**	**Dilution**	**Tissue**	**Conjugate**
Goat anti-mouse	Abcam	ab97035	Goat	1:1000	Frozen	Cy3
Goat- anti-rabbit	Thermo Fisher	A-11008	Goat	1:1000	Frozen	Alexa488
Goat- anti-mouse	Thermo Fisher	A-11001	Goat	1:1000	Frozen	Alexa488
Goat anti-rat	Thermo Fisher	A-11007	Goat	1:1000	Frozen	Alexa594
Donkey anti-rabbit	Thermo Fisher	A-10042	Donkey	1:1000	Frozen	Alexa568
Goat anti-chicken	Thermo Fisher	A-11039	Goat	1:1000	Frozen	Alexa555
Goat anti-mouse	Thermo Fisher	A-11005	Goat	1:1000/1:500	Frozen/JB4 embedded	Alexa594

Antigen retrieval			
Method	**Reagents**	**Cat#**	**Protocol**
Trypsin	Trypsin from porcine pancreas	Sigma-aldrich,T7168	Dissolve 1 tablet/100mL ddH2O. Incubate slides at 37C for 30m
Sodium citrate buffer	Citric acid	Sigma-aldrich, 251275	10mM Sodium citrate, 0.05% Tween-20. pH=6.0. Incubate slides at 97C for 30m. Cool for 30 m at room temperature
	Tween-20	Sigma-aldrich, P1379	

Appendix B RT-PCR primer sequence

Table 2 RT-PCR primer sequences

Gene	Forward primer sequence	Reverse primer sequence
hdac8	GCCCACCCTCTTGTGTTTCA	CACCTAATATTCTCTCTTGCCGTA
p21	CCTACGTTCACTCGGTAA	CTGTGATGTTGGTCTGTTT
actb1	CCGTGACATCAAGGATAAGCT	TCGTGGATACCGCAAGATTCC
eef1a1l1	ATCGACCGTCGTTCTGGCAAG	AACGGTGTGATTTGAGGGAA
kim1	CGCTAGAAGTAAGGCAGAA	CACTGTTCGTATTCGCTTTC
bactin	CGTGCTGTCTTCCCATCCA	TCACCAACGTAGCTGTCTTTCTG

Bibliography

1. Ronco, C., Bellomo, R. & Kellum, J.A. Acute kidney injury. *Lancet* **394**, 1949-1964 (2019).

2. Davies, J.A. Morphogenesis of the metanephric kidney. *ScientificWorldJournal* **2**, 1937-50 (2002).

3. Gerlach, G.F. & Wingert, R.A. Kidney organogenesis in the zebrafish: insights into vertebrate nephrogenesis and regeneration. *Wiley Interdiscip Rev Dev Biol* **2**, 559-85 (2013).

4. Desgrange, A. & Cereghini, S. Nephron Patterning: Lessons from Xenopus, Zebrafish, and Mouse Studies. *Cells* **4**, 483-99 (2015).

5. McMahon, A.P. Development of the Mammalian Kidney. *Curr Top Dev Biol* **117**, 31-64 (2016).

6. Little, M.H. & McMahon, A.P. Mammalian kidney development: principles, progress, and projections. *Cold Spring Harb Perspect Biol* **4**(2012).

7. Tang, M.J., Cai, Y., Tsai, S.J., Wang, Y.K. & Dressler, G.R. Ureteric bud outgrowth in response to RET activation is mediated by phosphatidylinositol 3-kinase. *Dev Biol* **243**, 128-36 (2002).

8. Jain, S., Encinas, M., Johnson, E.M., Jr. & Milbrandt, J. Critical and distinct roles for key RET tyrosine docking sites in renal development. *Genes Dev* **20**, 321-33 (2006).

9. Costantini, F. GDNF/Ret signaling and renal branching morphogenesis: From mesenchymal signals to epithelial cell behaviors. *Organogenesis* **6**, 252-62 (2010).

10. Hatini, V., Huh, S.O., Herzlinger, D., Soares, V.C. & Lai, E. Essential role of stromal mesenchyme in kidney morphogenesis revealed by targeted disruption of Winged Helix transcription factor BF-2. *Genes Dev* **10**, 1467-78 (1996).

11. Humphreys, B.D. *et al.* Fate tracing reveals the pericyte and not epithelial origin of myofibroblasts in kidney fibrosis. *Am J Pathol* **176**, 85-97 (2010).

12. Boyle, S. *et al.* Fate mapping using Cited1-CreERT2 mice demonstrates that the cap mesenchyme contains self-renewing progenitor cells and gives rise exclusively to nephronic epithelia. *Dev Biol* **313**, 234-45 (2008).

13. Kobayashi, A. *et al.* Six2 defines and regulates a multipotent self-renewing nephron progenitor population throughout mammalian kidney development. *Cell Stem Cell* **3**, 169-81 (2008).

14. Toyama, R., Kobayashi, M., Tomita, T. & Dawid, I.B. Expression of LIM-domain binding protein (ldb) genes during zebrafish embryogenesis. *Mech Dev* **71**, 197-200 (1998).

15. Pfeffer, P.L., Gerster, T., Lun, K., Brand, M. & Busslinger, M. Characterization of three novel members of the zebrafish Pax2/5/8 family: dependency of Pax5 and Pax8 expression on the Pax2.1 (noi) function. *Development* **125**, 3063-74 (1998).

16. Wingert, R.A. & Davidson, A.J. Zebrafish nephrogenesis involves dynamic spatiotemporal expression changes in renal progenitors and essential signals from retinoic acid and irx3b. *Dev Dyn* **240**, 2011-27 (2011).

17. Miller-Bertoglio, V.E., Fisher, S., Sanchez, A., Mullins, M.C. & Halpern, M.E. Differential regulation of chordin expression domains in mutant zebrafish. *Dev Biol* **192**, 537-50 (1997).

18. Diep, C.Q. *et al.* Development of the zebrafish mesonephros. *Genesis* **53**, 257-69 (2015).

19. Hoy, W.E., Hughson, M.D., Bertram, J.F., Douglas-Denton, R. & Amann, K. Nephron number, hypertension, renal disease, and renal failure. *J Am Soc Nephrol* **16**, 2557-64 (2005).

20. Zuk, A. & Bonventre, J.V. Acute Kidney Injury. *Annu Rev Med* **67**, 293-307 (2016).

21. Levey, A.S. & James, M.T. Acute Kidney Injury. *Ann Intern Med* **167**, ITC66-ITC80 (2017).

22. Makris, K. & Spanou, L. Acute Kidney Injury: Definition, Pathophysiology and Clinical Phenotypes. *Clin Biochem Rev* **37**, 85-98 (2016).

23. Susantitaphong, P. *et al.* World incidence of AKI: a meta-analysis. *Clin J Am Soc Nephrol* **8**, 1482-93 (2013).

24. Silver, S.A. & Chertow, G.M. The Economic Consequences of Acute Kidney Injury. *Nephron* **137**, 297-301 (2017).

25. Morales, A.I. *et al.* Metformin prevents experimental gentamicin-induced nephropathy by a mitochondria-dependent pathway. *Kidney Int* **77**, 861-9 (2010).

26. Morales, A.I. *et al.* Resveratrol inhibits gentamicin-induced mesangial cell contraction. *Life Sci* **78**, 2373-7 (2006).

27. Brown, J.R., Rezaee, M.E., Marshall, E.J. & Matheny, M.E. Hospital Mortality in the United States following Acute Kidney Injury. *Biomed Res Int* **2016**, 4278579 (2016).

28. Rewa, O. & Bagshaw, S.M. Acute kidney injury-epidemiology, outcomes and economics. *Nat Rev Nephrol* **10**, 193-207 (2014).

29. Kellum, J.A. KDIGO Clinical Practice Guideline for Acute Kidney Injury. *Kidney Int* **2**(2012).

30. Panesar, K. Acute Kidney Injury: An Overview. **40**(2015).

31. Forni, L.G. *et al.* Renal recovery after acute kidney injury. *Intensive Care Med* **43**, 855-866 (2017).

32. Kellum, J.A., Sileanu, F.E., Bihorac, A., Hoste, E.A. & Chawla, L.S. Recovery after Acute Kidney Injury. *Am J Respir Crit Care Med* **195**, 784-791 (2017).

33. Lafrance, J.P. & Miller, D.R. Acute kidney injury associates with increased long-term mortality. *J Am Soc Nephrol* **21**, 345-52 (2010).

34. Clark, J.Z. *et al.* Representation and relative abundance of cell-type selective markers in whole-kidney RNA-Seq data. *Kidney Int* **95**, 787-796 (2019).

35. McKee, R. & Wingert, R. Zebrafish Renal Pathology: Emerging Models of Acute Kidney Injury. *Current Pathobiology Reports* **3**, 171-181 (2015).

36. Zuk, A. & Bonventre, J.V. Recent advances in acute kidney injury and its consequences and impact on chronic kidney disease. *Curr Opin Nephrol Hypertens* **28**, 397-405 (2019).

37. Koyner, J.L. *et al.* Biomarkers predict progression of acute kidney injury after cardiac surgery. *J Am Soc Nephrol* **23**, 905-14 (2012).

38. Bonventre, J.V. & Yang, L. Cellular pathophysiology of ischemic acute kidney injury. *J Clin Invest* **121**, 4210-21 (2011).

39. Brooks, C.R. *et al.* KIM-1-/TIM-1-mediated phagocytosis links ATG5-/ULK1-dependent clearance of apoptotic cells to antigen presentation. *EMBO J* **34**, 2441-64 (2015).

40. Yin, W. *et al.* Mammalian Target of Rapamycin Mediates Kidney Injury Molecule 1-Dependent Tubule Injury in a Surrogate Model. *J Am Soc Nephrol* **27**, 1943-57 (2016).

41. Emlet, D.R. *et al.* Insulin-like growth factor binding protein 7 and tissue inhibitor of metalloproteinases-2: differential expression and secretion in human kidney tubule cells. *Am J Physiol Renal Physiol* **312**, F284-F296 (2017).

42. Wen, X. *et al.* A zebrafish model of infection-associated acute kidney injury. *Am J Physiol Renal Physiol* **315**, F291-F299 (2018).

43. Yamanishi, Y. *et al.* TIM1 is an endogenous ligand for LMIR5/CD300b: LMIR5 deficiency ameliorates mouse kidney ischemia/reperfusion injury. *J Exp Med* **207**, 1501-11 (2010).

44. Yin, C. & Wang, N. Kidney injury molecule-1 in kidney disease. *Ren Fail* **38**, 1567-1573 (2016).

45. Yang, L. *et al.* KIM-1-mediated phagocytosis reduces acute injury to the kidney. *J Clin Invest* **125**, 1620-36 (2015).

46. Chien, C.T. *et al.* De novo demonstration and co-localization of free-radical production and apoptosis formation in rat kidney subjected to ischemia/reperfusion. *J Am Soc Nephrol* **12**, 973-82 (2001).

47. Kellum, J.A. & Chawla, L.S. Cell-cycle arrest and acute kidney injury: the light and the dark sides. *Nephrol Dial Transplant* **31**, 16-22 (2016).

48. Nigam e, S. & Lieberthal, W. Acute renal failure. III. The role of growth factors in the process of renal regeneration and repair. *Am J Physiol Renal Physiol* **279**, F3-F11 (2000).

49. Murugan, R. & Kellum, J.A. Acute kidney injury: what's the prognosis? *Nat Rev Nephrol* **7**, 209-17 (2011).

50. Prescott, L.F. The normal urinary excretion rates of renal tubular cells, leucocytes and red blood cells. *Clin Sci* **31**, 425-35 (1966).

51. Nadasdy, T., Laszik, Z., Blick, K.E., Johnson, L.D. & Silva, F.G. Proliferative activity of intrinsic cell populations in the normal human kidney. *J Am Soc Nephrol* **4**, 2032-9 (1994).

52. Humphreys, B.D. *et al.* Intrinsic epithelial cells repair the kidney after injury. *Cell Stem Cell* **2**, 284-91 (2008).

53. Thadhani, R., Pascual, M. & Bonventre, J.V. Acute renal failure. *N Engl J Med* **334**, 1448-60 (1996).

54. Kusaba, T., Lalli, M., Kramann, R., Kobayashi, A. & Humphreys, B.D. Differentiated kidney epithelial cells repair injured proximal tubule. *Proc Natl Acad Sci U S A* **111**, 1527-32 (2014).

55. Witzgall, R., Brown, D., Schwarz, C. & Bonventre, J.V. Localization of proliferating cell nuclear antigen, vimentin, c-Fos, and clusterin in the postischemic kidney. Evidence for a heterogenous genetic response among nephron segments, and a large pool of mitotically active and dedifferentiated cells. *J Clin Invest* **93**, 2175-88 (1994).

56. Abbate, M., Brown, D. & Bonventre, J.V. Expression of NCAM recapitulates tubulogenic development in kidneys recovering from acute ischemia. *Am J Physiol* **277**, F454-63 (1999).

57. Benigni, A., Morigi, M., Remuzzi, G. Kidney Regeneration. *Lancet* **375**, 1310-1317 (2010).

58. Villanueva, S., Cespedes, C. & Vio, C.P. Ischemic acute renal failure induces the expression of a wide range of nephrogenic proteins. *Am J Physiol Regul Integr Comp Physiol* **290**, R861-70 (2006).

59. Terada, Y. *et al.* Expression and function of the developmental gene Wnt-4 during experimental acute renal failure in rats. *J Am Soc Nephrol* **14**, 1223-33 (2003).

60. Imgrund, M. *et al.* Re-expression of the developmental gene Pax-2 during experimental acute tubular necrosis in mice 1. *Kidney Int* **56**, 1423-31 (1999).

61. Cirio, M.C., de Caestecker, M.P. & Hukriede, N.A. Zebrafish Models of Kidney Damage and Repair. *Curr Pathobiol Rep* **3**, 163-170 (2015).

62. Chang-Panesso, M. *et al.* FOXM1 drives proximal tubule proliferation during repair from acute ischemic kidney injury. *J Clin Invest* **129**, 5501-5517 (2019).

63. Chang-Panesso, M. & Humphreys, B.D. Cellular plasticity in kidney injury and repair. *Nat Rev Nephrol* **13**, 39-46 (2017).

64. Yu, S.M. & Bonventre, J.V. Acute kidney injury and maladaptive tubular repair leading to renal fibrosis. *Curr Opin Nephrol Hypertens* **29**, 310-318 (2020).

65. Canaud, G. & Bonventre, J.V. Cell cycle arrest and the evolution of chronic kidney disease from acute kidney injury. *Nephrol Dial Transplant* **30**, 575-83 (2015).

66. Eardley, K.S. *et al.* The relationship between albuminuria, MCP-1/CCL2, and interstitial macrophages in chronic kidney disease. *Kidney Int* **69**, 1189-97 (2006).

67. Yang, L., Besschetnova, T.Y., Brooks, C.R., Shah, J.V. & Bonventre, J.V. Epithelial cell cycle arrest in G2/M mediates kidney fibrosis after injury. *Nat Med* **16**, 535-43, 1p following 143 (2010).

68. Venkatachalam, M.A., Weinberg, J.M., Kriz, W. & Bidani, A.K. Failed Tubule Recovery, AKI-CKD Transition, and Kidney Disease Progression. *J Am Soc Nephrol* **26**, 1765-76 (2015).

69. Kalluri, R. & Weinberg, R.A. The basics of epithelial-mesenchymal transition. *J Clin Invest* **119**, 1420-8 (2009).

70. Funk, J.A. & Schnellmann, R.G. Accelerated recovery of renal mitochondrial and tubule homeostasis with SIRT1/PGC-1alpha activation following ischemia-reperfusion injury. *Toxicol Appl Pharmacol* **273**, 345-54 (2013).

71. Yang, H. & Fogo, A.B. Cell senescence in the aging kidney. *J Am Soc Nephrol* **21**, 1436-9 (2010).

72. Lovisa, S. *et al.* Epithelial-to-mesenchymal transition induces cell cycle arrest and parenchymal damage in renal fibrosis. *Nat Med* **21**, 998-1009 (2015).

73. Grande, M.T. *et al.* Snail1-induced partial epithelial-to-mesenchymal transition drives renal fibrosis in mice and can be targeted to reverse established disease. *Nat Med* **21**, 989-97 (2015).

74. Vega, S. *et al.* Snail blocks the cell cycle and confers resistance to cell death. *Genes Dev* **18**, 1131-43 (2004).

75. Moonen, L., D'Haese, P.C. & Vervaet, B.A. Epithelial Cell Cycle Behaviour in the Injured Kidney. *Int J Mol Sci* **19**(2018).

76. Schmitt, R. & Cantley, L.G. The impact of aging on kidney repair. *Am J Physiol Renal Physiol* **294**, F1265-72 (2008).

77. Burma, S., Chen, B.P., Murphy, M., Kurimasa, A. & Chen, D.J. ATM phosphorylates histone H2AX in response to DNA double-strand breaks. *J Biol Chem* **276**, 42462-7 (2001).

78. Shaltiel, I.A., Krenning, L., Bruinsma, W. & Medema, R.H. The same, only different - DNA damage checkpoints and their reversal throughout the cell cycle. *J Cell Sci* **128**, 607-20 (2015).

79. Harper, J.W., Adami, G.R., Wei, N., Keyomarsi, K. & Elledge, S.J. The p21 Cdk-interacting protein Cip1 is a potent inhibitor of G1 cyclin-dependent kinases. *Cell* **75**, 805-16 (1993).

80. Price, P.M. *et al.* Dependence of cisplatin-induced cell death in vitro and in vivo on cyclin-dependent kinase 2. *J Am Soc Nephrol* **17**, 2434-42 (2006).

81. Wei, L. *et al.* Inhibition of CDK4/6 protects against radiation-induced intestinal injury in mice. *J Clin Invest* **126**, 4076-4087 (2016).

82. Pabla, N. *et al.* Mitigation of acute kidney injury by cell-cycle inhibitors that suppress both CDK4/6 and OCT2 functions. *Proc Natl Acad Sci U S A* **112**, 5231-6 (2015).

83. DiRocco, D.P. *et al.* CDK4/6 inhibition induces epithelial cell cycle arrest and ameliorates acute kidney injury. *Am J Physiol Renal Physiol* **306**, F379-88 (2014).

84. Megyesi, J., Andrade, L., Vieira, J.M., Jr., Safirstein, R.L. & Price, P.M. Positive effect of the induction of p21WAF1/CIP1 on the course of ischemic acute renal failure. *Kidney Int* **60**, 2164-72 (2001).

85. Megyesi, J., Price, P.M., Tamayo, E. & Safirstein, R.L. The lack of a functional p21(WAF1/CIP1) gene ameliorates progression to chronic renal failure. *Proc Natl Acad Sci U S A* **96**, 10830-5 (1999).

86. Bencokova, Z. *et al.* ATM activation and signaling under hypoxic conditions. *Mol Cell Biol* **29**, 526-37 (2009).

87. Bassermann, F. *et al.* The Cdc14B-Cdh1-Plk1 axis controls the G2 DNA-damage-response checkpoint. *Cell* **134**, 256-67 (2008).

88. Lee, J., Kim, J.A., Barbier, V., Fotedar, A. & Fotedar, R. DNA damage triggers p21WAF1-dependent Emi1 down-regulation that maintains G2 arrest. *Mol Biol Cell* **20**, 1891-902 (2009).

89. Sudo, T. *et al.* Activation of Cdh1-dependent APC is required for G1 cell cycle arrest and DNA damage-induced G2 checkpoint in vertebrate cells. *EMBO J* **20**, 6499-508 (2001).

90. Wiebusch, L. & Hagemeier, C. p53- and p21-dependent premature APC/C-Cdh1 activation in G2 is part of the long-term response to genotoxic stress. *Oncogene* **29**, 3477-89 (2010).

91. Johmura, Y. *et al.* Necessary and sufficient role for a mitosis skip in senescence induction. *Mol Cell* **55**, 73-84 (2014).

92. Krenning, L., Feringa, F.M., Shaltiel, I.A., van den Berg, J. & Medema, R.H. Transient activation of p53 in G2 phase is sufficient to induce senescence. *Mol Cell* **55**, 59-72 (2014).

93. Krenning, L. & Medema, R.H. Enter the nucleus to exit the cycle. *Cell Cycle* **13**, 2651-2 (2014).

94. Lindqvist, A. *et al.* Wip1 confers G2 checkpoint recovery competence by counteracting p53-dependent transcriptional repression. *EMBO J* **28**, 3196-206 (2009).

95. Canaud, G. *et al.* Cyclin G1 and TASCC regulate kidney epithelial cell G2-M arrest and fibrotic maladaptive repair. *Sci Transl Med* **11**(2019).

96. Alexakis, C., Maxwell, P. & Bou-Gharios, G. Organ-specific collagen expression: implications for renal disease. *Nephron Exp Nephrol* **102**, e71-5 (2006).

97. Ko, Y.A. *et al.* Cytosine methylation changes in enhancer regions of core pro-fibrotic genes characterize kidney fibrosis development. *Genome Biol* **14**, R108 (2013).

98. Kumar, S. Cellular and molecular pathways of renal repair after acute kidney injury. *Kidney Int* **93**, 27-40 (2018).

99. Iwakura, T. *et al.* Acquired resistance to rechallenge injury after acute kidney injury in rats is associated with cell cycle arrest in proximal tubule cells. *Am J Physiol Renal Physiol* **310**, F872-84 (2016).

100. Zager, R.A. & Johnson, A.C.M. Acute kidney injury induces dramatic p21 upregulation via a novel, glucocorticoid-activated, pathway. *Am J Physiol Renal Physiol* **316**, F674-F681 (2019).

101. van Furth, R. *et al.* The mononuclear phagocyte system: a new classification of macrophages, monocytes, and their precursor cells. *Bull World Health Organ* **46**, 845-52 (1972).

102. Varol, C., Mildner, A. & Jung, S. Macrophages: development and tissue specialization. *Annu Rev Immunol* **33**, 643-75 (2015).

103. Davidson, A.J. & Zon, L.I. The 'definitive' (and 'primitive') guide to zebrafish hematopoiesis. *Oncogene* **23**, 7233-46 (2004).

104. Gentek R., M., K., Sieweke, M.H. Tissue macrophage identity and self-renewal. *Immunological Reviews* **262**, 56-73 (2014).

105. Conger, J. Hemodynamic factors in acute renal failure. *Adv Ren Replace Ther* **4**, 25-37 (1997).

106. Brooks, D.P. Role of endothelin in renal function and dysfunction. *Clin Exp Pharmacol Physiol* **23**, 345-48 (1996).

107. Bonavia, A. & Singbartl, K. A review of the role of immune cells in acute kidney injury. *Pediatr Nephrol* **33**, 1629-1639 (2018).

108. Ysebaert, D.K. *et al.* Identification and kinetics of leukocytes after severe ischaemia/reperfusion renal injury. *Nephrol Dial Transplant* **15**, 1562-74 (2000).

109. Ozkok, A. & Edelstein, C.L. Pathophysiology of cisplatin-induced acute kidney injury. *Biomed Res Int* **2014**, 967826 (2014).

110. Chauhan, P., Sodhi, A. & Shrivastava, A. Cisplatin primes murine peritoneal macrophages for enhanced expression of nitric oxide, proinflammatory cytokines, TLRs, transcription factors and activation of MAP kinases upon co-incubation with L929 cells. *Immunobiology* **214**, 197-209 (2009).

111. Zhang, M.Z. *et al.* CSF-1 signaling mediates recovery from acute kidney injury. *J Clin Invest* **122**, 4519-32 (2012).

112. Nourshargh, S. & Alon, R. Leukocyte migration into inflamed tissues. *Immunity* **41**, 694-707 (2014).

113. Klei, T.R., Meinderts, S.M., van den Berg, T.K. & van Bruggen, R. From the Cradle to the Grave: The Role of Macrophages in Erythropoiesis and Erythrophagocytosis. *Front Immunol* **8**, 73 (2017).

114. Mosser, D.M. & Edwards, J.P. Exploring the full spectrum of macrophage activation. *Nat Rev Immunol* **8**, 958-69 (2008).

115. Lee, S. *et al.* Distinct macrophage phenotypes contribute to kidney injury and repair. *J Am Soc Nephrol* **22**, 317-26 (2011).

116. Novak, M.L. & Koh, T.J. Macrophage phenotypes during tissue repair. *J Leukoc Biol* **93**, 875-81 (2013).

117. Kroner, A. *et al.* TNF and increased intracellular iron alter macrophage polarization to a detrimental M1 phenotype in the injured spinal cord. *Neuron* **83**, 1098-116 (2014).

118. Huen, S.C. *et al.* GM-CSF Promotes Macrophage Alternative Activation after Renal Ischemia/Reperfusion Injury. *J Am Soc Nephrol* **26**, 1334-45 (2015).

119. de Gaetano, M., Crean, D., Barry, M. & Belton, O. M1- and M2-Type Macrophage Responses Are Predictive of Adverse Outcomes in Human Atherosclerosis. *Front Immunol* **7**, 275 (2016).

120. Klinkert, K. *et al.* Selective M2 Macrophage Depletion Leads to Prolonged Inflammation in Surgical Wounds. *Eur Surg Res* **58**, 109-120 (2017).

121. Melgar-Lesmes, P. & Edelman, E.R. Monocyte-endothelial cell interactions in the regulation of vascular sprouting and liver regeneration in mouse. *J Hepatol* **63**, 917-25 (2015).

122. Lee, H., Liao, J.J., Graeler, M., Huang, M.C. & Goetzl, E.J. Lysophospholipid regulation of mononuclear phagocytes. *Biochim Biophys Acta* **1582**, 175-7 (2002).

123. Roszer, T. Understanding the Mysterious M2 Macrophage through Activation Markers and Effector Mechanisms. *Mediators Inflamm* **2015**, 816460 (2015).

124. Kruger, P. *et al.* Neutrophils: Between host defence, immune modulation, and tissue injury. *PLoS Pathog* **11**, e1004651 (2015).

125. McGrath, K.E. *et al.* Distinct Sources of Hematopoietic Progenitors Emerge before HSCs and Provide Functional Blood Cells in the Mammalian Embryo. *Cell Rep* **11**, 1892-904 (2015).

126. Futosi, K., Fodor, S. & Mocsai, A. Neutrophil cell surface receptors and their intracellular signal transduction pathways. *Int Immunopharmacol* **17**, 638-50 (2013).

127. Keightley, M.C., Wang, C.H., Pazhakh, V. & Lieschke, G.J. Delineating the roles of neutrophils and macrophages in zebrafish regeneration models. *Int J Biochem Cell Biol* **56**, 92-106 (2014).

128. Kim, N.D. & Luster, A.D. The role of tissue resident cells in neutrophil recruitment. *Trends Immunol* **36**, 547-55 (2015).

129. Vieira, S.M. *et al.* A crucial role for TNF-alpha in mediating neutrophil influx induced by endogenously generated or exogenous chemokines, KC/CXCL1 and LIX/CXCL5. *Br J Pharmacol* **158**, 779-89 (2009).

130. De Filippo, K. *et al.* Mast cell and macrophage chemokines CXCL1/CXCL2 control the early stage of neutrophil recruitment during tissue inflammation. *Blood* **121**, 4930-7 (2013).

131. Mantovani, A., Cassatella, M.A., Costantini, C. & Jaillon, S. Neutrophils in the activation and regulation of innate and adaptive immunity. *Nat Rev Immunol* **11**, 519-31 (2011).

132. Eken, C. *et al.* Polymorphonuclear neutrophil-derived ectosomes interfere with the maturation of monocyte-derived dendritic cells. *J Immunol* **180**, 817-24 (2008).

133. Gasser, O. & Schifferli, J.A. Activated polymorphonuclear neutrophils disseminate anti-inflammatory microparticles by ectocytosis. *Blood* **104**, 2543-8 (2004).

134. Biswas, S.K. & Mantovani, A. Macrophage plasticity and interaction with lymphocyte subsets: cancer as a paradigm. *Nat Immunol* **11**, 889-96 (2010).

135. Jones, H.R., Robb, C.T., Perretti, M. & Rossi, A.G. The role of neutrophils in inflammation resolution. *Semin Immunol* **28**, 137-45 (2016).

136. Martin, K.R., Ohayon, D. & Witko-Sarsat, V. Promoting apoptosis of neutrophils and phagocytosis by macrophages: novel strategies in the resolution of inflammation. *Swiss Med Wkly* **145**, w14056 (2015).

137. Hoodless, L.J. *et al.* Genetic and pharmacological inhibition of CDK9 drives neutrophil apoptosis to resolve inflammation in zebrafish in vivo. *Sci Rep* **5**, 36980 (2016).

138. Mathias, J.R. *et al.* Resolution of inflammation by retrograde chemotaxis of neutrophils in transgenic zebrafish. *J Leukoc Biol* **80**, 1281-8 (2006).

139. Vatankhah, N. *et al.* Predictive value of neutrophil-to-lymphocyte ratio in diabetic wound healing. *J Vasc Surg* **65**, 478-483 (2017).

140. Antonucci, E. *et al.* Neutrophil gelatinase-associated lipocalin (NGAL): a promising biomarker for the early diagnosis of acute kidney injury (AKI). *Acta Biomed* **85**, 289-94 (2014).

141. Castoldi, A. *et al.* TLR2, TLR4 and the MYD88 signaling pathway are crucial for neutrophil migration in acute kidney injury induced by sepsis. *PLoS One* **7**, e37584 (2012).

142. Kimura, A. *et al.* Interferon-gamma is protective in cisplatin-induced renal injury by enhancing autophagic flux. *Kidney Int* **82**, 1093-104 (2012).

143. Saha, S. *et al.* Macrophage-derived extracellular vesicle-packaged WNTs rescue intestinal stem cells and enhance survival after radiation injury. *Nat Commun* **7**, 13096 (2016).

144. Long, M.E. *et al.* MEK1/2 Inhibition Promotes Macrophage Reparative Properties. *J Immunol* **198**, 862-872 (2017).

145. Lin, S.L. *et al.* Macrophage Wnt7b is critical for kidney repair and regeneration. *Proc Natl Acad Sci U S A* **107**, 4194-9 (2010).

146. Howe, K. *et al.* The zebrafish reference genome sequence and its relationship to the human genome. *Nature* **496**, 498-503 (2013).

147. Balasubramanian, S., Raghunath, A. & Perumal, E. Role of epigenetics in zebrafish development. *Gene* **718**, 144049 (2019).

148. de Groh, E.D. *et al.* Inhibition of histone deacetylase expands the renal progenitor cell population. *J Am Soc Nephrol* **21**, 794-802 (2010).

149. Dooley, K. & Zon, L.I. Zebrafish: a model system for the study of human disease. *Curr Opin Genet Dev* **10**, 252-6 (2000).

150. MacRae, C.A. & Peterson, R.T. Zebrafish as tools for drug discovery. *Nat Rev Drug Discov* **14**, 721-31 (2015).

151. Marques, I.J., Lupi, E. & Mercader, N. Model systems for regeneration: zebrafish. *Development* **146**(2019).

152. McKee, R.A. & Wingert, R.A. Zebrafish Renal Pathology: Emerging Models of Acute Kidney Injury. *Curr Pathobiol Rep* **3**, 171-181 (2015).

153. Perazella, M.A. Pharmacology behind Common Drug Nephrotoxicities. *Clin J Am Soc Nephrol* **13**, 1897-1908 (2018).

154. Hentschel, D.M. *et al.* Acute renal failure in zebrafish: a novel system to study a complex disease. *Am J Physiol Renal Physiol* **288**, F923-9 (2005).

155. Cianciolo Cosentino, C., Roman, B.L., Drummond, I.A. & Hukriede, N.A. Intravenous microinjections of zebrafish larvae to study acute kidney injury. *J Vis Exp* (2010).

156. Cianciolo Cosentino, C. *et al.* Histone deacetylase inhibitor enhances recovery after AKI. *J Am Soc Nephrol* **24**, 943-53 (2013).

157. Chiba, T. *et al.* Retinoic Acid Signaling Coordinates Macrophage-Dependent Injury and Repair after AKI. *J Am Soc Nephrol* **27**, 495-508 (2016).

158. Brilli Skvarca, L. *et al.* Enhancing regeneration after acute kidney injury by promoting cellular dedifferentiation in zebrafish. *Dis Model Mech* **12**(2019).

159. Dressler, G.R. & Woolf, A.S. Pax2 in development and renal disease. *Int J Dev Biol* **43**, 463-8 (1999).

160. Sharma, R., Sanchez-Ferras, O. & Bouchard, M. Pax genes in renal development, disease and regeneration. *Semin Cell Dev Biol* **44**, 97-106 (2015).

161. Majumdar, A., Lun, K., Brand, M. & Drummond, I.A. Zebrafish no isthmus reveals a role for pax2.1 in tubule differentiation and patterning events in the pronephric primordia. *Development* **127**, 2089-98 (2000).

162. Wingert, R.A. *et al.* The cdx genes and retinoic acid control the positioning and segmentation of the zebrafish pronephros. *PLoS Genet* **3**, 1922-38 (2007).

163. Li, Y., Cheng, C.N., Verdun, V.A. & Wingert, R.A. Zebrafish nephrogenesis is regulated by interactions between retinoic acid, mecom, and Notch signaling. *Dev Biol* **386**, 111-22 (2014).

164. Bollig, F. *et al.* A highly conserved retinoic acid responsive element controls wt1a expression in the zebrafish pronephros. *Development* **136**, 2883-92 (2009).

165. Tomar, R., Mudumana, S.P., Pathak, N., Hukriede, N.A. & Drummond, I.A. osr1 is required for podocyte development downstream of wt1a. *J Am Soc Nephrol* **25**, 2539-45 (2014).

166. Wu, J. *et al.* Retinoic acid attenuates contrast-induced acute kidney injury in a miniature pig model. *Biochem Biophys Res Commun* **512**, 163-169 (2019).

167. Ellett, F., Pase, L., Hayman, J.W., Andrianopoulos, A. & Lieschke, G.J. mpeg1 promoter transgenes direct macrophage-lineage expression in zebrafish. *Blood* **117**, e49-e56 (2011).

168. Murayama, E. *et al.* Tracing hematopoietic precursor migration to successive hematopoietic organs during zebrafish development. *Immunity* **25**, 963-75 (2006).

169. Yu, C.C., Chien, C.T. & Chang, T.C. M2 macrophage polarization modulates epithelial-mesenchymal transition in cisplatin-induced tubulointerstitial fibrosis. *Biomedicine (Taipei)* **6**, 5 (2016).

170. Nguyen-Chi, M. *et al.* Identification of polarized macrophage subsets in zebrafish. *Elife* **4**, e07288 (2015).

171. Lieschke, G.J., Oates, A.C., Crowhurst, M.O., Ward, A.C. & Layton, J.E. Morphologic and functional characterization of granulocytes and macrophages in embryonic and adult zebrafish. *Blood* **98**, 3087-96 (2001).

172. Campana, L. *et al.* The STAT3-IL-10-IL-6 Pathway Is a Novel Regulator of Macrophage Efferocytosis and Phenotypic Conversion in Sterile Liver Injury. *J Immunol* **200**, 1169-1187 (2018).

173. Petrie, T.A., Strand, N.S., Yang, C.T., Rabinowitz, J.S. & Moon, R.T. Macrophages modulate adult zebrafish tail fin regeneration. *Development* **141**, 2581-91 (2014).

174. Simoes, F.C. *et al.* Macrophages directly contribute collagen to scar formation during zebrafish heart regeneration and mouse heart repair. *Nat Commun* **11**, 600 (2020).

175. Fass, D.M. *et al.* Effect of Inhibiting Histone Deacetylase with Short-Chain Carboxylic Acids and Their Hydroxamic Acid Analogs on Vertebrate Development and Neuronal Chromatin. *ACS Med Chem Lett* **2**, 39-42 (2010).

176. Skrypnyk, N.I. *et al.* Delayed treatment with PTBA analogs reduces postinjury renal fibrosis after kidney injury. *Am J Physiol Renal Physiol* **310**, F705-F716 (2016).

177. Novitskaya, T. *et al.* A PTBA small molecule enhances recovery and reduces postinjury fibrosis after aristolochic acid-induced kidney injury. *American Journal of Physiology - Renal Physiology* **306**, F496-F504 (2014).

178. Brilli, L.L., Swanhart, L.M., de Caestecker, M.P. & Hukriede, N.A. HDAC inhibitors in kidney development and disease. *Pediatr Nephrol* **28**, 1909-21 (2013).

179. Skvarca, L.B. Acute kidney injury in zebrafish larvae as a regeneration model for drug discovery *University of Pittsburgh* (2015).

180. Banerjee, S., Adhikari, N., Amin, S.A. & Jha, T. Histone deacetylase 8 (HDAC8) and its inhibitors with selectivity to other isoforms: An overview. *Eur J Med Chem* **164**, 214-240 (2019).

181. Kleff, S., Andrulis, E.D., Anderson, C.W. & Sternglanz, R. Identification of a gene encoding a yeast histone H4 acetyltransferase. *J Biol Chem* **270**, 24674-7 (1995).

182. Haberland, M., Mokalled, M.H., Montgomery, R.L. & Olson, E.N. Epigenetic control of skull morphogenesis by histone deacetylase 8. *Genes Dev* **23**, 1625-30 (2009).

183. Hu, E. *et al.* Cloning and characterization of a novel human class I histone deacetylase that functions as a transcription repressor. *J Biol Chem* **275**, 15254-64 (2000).

184. Vanaja, G.R., Ramulu, H.G. & Kalle, A.M. Overexpressed HDAC8 in cervical cancer cells shows functional redundancy of tubulin deacetylation with HDAC6. *Cell Commun Signal* **16**, 20 (2018).

185. Joshi, P. *et al.* The functional interactome landscape of the human histone deacetylase family. *Mol Syst Biol* **9**, 672 (2013).

186. Dasgupta, T., Antony, J., Braithwaite, A.W. & Horsfield, J.A. HDAC8 Inhibition Blocks SMC3 Deacetylation and Delays Cell Cycle Progression without Affecting Cohesin-dependent Transcription in MCF7 Cancer Cells. *J Biol Chem* **291**, 12761-70 (2016).

187. Kaiser, F.J. *et al.* Loss-of-function HDAC8 mutations cause a phenotypic spectrum of Cornelia de Lange syndrome-like features, ocular hypertelorism, large fontanelle and X-linked inheritance. *Hum Mol Genet* **23**, 2888-900 (2014).

188. Deardorff, M.A. *et al.* HDAC8 mutations in Cornelia de Lange syndrome affect the cohesin acetylation cycle. *Nature* **489**, 313-7 (2012).

189. Caby, S. *et al.* Analysis of the interactome of Schistosoma mansoni histone deacetylase 8. *PLoS Negl Trop Dis* **11**, e0006089 (2017).

190. Deardorff, M.A., Porter, N.J. & Christianson, D.W. Structural aspects of HDAC8 mechanism and dysfunction in Cornelia de Lange syndrome spectrum disorders. *Protein Sci* **25**, 1965-1976 (2016).

191. Li, R.F. *et al.* Roles of HDAC2 and HDAC8 in Cardiac Remodeling in Renovascular Hypertensive Rats and the Effects of Valproic Acid Sodium. *Pharmacology* **99**, 27-39 (2017).

192. Choi, S.Y. *et al.* Piceatannol Attenuates Renal Fibrosis Induced by Unilateral Ureteral Obstruction via Downregulation of Histone Deacetylase 4/5 or p38-MAPK Signaling. *PLoS One* **11**, e0167340 (2016).

193. Kee, H.J. *et al.* HDAC inhibition suppresses cardiac hypertrophy and fibrosis in DOCA-salt hypertensive rats via regulation of HDAC6/HDAC8 enzyme activity. *Kidney Blood Press Res* **37**, 229-39 (2013).

194. Fragiadaki, M. & Mason, R.M. Epithelial-mesenchymal transition in renal fibrosis - evidence for and against. *Int J Exp Pathol* **92**, 143-50 (2011).

195. Zhang, Y. *et al.* Identification of histone deacetylase 8 as a novel therapeutic target for renal fibrosis. *FASEB J* (2020).

196. Yoshikawa, M., Hishikawa, K., Marumo, T. & Fujita, T. Inhibition of histone deacetylase activity suppresses epithelial-to-mesenchymal transition induced by TGF-beta1 in human renal epithelial cells. *J Am Soc Nephrol* **18**, 58-65 (2007).

197. Zeisberg, M. *et al.* BMP-7 counteracts TGF-beta1-induced epithelial-to-mesenchymal transition and reverses chronic renal injury. *Nat Med* **9**, 964-8 (2003).

198. Lin, F.L. *et al.* HADC8 Inhibitor WK2-16 Therapeutically Targets Lipopolysaccharide-Induced Mouse Model of Neuroinflammation and Microglial Activation. *Int J Mol Sci* **20**(2019).

199. Ferenbach, D.A. & Bonventre, J.V. Mechanisms of maladaptive repair after AKI leading to accelerated kidney ageing and CKD. *Nat Rev Nephrol* **11**, 264-76 (2015).

200. Mishra, A. *et al.* Both interaction surfaces within cohesin's hinge domain are essential for its stable chromosomal association. *Curr Biol* **20**, 279-89 (2010).

201. Xiong, B., Lu, S. & Gerton, J.L. Hos1 is a lysine deacetylase for the Smc3 subunit of cohesin. *Curr Biol* **20**, 1660-5 (2010).

202. Borges, V. *et al.* Hos1 deacetylates Smc3 to close the cohesin acetylation cycle. *Mol Cell* **39**, 677-88 (2010).

203. Gil-Rodriguez, M.C. *et al.* De novo heterozygous mutations in SMC3 cause a range of Cornelia de Lange syndrome-overlapping phenotypes. *Hum Mutat* **36**, 454-62 (2015).

204. Papassotiriou, G.P. *et al.* Neutrophil Gelatinase--Associated Lipocalin and Cystatin C Are Sensitive Markers of Renal Injury in Patients With Multiple Myeloma. *Clin Lymphoma Myeloma Leuk* **16**, 29-35 (2016).

205. Piche, J., Van Vliet, P.P., Puceat, M. & Andelfinger, G. The expanding phenotypes of cohesinopathies: one ring to rule them all! *Cell Cycle* **18**, 2828-2848 (2019).

206. Borrie, M.S., Campor, J.S., Joshi, H. & Gartenberg, M.R. Binding, sliding, and function of cohesin during transcriptional activation. *Proc Natl Acad Sci U S A* **114**, E1062-E1071 (2017).

207. Yun, J. *et al.* Dynamic cohesin-mediated chromatin architecture controls epithelial-mesenchymal plasticity in cancer. *EMBO Rep* **17**, 1343-59 (2016).

208. Meier, M. *et al.* Cohesin facilitates zygotic genome activation in zebrafish. *Development* **145**(2018).

209. Swanhart, L.M. *et al.* Zebrafish kidney development: basic science to translational research. *Birth Defects Res C Embryo Today* **93**, 141-56 (2011).

210. Chiba, T., Hukriede, N. & de Caestecker, M.P. Kidney Regeneration: Lessons from Development. *Curr Pathobiol Rep* **3**, 67-79 (2015).

211. Wen, X. *et al.* Time-dependent effects of histone deacetylase inhibition in sepsis-associated acute kidney injury. *Intensive Care Med Exp* **8**, 9 (2020).

212. Humphreys, B.D. *et al.* Repair of injured proximal tubule does not involve specialized progenitors. *Proc Natl Acad Sci U S A* **108**, 9226-31 (2011).

213. Maeshima, A., Maeshima, K., Nojima, Y. & Kojima, I. Involvement of Pax-2 in the action of activin A on tubular cell regeneration. *J Am Soc Nephrol* **13**, 2850-9 (2002).

214. Ichimura, T. *et al.* Kidney injury molecule-1 (KIM-1), a putative epithelial cell adhesion molecule containing a novel immunoglobulin domain, is up-regulated in renal cells after injury. *J Biol Chem* **273**, 4135-42 (1998).

215. Humphreys, B.D. *et al.* Chronic epithelial kidney injury molecule-1 expression causes murine kidney fibrosis. *J Clin Invest* **123**, 4023-35 (2013).

216. Rosselot, C. *et al.* Non-cell-autonomous retinoid signaling is crucial for renal development. *Development* **137**, 283-92 (2010).

217. Burrow, C.R. Retinoids and renal development. *Exp Nephrol* **8**, 219-25 (2000).

218. Takayama, M., Miyatake, K. & Nishida, E. Identification and characterization of retinoic acid-responsive genes in mouse kidney development. *Genes Cells* **19**, 637-49 (2014).

219. Pogoda, H.M. *et al.* Direct activation of chordoblasts by retinoic acid is required for segmented centra mineralization during zebrafish spine development. *Development* **145**(2018).

220. Waxman, J.S., Keegan, B.R., Roberts, R.W., Poss, K.D. & Yelon, D. Hoxb5b acts downstream of retinoic acid signaling in the forelimb field to restrict heart field potential in zebrafish. *Dev Cell* **15**, 923-34 (2008).

221. Waxman, J.S. & Yelon, D. Zebrafish retinoic acid receptors function as context-dependent transcriptional activators. *Dev Biol* **352**, 128-40 (2011).

222. Westerfield, M. The zebrafish book. A guide for the laboratory use of zebrafish (Danio rerio). *University of Oregon Press* (2000).

223. Chien, K.M.K.E.F.C.G.B.D.M.M.E.H.D.S.C.J.M.P.H.J.Y.J.P.K.C.B. The Tol2kit: A multisite gateway-based construction kit for Tol2 transposon transgenesis constructs. *Developmental Dynamics* **236**, 3088-3099 (2007).

224. Drummond, I.A. & Davidson, A.J. Zebrafish kidney development. *Methods Cell Biol* **100**, 233-60 (2010).

225. Liao, Y., Smyth, G.K. & Shi, W. featureCounts: an efficient general purpose program for assigning sequence reads to genomic features. *Bioinformatics* **30**, 923-30 (2014).

226. Robinson, M.D., McCarthy, D.J. & Smyth, G.K. edgeR: a Bioconductor package for differential expression analysis of digital gene expression data. *Bioinformatics* **26**, 139-40 (2010).

227. Andrianova, N.V. *et al.* Kidney Cells Regeneration: Dedifferentiation of Tubular Epithelium, Resident Stem Cells and Possible Niches for Renal Progenitors. *Int J Mol Sci* **20**(2019).

228. Buzhor, E. *et al.* Reactivation of NCAM1 defines a subpopulation of human adult kidney epithelial cells with clonogenic and stem/progenitor properties. *Am J Pathol* **183**, 1621-1633 (2013).

229. Subramanian, P., Mitroulis, I., Hajishengallis, G. & Chavakis, T. Regulation of tissue infiltration by neutrophils: role of integrin alpha3beta1 and other factors. *Curr Opin Hematol* **23**, 36-43 (2016).

230. Souza, A.C. *et al.* TLR4 mutant mice are protected from renal fibrosis and chronic kidney disease progression. *Physiol Rep* **3**(2015).

231. Lee, S. *et al.* Distinct Macrophage Phenotypes Contribute to Kidney Injury and Repair. *JASN* **22**, 317-326 (2011).

232. Han, W.K., Bailly, V., Abichandani, R., Thadhani, R. & Bonventre, J.V. Kidney Injury Molecule-1 (KIM-1): a novel biomarker for human renal proximal tubule injury. *Kidney Int* **62**, 237-44 (2002).

233. Li, L., Yan, B., Shi, Y.Q., Zhang, W.Q. & Wen, Z.L. Live imaging reveals differing roles of macrophages and neutrophils during zebrafish tail fin regeneration. *J Biol Chem* **287**, 25353-60 (2012).

234. Ricardo, S.D., van Goor, H. & Eddy, A.A. Macrophage diversity in renal injury and repair. *J Clin Invest* **118**, 3522-30 (2008).

235. Cao, Q. *et al.* IL-10/TGF-β–Modified Macrophages Induce Regulatory T Cells and Protect against Adriamycin Nephrosis. *J Am Soc Nephrol* **21**, 933-42 (2010).

236. Jo, S.K., Sung, S.A., Cho, W.Y., Go, K.J. & Kim, H.K. Macrophages contribute to the initiation of ischaemic acute renal failure in rats. *Nephrol Dial Transplant* **21**, 1231-9 (2006).

237. Sanker, S. *et al.* Development of high-content assays for kidney progenitor cell expansion in transgenic zebrafish. *J Biomol Screen* **18**, 1193-202 (2013).

238. Kitaguchi, T., Kawakami, K. & Kawahara, A. Transcriptional regulation of a myeloid-lineage specific gene lysozyme C during zebrafish myelopoiesis. *Mech Dev* **126**, 314-23 (2009).

239. Harvie, E.A., Green, J.M., Neely, M.N. & Huttenlocher, A. Innate immune response to Streptococcus iniae infection in zebrafish larvae. *Infect Immun* **81**, 110-21 (2013).

240. Wiegertjes, G.F., Wentzel, A.S., Spaink, H.P., Elks, P.M. & Fink, I.R. Polarization of immune responses in fish: The 'macrophages first' point of view. *Mol Immunol* **69**, 146-56 (2016).

241. Herbomel, P., Thisse, B. & Thisse, C. Ontogeny and behaviour of early macrophages in the zebrafish embryo. *Development* **126**, 3735-45 (1999).

242. Selders, G.S., Fetz, A.E., Radic, M.Z. & Bowlin, G.L. An overview of the role of neutrophils in innate immunity, inflammation and host-biomaterial integration. *Regen Biomater* **4**, 55-68 (2017).

243. Oliveira, L.M., Teixeira, F.M.E. & Sato, M.N. Impact of Retinoic Acid on Immune Cells and Inflammatory Diseases. *Mediators Inflamm* **2018**, 3067126 (2018).

244. Na, S.Y. *et al.* Retinoids inhibit interleukin-12 production in macrophages through physical associations of retinoid X receptor and NFkappaB. *J Biol Chem* **274**, 7674-80 (1999).

245. Gundra, U.M. *et al.* Vitamin A mediates conversion of monocyte-derived macrophages into tissue-resident macrophages during alternative activation. *Nat Immunol* **18**, 642-653 (2017).

246. Rafa, H. *et al.* All-Trans Retinoic Acid Modulates TLR4/NF-kappaB Signaling Pathway Targeting TNF-alpha and Nitric Oxide Synthase 2 Expression in Colonic Mucosa during

Ulcerative Colitis and Colitis Associated Cancer. *Mediators Inflamm* **2017**, 7353252 (2017).

247. Sierra-Mondragon, E. *et al.* All-Trans Retinoic Acid Attenuates Fibrotic Processes by Downregulating TGF-beta1/Smad3 in Early Diabetic Nephropathy. *Biomolecules* **9**(2019).

248. Tang, J. *et al.* Class I HDAC activity is required for renal protection and regeneration after acute kidney injury. *Am J Physiol Renal Physiol* **307**, F303-16 (2014).

249. Li, W. & Sun, Z. Mechanism of Action for HDAC Inhibitors-Insights from Omics Approaches. *Int J Mol Sci* **20**(2019).

250. Massey, A.J. A high content, high throughput cellular thermal stability assay for measuring drug-target engagement in living cells. *PLoS One* **13**, e0195050 (2018).

251. Ishii, T. *et al.* CETSA quantitatively verifies in vivo target engagement of novel RIPK1 inhibitors in various biospecimens. *Sci Rep* **7**, 13000 (2017).

252. Axelsson, H., Almqvist, H., Seashore-Ludlow, B. & Lundback, T. Screening for Target Engagement using the Cellular Thermal Shift Assay - CETSA. in *Assay Guidance Manual* (eds. Sittampalam, G.S. *et al.*) (Bethesda (MD), 2004).

253. Martinez Molina, D. & Nordlund, P. The Cellular Thermal Shift Assay: A Novel Biophysical Assay for In Situ Drug Target Engagement and Mechanistic Biomarker Studies. *Annu Rev Pharmacol Toxicol* **56**, 141-61 (2016).

254. Jensen, A.J., Martinez Molina, D. & Lundback, T. CETSA: a target engagement assay with potential to transform drug discovery. *Future Med Chem* **7**, 975-8 (2015).

255. Jafari, R. *et al.* The cellular thermal shift assay for evaluating drug target interactions in cells. *Nat Protoc* **9**, 2100-22 (2014).

256. Martinez Molina, D. *et al.* Monitoring drug target engagement in cells and tissues using the cellular thermal shift assay. *Science* **341**, 84-7 (2013).

257. Balasubramanian, S. *et al.* A novel histone deacetylase 8 (HDAC8)-specific inhibitor PCI-34051 induces apoptosis in T-cell lymphomas. *Leukemia* **22**, 1026-34 (2008).

258. Busch-Nentwich, E., Kettleborough, R., Dooley, C. M., Scahill, C., Sealy, I., White, R., Herd, C., Mehroke, S., Wali, N., Carruthers, S., Hall, A., Collins, J., Gibbons, R., Pusztai, Z., Clark, R., and Stemple, D.L. Sanger Institute Zebrafish Mutation Project mutant data submission

. *ZFIN Direct Data Submission* (2013).

259. Alam, N. *et al.* Structure-based identification of HDAC8 non-histone substrates. *Structure* **24**, 458-468 (2016).

260. Lopez, J.E., Haynes, S.E., Majmudar, J.D., Martin, B.R. & Fierke, C.A. HDAC8 Substrates Identified by Genetically Encoded Active Site Photocrosslinking. *J Am Chem Soc* **139**, 16222-16227 (2017).

261. Hendzel, M.J. *et al.* Mitosis-specific phosphorylation of histone H3 initiates primarily within pericentromeric heterochromatin during G2 and spreads in an ordered fashion coincident with mitotic chromosome condensation. *Chromosoma* **106**, 348-60 (1997).

262. Van Hooser, A., Goodrich, D.W., Allis, C.D., Brinkley, B.R. & Mancini, M.A. Histone H3 phosphorylation is required for the initiation, but not maintenance, of mammalian chromosome condensation. *J Cell Sci* **111 (Pt 23)**, 3497-506 (1998).

263. Hans, F. & Dimitrov, S. Histone H3 phosphorylation and cell division. *Oncogene* **20**, 3021-7 (2001).

264. LaBaer, J. *et al.* New functional activities for the p21 family of CDK inhibitors. *Genes Dev* **11**, 847-62 (1997).

265. Cheng, M. *et al.* The p21(Cip1) and p27(Kip1) CDK 'inhibitors' are essential activators of cyclin D-dependent kinases in murine fibroblasts. *EMBO J* **18**, 1571-83 (1999).

266. Sugimoto, M. *et al.* Activation of cyclin D1-kinase in murine fibroblasts lacking both p21(Cip1) and p27(Kip1). *Oncogene* **21**, 8067-74 (2002).

267. Thomasova, D. & Anders, H.J. Cell cycle control in the kidney. *Nephrol Dial Transplant* **30**, 1622-30 (2015).

268. Monnich, M., Kuriger, Z., Print, C.G. & Horsfield, J.A. A zebrafish model of Roberts syndrome reveals that Esco2 depletion interferes with development by disrupting the cell cycle. *PLoS One* **6**, e20051 (2011).

269. Alam, N. *et al.* Structure-Based Identification of HDAC8 Non-histone Substrates. *Structure* **24**, 458-68 (2016).

270. Rivera, T. & Losada, A. Recycling cohesin rings by deacetylation. *Mol Cell* **39**, 657-9 (2010).

271. Gelbert, L.M. *et al.* Preclinical characterization of the CDK4/6 inhibitor LY2835219: in-vivo cell cycle-dependent/independent anti-tumor activities alone/in combination with gemcitabine. *Invest New Drugs* **32**, 825-37 (2014).

272. Wang, Y., Sun, Z.H., Zhou, L., Li, Z. & Gui, J.F. Grouper tshbeta promoter-driven transgenic zebrafish marks proximal kidney tubule development. *PLoS One* **9**, e97806 (2014).

273. Johnson, A.C.M. & Zager, R.A. Mechanisms and consequences of oxidant-induced renal preconditioning: an Nrf2-dependent, P21-independent, anti-senescence pathway. *Nephrol Dial Transplant* **33**, 1927-1941 (2018).

274. Yan, M., Tang, C., Ma, Z., Huang, S. & Dong, Z. DNA damage response in nephrotoxic and ischemic kidney injury. *Toxicol Appl Pharmacol* **313**, 104-108 (2016).

275. Ajay, A.K. *et al.* A bioinformatics approach identifies signal transducer and activator of transcription-3 and checkpoint kinase 1 as upstream regulators of kidney injury molecule-1 after kidney injury. *J Am Soc Nephrol* **25**, 105-18 (2014).

276. Jorgensen, P.L. Structure, function and regulation of Na,K-ATPase in the kidney. *Kidney Int* **29**, 10-20 (1986).

277. Fragkos, M., Jurvansuu, J. & Beard, P. H2AX is required for cell cycle arrest via the p53/p21 pathway. *Mol Cell Biol* **29**, 2828-40 (2009).

278. Branzei, D. & Foiani, M. The checkpoint response to replication stress. *DNA Repair (Amst)* **8**, 1038-46 (2009).

279. Plesca, D., Mazumder, S. & Almasan, A. DNA damage response and apoptosis. *Methods Enzymol* **446**, 107-22 (2008).

280. Branzei, D. & Foiani, M. Regulation of DNA repair throughout the cell cycle. *Nat Rev Mol Cell Biol* **9**, 297-308 (2008).

281. Podhorecka, M., Skladanowski, A. & Bozko, P. H2AX Phosphorylation: Its Role in DNA Damage Response and Cancer Therapy. *J Nucleic Acids* **2010**(2010).

282. Raudvere, U. *et al.* g:Profiler: a web server for functional enrichment analysis and conversions of gene lists (2019 update). *Nucleic Acids Res* **47**, W191-W198 (2019).

283. Bresciani, E., Broadbridge, E. & Liu, P.P. An efficient dissociation protocol for generation of single cell suspension from zebrafish embryos and larvae. *MethodsX* **5**, 1287-1290 (2018).

284. Kim, D., Langmead, B. & Salzberg, S.L. HISAT: a fast spliced aligner with low memory requirements. *Nat Methods* **12**, 357-60 (2015).

285. Rettig, I. *et al.* Selective inhibition of HDAC8 decreases neuroblastoma growth in vitro and in vivo and enhances retinoic acid-mediated differentiation. *Cell Death Dis* **6**, e1657 (2015).

286. Shan, Z.Y. *et al.* pCREB is involved in neural induction of mouse embryonic stem cells by RA. *Anat Rec (Hoboken)* **291**, 519-26 (2008).

287. Puri, P. *et al.* Ectopic Phosphorylated Creb Marks Dedifferentiated Proximal Tubules in Cystic Kidney Disease. *Am J Pathol* **188**, 84-94 (2018).

288. Stewart, R., Flechner, L., Montminy, M. & Berdeaux, R. CREB is activated by muscle injury and promotes muscle regeneration. *PLoS One* **6**, e24714 (2011).

289. Ortega-Martinez, S. A new perspective on the role of the CREB family of transcription factors in memory consolidation via adult hippocampal neurogenesis. *Front Mol Neurosci* **8**, 46 (2015).

290. Gao, J., Siddoway, B., Huang, Q. & Xia, H. Inactivation of CREB mediated gene transcription by HDAC8 bound protein phosphatase,. *Biochemical and Biophysical Research Communications* **379**, 1-5 (2009).

291. Ha, S.D., Han, C.Y., Reid, C. & Kim, S.O. HDAC8-mediated epigenetic reprogramming plays a key role in resistance to anthrax lethal toxin-induced pyroptosis in macrophages. *J Immunol* **193**, 1333-43 (2014).

292. Li, J. *et al.* Histone deacetylase 8 regulates cortactin deacetylation and contraction in smooth muscle tissues. *Am J Physiol Cell Physiol* **307**, C288-95 (2014).

293. Zhang, X. *et al.* HDAC6 modulates cell motility by altering the acetylation level of cortactin. *Mol Cell* **27**, 197-213 (2007).

294. Kirkbride, K.C., Sung, B.H., Sinha, S. & Weaver, A.M. Cortactin: a multifunctional regulator of cellular invasiveness. *Cell Adh Migr* **5**, 187-98 (2011).

295. Yan, B. *et al.* HDAC6 deacetylase activity is critical for lipopolysaccharide-induced activation of macrophages. *PLoS One* **9**, e110718 (2014).

296. Schenone, M., Dancik, V., Wagner, B.K. & Clemons, P.A. Target identification and mechanism of action in chemical biology and drug discovery. *Nat Chem Biol* **9**, 232-40 (2013).

297. Przepiorski, A. *et al.* A Simple Bioreactor-Based Method to Generate Kidney Organoids from Pluripotent Stem Cells. *Stem Cell Reports* **11**, 470-484 (2018).

298. Przepiorski, A., Crunk, A.E., Espiritu, E.B., Hukriede, N.A. & Davidson, A.J. The Utility of Human Kidney Organoids in Modeling Kidney Disease. *Semin Nephrol* **40**, 188-198 (2020).